

AD-A258 484



ON PAGE

Form Approved
OMB No 0704-0188

2

Public
gathe
collec
Davis

1 hour per response, including the time for reviewing instructions, searching existing data sources, collection of information. Send comments regarding this burden estimate or any other aspect of this Washington Headquarters Services, Directorate for Information Operations and Reports, 1215 Jefferson Management and Budget, Paperwork Reduction Project (0704-0188) Washington, DC 20503

1. AGENCY USE ONLY (Leave blank)

3. REPORT TYPE AND DATES COVERED

FINAL 21 Aug 89 - 20 Aug 92

4. TITLE AND SUBTITLE

"DEVELOP, APPLY AND EVALUATE WAVELET TECHNOLOGY" (U)

5. FUNDING NUMBERS

7092/00/DARPA

6. AUTHOR(S)

Dr. Howard L. Resnikoff & Aware Staff

7. PERFORMING ORGANIZATION NAME(S) AND ADDRESS(ES)

Aware, Inc.
One Memorial Drive
Fourth Floor
Cambridge, MA 02142

8. PERFORMING ORGANIZATION
REPORT NUMBER

9. SPONSORING/MONITORING AGENCY NAME(S) AND ADDRESS(ES)

AFOSR/NM
Bldg 410
Bolling AFB DC 20332-6448

10. SPONSORING MONITORING
AGENCY REPORT NUMBER

F49620-89-C-0125

11. SUPPLEMENTARY NOTES

DTIC
SELECTE
NOV 23 1992
S B D

12a. DISTRIBUTION/AVAILABILITY STATEMENT

Approved for public release;
Distribution unlimited

12b. DISTRIBUTION CODE

UL

13. ABSTRACT (Maximum 200 words)

On this contract, they completed work in three major areas: the mathematical foundations of wavelet theory, and applications of wavelets to signal processing and partial differential equations. In the area of mathematical foundations, they have investigated both discrete and continuous aspects of wavelet theory. In their investigations of the applications of wavelets to signal processing, they have had two major foci: image compression and computational algorithms. Furthermore they have investigated connections between the wavelet and Fourier transforms and described the characteristics of some fundamental signals in wavelet phase space. They have applied wavelet based numerical methods to the solution of partial differential equations. Specifically, they compare the Wavelet-Galerkin method to standard numerical methods for the numerical solution of (1) the Euler equations of a two-dimensional, incompressible fluid in a periodic domain, (2) the Biharmonic Helmholtz equation and the Reduced Wave equation in nonseparable, two-dimensional geometry and (3) the Euler and Navier-Stokes equations in nonseparable, two dimensional geometry. The wavelet methods have significant advantages with regard to stability, accuracy, and rate of convergence.

14. SUBJECT TERMS

15. NUMBER OF PAGES

125

16. PRICE CODE

17. SECURITY CLASSIFICATION
OF REPORT

UNCLASSIFIED

18. SECURITY CLASSIFICATION
OF THIS PAGE

UNCLASSIFIED

19. SECURITY CLASSIFICATION
OF ABSTRACT

UNCLASSIFIED

20. LIMITATION OF ABSTRACT

SAR

Final Summary Technical Report

“Develop, Apply, and Evaluate Wavelet Technology”

ARPA Order #7092

AFOSR Contract #F49620-89-C-0125

Staff of Aware
Aware, Inc.
One Memorial Drive, 4th Floor
Cambridge, MA 02142 USA
617-577-1700 617-577-1710 FAX

©1992 Aware, Inc.

AD921020

20 October 1992

012550
92-30011
21288

92 11 20 084

Abstract

This is the Final Report of a three year project to "Develop, Apply, and Evaluate Wavelet Technology" conducted under ARPA Order #7092, AFOSR Contract #F49620-89-C-0125.

The Final Report has two parts. This part contains a summary technical report, and appendices that describe outreach activities to the scientific, commercial, and governmental communities under the program.

The second part of the Final Report is a separately bound monograph titled *The scalable structure of information: An essay on wavelet technology and its application to bandwidth management*. It is a semi-technical presentation for people who want to know what wavelets are, how they are related to conventional mathematical tools, and what they are good for. The *Essay* describes the foundations of wavelet technology; provides an informal introduction (i.e., many figures; no proofs) to the many types of compactly supported wavelets; and describes their application in bandwidth management. The applications emphasize *compression, channel coding, and numerical solution of partial differential equations*.

Keywords: Audio compression; Bandwidth compression; Biorthogonal wavelets; Channel coding; Complex wavelets; Connection coefficients; Discrete functions; Formal derivatives of wavelets; Higher rank wavelets; Image compression; Numerical solution of partial differential equations; Orthogonal wavelets; Scaling function; Transient signal analysis; Wavelet bases; Wavelet-Capacitance matrix; Wavelet-Galerkin method; Wavelet matrices; Wavelet matrix expansion.

Contents

1	Report Summary	4
2	Mathematical Foundations	5
2.1	Higher Rank Wavelets	5
2.2	Parametrization of Wavelets	9
2.3	Wavelets and Classical Analysis	11
2.4	Wavelet Frames and the Wavelet-Galerkin Operator	12
2.5	Future Directions	13
3	Signal Processing	14
3.1	Image Processing	14
3.2	Signal Detection and Classification	16
4	Wavelets and the Numerical Solution of Partial Differential Equations	20
5	Channel Coding	23
6	Appendices	30
6.1	About Aware, Inc.	30
6.2	Government contracts related to this contract	31
6.3	Aware reports and presentations supported in part by this contract	31
6.3.1	Reports and publications supported in part by this contract	31
6.3.2	Related reports	34
6.4	Wavelet technology in the popular press	34
6.5	Lectures and presentations supported in part by this contract	34
6.6	Academic relationships	35
6.6.1	Student internships	36

List of Figures

1	Frequency response for regular wavelet filters: $N = 1, m = 2, 3, 4$	7
2	Basis elements $\varphi, \psi^1, \psi^2, \psi^3$ with regularity $N = 3$	8

3	Novon scaling function with regularity order $N = 1$	10
4	Aware's wavelet-based image compression system	14
5	Mallat decomposition	15
6	Wavelet phase space plot of the Dirac distribution	20

Executive Summary

This is the Final Report of a three year project to "Develop, Apply, and Evaluate Wavelet Technology" conducted under ARPA Order #7092, AFOSR Contract #F49620-89-C-0125. The Final Report has two parts. This part contains a summary technical report, and appendices that describe outreach activities to the scientific, commercial, and governmental communities under the program.

The second part of the Final Report is a separately bound monograph titled *The scalable structure of information: An essay on wavelet technology and its application to bandwidth management*. It is a semi-technical presentation for people who want to know what wavelets are, how they are related to conventional mathematical tools, and what they are good for. The *Essay* describes the foundations of wavelet technology; provides an informal introduction (i.e., many figures; no proofs) to the many types of compactly supported wavelets; and describes their application in bandwidth management. The applications emphasize *compression, channel coding, and numerical solution of partial differential equations*.

DTIC QUALITY INSPECTED 4

Accession For	
NTIS GRA&I	<input checked="" type="checkbox"/>
DTIC TAB	<input type="checkbox"/>
Unannounced	<input type="checkbox"/>
Justification	
By _____	
Distribution/	
Availability Codes	
Dist	Avail and/or Special
A-1	

1 Report Summary

In our work on this contract, we completed work in three major areas: the mathematical foundations of wavelet theory, and applications of wavelets to signal processing and partial differential equations. In this final technical report we summarize the results of our investigations in these three areas and report on directions for further research.

In the area of mathematical foundations, we have investigated both discrete and continuous aspects of wavelet theory. The original wavelets of Daubechies [2] and Mallat [25] correspond to 2-band filter banks; they split a signal (or subspace of functions) into *two* parts. We have developed [17, 14] a far-reaching generalization of the wavelet concept (“higher rank wavelets”) to the case where a signal is split into m different pieces or frequency bands¹. This generalization encompasses block transforms such as the FFT as well as overlapped transforms, all within a multiresolution framework. We have carried out much of the detail work necessary to implement this generalization (cf. [12, 13]). We have also developed two distinct parametrizations of the “rank 2” wavelets, which prove useful in adaptive choice of a wavelet for engineering applications. In the continuous realm, we have investigated wavelet expansions of function spaces – characterizing those wavelets which yield orthonormal bases of $L^2(\mathbf{R})$ and describing the local behavior of wavelet functions, establishing connections with classical analysis.

In our investigations of the applications of wavelets to signal processing, we have had two major foci: image compression and computational algorithms. We have developed a wavelet-based still image compression system [56] with performance superior to that of traditional DCT-based algorithms. Gopinath and Burrus [8] have studied computation with the wavelet transform, and Gopinath, Burrus, and Lawton [11] have investigated the approximation of linear translation-invariant operators with the wavelet-Galerkin operator. Furthermore, we have investigated connections between the wavelet and Fourier transforms and described the characteristics of some fundamental signals in wavelet phase space.

We have applied wavelet based numerical methods to the solution of partial differential equations [6, 18, 19, 33, 34, 35, 54]. Specifically, we compare the Wavelet-Galerkin method to standard numerical methods for the numer-

¹here m is an integer greater than or equal to two.

ical solution of

- The Euler equations of a two-dimensional, incompressible fluid in a periodic domain.
- The Biharmonic Helmholtz equation and the Reduced Wave equation in nonseparable, two-dimensional geometry.
- The Euler and Navier-Stokes equations in nonseparable, two-dimensional geometry.

The wavelet methods have significant advantages with regard to stability, accuracy, and rate of convergence.

2 Mathematical Foundations

2.1 Higher Rank Wavelets

We have generalized the two-band wavelets of Daubechies and Mallat to the m -band (or *rank* m) case, yielding a large family of transforms which include block transforms such as the FFT, as well as overlapping generalizations of these $m \times m$ block transforms. Furthermore, these "higher rank wavelets" are well-suited to use in a multiresolution analysis tree. They have applications in a broad range of areas from image and audio compression to interference cancellation and transient detection.

A wavelet matrix is an $m \times mg$ matrix A with complex entries a_k^s satisfying

$$\sum_k a_k^s \bar{a}_{k+ml}^{s'} = m \delta^{s,s'} \delta_{l,0}, \quad \text{and} \quad (1)$$

$$\sum_k a_k^s = m \delta^{s,0}. \quad (2)$$

The first row a_k^0 of the wavelet matrix is called the lowpass row since it corresponds to a lowpass filter, and the other rows are the wavelet or highpass rows. The genus g is the number of $m \times m$ blocks which make up the wavelet matrix. The conditions (1)-(2) can be rephrased in the language of polyphase factorizations of filter banks; for details see [17].

The wavelet matrices of genus 1 play a special role; these $m \times m$ matrices are called Haar wavelet matrices; they include a wide range of block transforms such as the FFT, Discrete Cosine Transform, and Hadamard-Walsh

transform. Furthermore, each wavelet matrix (of arbitrary genus) has such a Haar matrix associated with it, by

$$H_A = (h_r^s), \quad h_r^s = \sum_l a_{r+lm}^s. \quad (3)$$

This Haar matrix determines the frequency partitioning properties of the corresponding wavelet filter bank.

Pollen [27] at Aware has carried out a parametrization of the rank 2 wavelets, describing a genus g wavelet by means of $g - 1$ angular parameters. We are currently working on the generalization of this result to arbitrary rank.

We have observed [17] that the orthogonality condition (1) implies that a wavelet system provides an orthonormal representation for discrete functions:

Theorem 2.1 *Given a signal $f(n)$ and an $m \times mg$ wavelet system a_k^s , then f has a unique wavelet expansion*

$$f(n) = \sum_{s=0}^{m-1} \sum_{l=-\infty}^{\infty} c_l^s a_{n+lm}^s$$

where

$$c_l^s = \frac{1}{m} \sum_n f(n) \bar{a}_{m l+n}^s.$$

Higher Rank Daubechies Wavelets

One of the first questions to arise in the theory of higher rank wavelets is "what is the generalization of Daubechies' regular compactly supported wavelets to the rank m setting?" Regularity is important because regular filters "pass through" polynomial information and because regular filters lead to regular (smooth) scaling functions. Given an m -band FIR wavelet filter (a_0, a_1, \dots, a_N) with frequency response

$$A(e^{i\omega}) = \sum_k a_k e^{ik\omega}$$

we say that the filter is *regular of order N* iff the frequency response A is flat (has a zero) of order $N + 1$ at the m -th roots of unity $\omega = 2\pi i/m$. There are numerous equivalent formulations of regularity; they are discussed

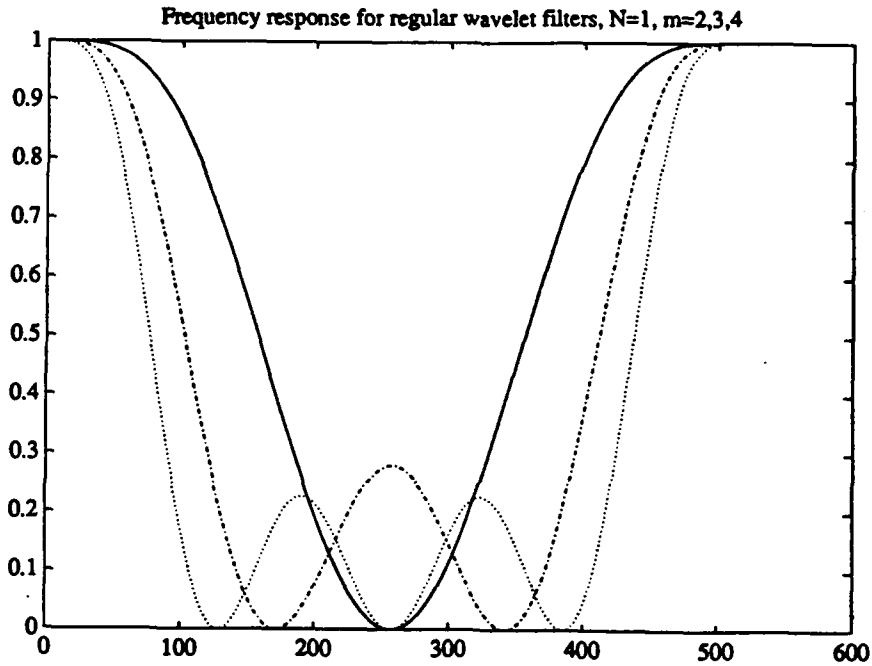


Figure 1: Frequency response for regular wavelet filters: $N = 1, m = 2, 3, 4$

in [13, 40]. We have constructed rank m wavelet lowpass filters with N -th order regularity and derived an explicit formula for the “scaling coefficients” (i.e. lowpass filter taps). The key is to begin with the Haar lowpass filter $h = (a_0 = 1, a_1 = 1, \dots, a_{m-1} = 1)$ and form

$$A(e^{i\omega}) = H^N(e^{i\omega})Q(e^{i\omega})$$

By examining the square modulus of A and enforcing the orthogonality condition (1), we find an explicit formula for $|Q(e^{i\omega})|^2$ and thus A ; the details appear in [13]. Figure 1 displays the frequency responses of the $N = 1$ regular wavelet filters for $m = 2, 3, 4$.

Having derived the rank m wavelet lowpass filter using the above construction, we are then able to construct a full rank m wavelet matrix, given the lowpass filter and the desired characteristic Haar matrix. This construction is described in [17] and [12]; it amounts to solving a set of $m + g - 1$ linear equations for a wavelet matrix of rank m and genus g . Furthermore, given a valid wavelet matrix with regularity of order N , we are able to construct rank m wavelet tight frames for $L^2(\mathbb{R})$. Specifically, the rank m scaling function is the solution of the equation

$$\varphi(x) = \sum_k a_k^0 \varphi(mx - k); \quad (4)$$

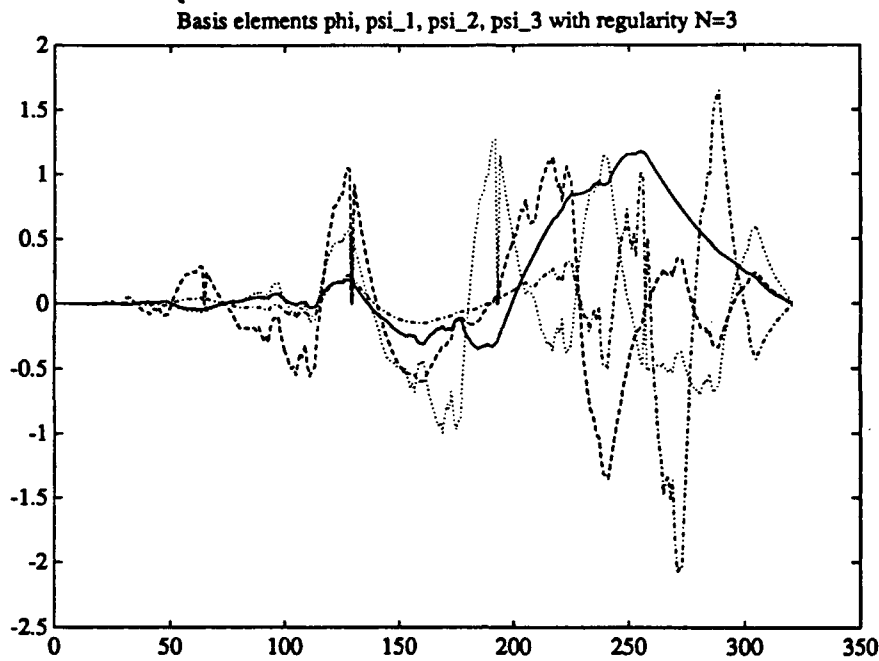


Figure 2: Basis elements $\varphi, \psi^1, \psi^2, \psi^3$ with regularity $N = 3$

if the scaling coefficient set has regularity of order N , then the resulting scaling function will have λN continuous derivatives, for some constant λ independent of N . We can then construct the $m - 1$ wavelet functions by

$$\psi^s(x) = \sum_k a_k^s \varphi(mx - k), \quad s = 1, 2, \dots, m - 1. \quad (5)$$

The collection of functions

$$\{m^{j/2} \psi^s(x/m^j)\}$$

form a tight frame and in most cases an orthonormal basis for $L^2(\mathbf{R})$; details are to be found in [14, 20]. Figure 2 shows the functions $\varphi, \psi^1, \psi^2, \psi^3$ for a rank 4 wavelet system with regularity order $N = 3$.

We have discovered [16] that when using a regular wavelet filter (of arbitrary rank and regularity order N), polynomials are *generalized eigenfunctions* for the wavelet transform. That is, a sequence $h(k)$ whose elements are a polynomial in k of degree less than or equal to N will emerge as a polynomial sequence of the same degree under the operation of convolution with a wavelet filter and decimation by a factor of m . This property characterizes regular wavelet lowpass filters, and should prove useful, for example in the detrending of signals with an underlying polynomial trend. When using a full wavelet filter bank, a purely polynomial input will produce nonzero outputs only for the lowpass filter.

We have also made significant steps [24] in the development of wavelet theory for dimensions greater than one. In this setting the *sampling sublattice* becomes paramount; in the classical one dimensional rank 2 case, the sampling sublattice is the even integers $2\mathbf{Z} \subset \mathbf{Z}$. While Mallat [25] introduced a separable wavelet theory in multiple dimensions (i.e., multidimensional wavelets as tensor products of one-dimensional wavelets), the fully general theory outlined in [24] permits the use of a nonseparable subsampling matrix M . Specifically, a general n -dimensional wavelet system is given by an n -dimensional lattice $\Lambda \subset \mathbf{R}^n$, a matrix M with integer entries and a set of coefficients a_λ satisfying:

- $M\Lambda \subseteq \Lambda$
- M is expansive (all eigenvalues strictly greater than one)
- $\sum_{\lambda \in \Lambda} a_\lambda^s \bar{a}_{\lambda+M\mu}^{s'} = \det M \delta^{s,s'} \delta_{\mu,0}$,
- $\sum_\lambda a_\lambda^s = \det M \delta^{s,0}$.

The scaling and wavelet functions will then be given by appropriate generalizations of the formulas (4) and (5). One can seek regular wavelets as we did above for the one dimensional rank m case; preliminary work on this problem is reported in [30]. Figure 3 displays a nonseparable two-dimensional wavelet (the "Novon" multiplier) with regularity order $N = 1$.

2.2 Parametrization of Wavelets

Parametrization of compactly supported wavelets is essential for effective choice of a wavelet basis in a particular application. We have arrived at two independent parametrizations of compactly supported wavelets, that of Pollen [27] cited earlier and one due to Wells [55]. We summarize Wells' parametrization of regular compactly supported wavelets here. Given a scaling coefficient set $\{a_k\}$ with frequency response $A(e^{i\omega})$, Daubechies describes the scaling coefficients with regularity of order N as those for which

$$A(e^{i\omega}) = (1 + e^{i\omega})^N Q(e^{i\omega}).$$

She solves for Q by changing variables to $y = \sin^2(\omega/2)$, examining

$$|A(e^{i\omega})|^2$$

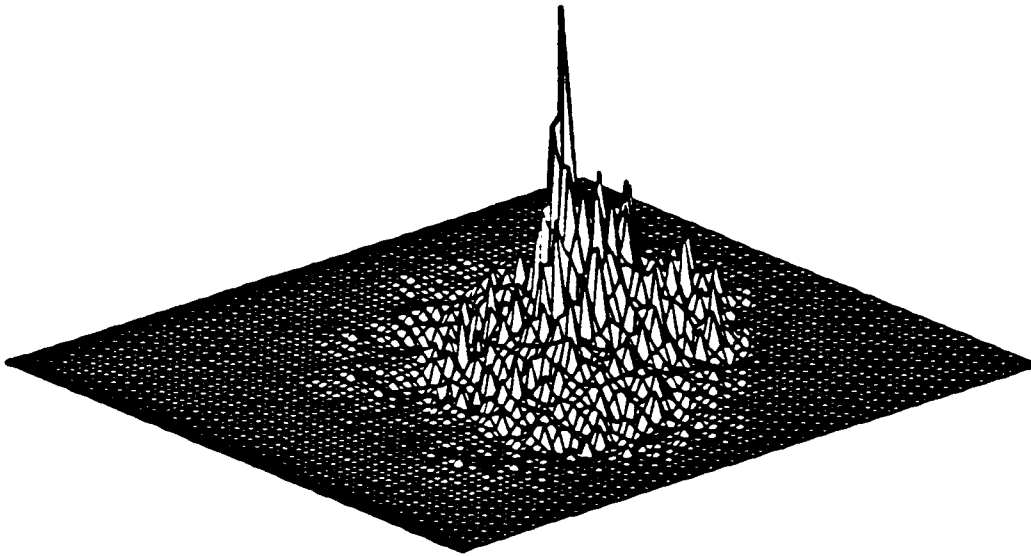


Figure 3: Novon scaling function with regularity order $N = 1$

and finding that

$$|Q(e^{i\omega})|^2 = \sum_{k=0}^{N-1} \binom{N-1+k}{N-1} y^k + y^N P(y), \quad (6)$$

subject to several constraints on the polynomial P . In particular,

$$P(1/2 - y) \quad \text{must be an odd polynomial} \quad (7)$$

and

$$\sum_{k=0}^{N-1} \binom{N-1+k}{N-1} y^k + y^N P(y) \geq 0. \quad (8)$$

Wells takes this description as a parametrization, called the *reduced moduli space*, of all wavelet scaling coefficients sets with regularity of order N . For each regularity order N and degree M of the polynomial P (i.e. M free parameters to the wavelet) he describes a polyhedron in parameter space, each point of which gives rise to a valid polynomial P satisfying (7) and (8). Furthermore, the vertices of the polyhedron lie on the boundary of the reduced moduli space, so that in some sense this polyhedron is maximal. The signal processor can then optimize over the parameter space for an additional desired trait (such as the stopband performance of the wavelet lowpass filter).

2.3 Wavelets and Classical Analysis

Wavelets and Weierstrass functions

Resnikoff [38] at Awaré has discovered a link between the compactly supported wavelets of Daubechies and Weierstrass' famous example of a nowhere differentiable continuous function. In particular, he has found that the scaling function φ can be expressed as an infinite series of *harmonics* of a Weierstrass function. Weierstrass' original example was the infinite series

$$\sum_{k=0}^{\infty} a^k \cos b^k \pi x ;$$

we generalize this to allow the parameter a to be an $n \times n$ matrix and define the *Weierstrass function with matrix parameter a* to be

$$W[a, b] := \sum_{k=0}^{\infty} a^k e^{2\pi i b^k x} . \quad (9)$$

We now break the scaling function φ of equation (4) into pieces defined on the unit interval $[0, 1]$:

$$\Phi_j(x) := \varphi(j + x) \chi_{[0,1]}(x) ; \quad (10)$$

here $\chi_{[0,1]}(x)$ denotes the characteristic function of the unit interval. Resnikoff [38] proves that the vector-valued function $\Phi(x) = \{\Phi_j(x)\}_{j=1}^N$ can be represented as a series of "Weierstrass harmonics":

$$\Phi(x) = C_0 + \sum_{q \text{ odd}} C_q W[T, 2](qx) \quad (11)$$

where the matrix

$$T := (T_{jk}) = \left(\frac{a_{2j-k} + a_{2j+1-k}}{2} \right)$$

is derived from the scaling coefficients a_k and the C_q can be determined from φ . Furthermore, Resnikoff has discovered that if the scaling function φ is regular of order N , (e.g. the wavelet moments vanish up through order N), then each of the functions Φ_j is a scalar multiple of the *Bernoulli polynomial* of degree j . A detailed discussion and proofs appear in Resnikoff [38].

Daubechies Scaling Function on $[0,3)$

Pollen [29] has used the first principles of analysis to investigate the scaling function φ_{D_4} associated with Daubechies 4-element scaling coefficient set "D4". He is able to prove the following results:

- φ_{D_4} takes its values in $\mathbb{Q}[\sqrt{3}]$.
- φ_{D_4} is continuous.
- φ_{D_4} is not right-differentiable at any dyadic integer ² in $[0, 3)$.
- φ_{D_4} is left-differentiable at every dyadic integer in $[0, 3)$.

2.4 Wavelet Frames and the Wavelet-Galerkin Operator

Lawton at Aware has investigated [20, 21, 22] the properties of rank 2 wavelet expansions of the function space $L^2(\mathbb{R})$. He has been able to prove that every compactly supported wavelet gives rise to a "tight frame" for $L^2(\mathbb{R})$, and he has also characterized the exceptional set of those wavelets which yield a tight frame but not an orthonormal basis. Lawton's approach keys on the wavelet-Galerkin operator, defined as follows:

Given a valid wavelet scaling sequence a , form the operator S_a on sequences in l^2 by

$$S_a(h)(k) = 2 \sum_m a_m \bar{a}_n h(2k + m - n). \quad (12)$$

The quadratic orthogonality condition (1) means that the Dirac sequence $\delta(k)$ is an eigenvector for S_a with eigenvalue 1. Denote by W the subset consisting of those scaling sequences for which S_a has more than one eigenvector with eigenvalue 1. Use V_N to denote the set of scaling sequences of length $2N$ and define $W_N = W \cap V_N$. In [20] Lawton proves the following

Theorem 2.2 *For $N \geq 1$, let $a \in V_N$, let φ and ψ be the scaling function and wavelet constructed from a , and let S_a be as above. Then the set of*

²A dyadic integer is a rational number x such that there exists $N_x \in \mathbb{Z}$ with $2^{N_x} x \in \mathbb{Z}$.

(normalized) dyadic scalings of integer translates of ψ forms a tight frame for $L^2(\mathbf{R})$, i.e. for any $g \in L^2(\mathbf{R})$,

$$g = \sum_{j,k} \langle \psi_{j,k} | g \rangle \psi_{j,k} .$$

Furthermore, for $N \geq 2$, W_N is a nonempty proper algebraic subset of V_N and the tight frame forms an orthonormal basis unless $a \in W_N$.

In [21], Lawton has been able to turn this result into a characterization of those wavelet bases which are orthonormal bases:

Theorem 2.3 *Let $a \in V_N$. Then the tight frame of wavelets constructed using a is not an orthonormal basis if and only if $a \in W_N$, i.e. iff S_a has 1 as an eigenvalue with multiplicity greater than 1.*

2.5 Future Directions

The theory of higher rank wavelets presented above provides a high-level, unified framework encompassing many of the transforms used in signal processing today. Promising research directions exist in this area: parametrization of the family of higher rank wavelets, the theory of biorthogonal rank m wavelets (the rank 2 theory was introduced in [1]), and the application of higher rank wavelet transforms to specific application areas, such as image processing and sonar transient detection.

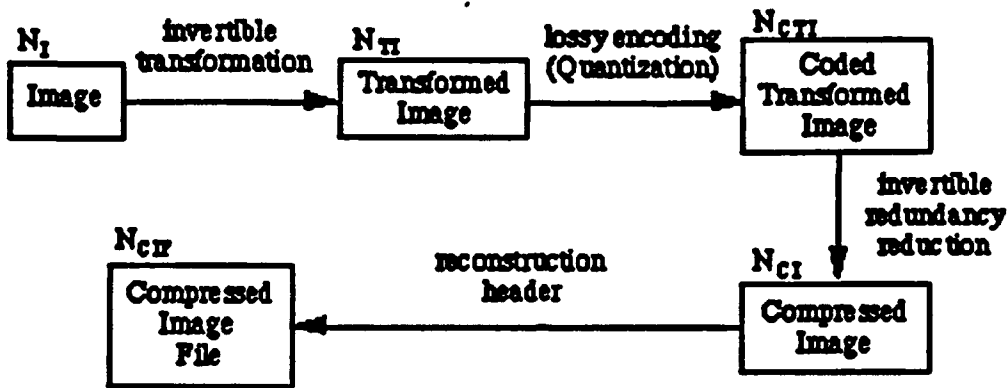


Figure 4: Aware's wavelet-based image compression system

3 Signal Processing

3.1 Image Processing

In the course of its work on the contract, Aware has developed a state-of-the-art wavelet-based still image compression system. We outline the design of the system and its performance below; greater detail appears in [56] and [37].

Our system for (lossy) compression of images is built of three components: a (wavelet) transform, a (lossy) quantizer, and a (lossless) encoder, depicted in Figure 4.

The transform is a rank 2 wavelet transform, which operates on a discrete data stream by convolution and decimation. In particular, we have two filters, a lowpass filter $\{a_k\}$ and a highpass filter $\{b_k\}$ with

$$b_k = (-1)^k a_{N-k}$$

and from a one-dimensional input signal $f(n)$ we obtain the two outputs

$$Lf(n) = (f * a)(2n) \quad (13)$$

and

$$Hf(n) = (f * b)(2n). \quad (14)$$

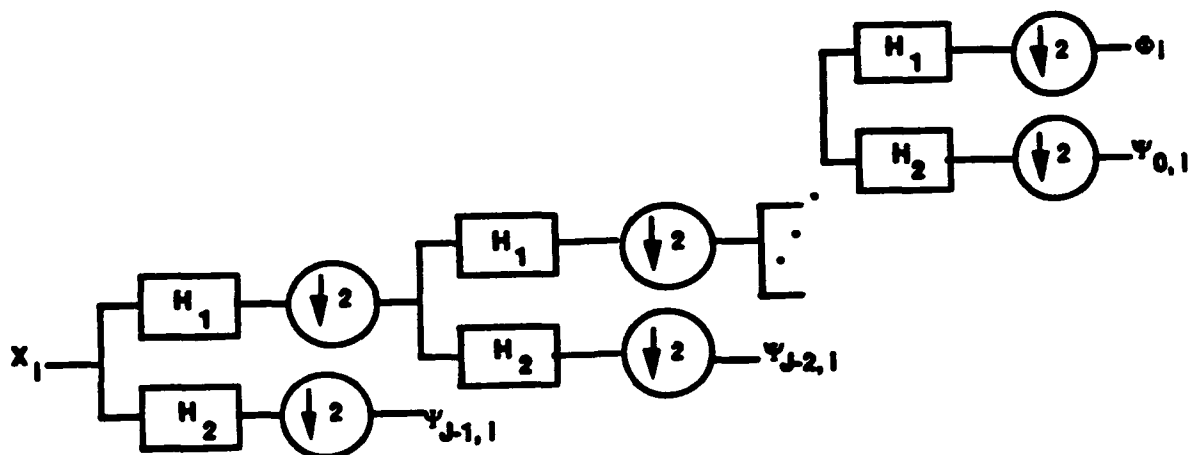


Figure 5: Mallat decomposition

In order to apply this one-dimensional transform to a two-dimensional array of pixels I representing an image, we apply the 1-d transform first in the x direction to produce two output images $L_x I$ and $H_x I$, and then apply the 1-d transform in the y direction to these to obtain 4 output images, $L_x L_y I$, $L_x H_y I$, $H_x L_y I$, $H_x H_y I$. We then *iterate* this procedure on the subimage $L_x L_y I$ in a Mallat tree structure.³ This iterative decomposition of an image is depicted in Figure 5. Observe that because of the critical decimation, the output of the transform has exactly as many data points as the input.

The next step is to *quantize* the values of the transform coefficients; we experimented with a number of scalar and vector quantizers, and ultimately found the most effective method to be a uniform scalar quantizer with different binwidths for the different output bands. One reason for this is that the high-frequency components (such as the $H_x H_y I$ output) are concentrated around edges, and image intensities at edge discontinuities are known to be approximately Laplacian-distributed. We can incorporate these Laplacian distributions into computations for a uniform scalar quantizer rather easily, as described in [7].

Once the transform coefficients have been quantized, we further exploit

³We have investigated alternative methods of iterating the transform, e.g. further decomposing the $L_x H_y I$ term in x ; details are presented in [37].

redundancies in the data by lossless encoding, such as Huffman coding or an adaptive coder such as the Q-coder developed at IBM [32]. We have obtained our best results with the (nonadaptive) Huffman coder.

Upon implementing this wavelet image compression system, we have found it to exhibit several advantages over Fourier-based methods. First, since we used compactly supported wavelet filters (cf. [2]), edges contribute to a small number of transform coefficients. This greatly reduces the “ringing” associated with Fourier methods, where a discontinuity has a broadband spectrum, and quantization can produce artifacts across the support of the Fourier components. Fourier methods such as the DCT require that the image be broken into subblocks (usually 8×8 or 16×16), both to bound the $O(N \log N)$ complexity and to limit the ringing just described. This produces quilt-like artifacts once the transform coefficients are quantized, as different subblocks end up with different total intensities. A significant advantage provided by our system is that no subblocking of the image is necessary (the wavelet transform has $O(N)$ complexity), and these blocking artifacts are eliminated. Finally, the local nature of the computations (13) and (14) enables efficient hardware layouts for wavelet transform computations.

3.2 Signal Detection and Classification

Workers at Aware have investigated numerous areas of signal processing with wavelets, including an analysis of wavelet transform computations [8], a study of wavelets and linear translation-invariant operators [11], an analysis of the effect of multirate filtering on convolution [15], discovery of new relationships between the wavelet and Fourier transforms [39], and an investigation of wavelet phase space [36].

Gopinath and Burrus [8] have developed efficient means of computing the continuous wavelet transform for an arbitrary wavelet by using the discrete wavelet transform as an intermediary. Define the continuous wavelet transform of a function f with respect to a wavelet w by

$$W_w f(s, \tau) = \int_{\mathbf{R}} f(t) 2^{s/2} w(2^s t - \tau) dt$$

and write the coefficients of the discrete wavelet transform of a function g with respect to the wavelet ψ (as in (22)) as

$$W_\psi g(j, k) .$$

Then Gopinath and Burrus find that

$$\mathcal{W}_w f(s, \tau) = \sum_{j', k', j, k} W_\psi f(j', k') W_\psi w(j, k) W_\psi \psi(s + j - j', 2^{u+j-j'} k + u^j \tau + k'). \quad (15)$$

In other words, a general continuous wavelet transform may be computed as a double summation of the *discrete* wavelet transform of f and w against a kernel which is the continuous wavelet transform of the wavelet ψ with itself. Notice that the kernel can be precomputed once (as may be the DWT of the wavelet w , once it is known), and so the continuous wavelet transform computation is reduced to a discrete wavelet transform computation, which may be done efficiently by lattice methods such as in [47].

Linear translation-invariant operators (such as differentiation) can be well-represented by the wavelet-Galerkin method; this is developed in Gopinath, Lawton, and Burrus [11]. Consider a linear translation-invariant operator T (e.g. $T = d^p/dx^p$); it can be represented as convolution with a kernel $t(x)$. In the case of the Galerkin method we approximate the operator T defined on $L^2(\mathbb{R})$ by an operator T_d which is the projection of T onto a subspace $V_{\Delta x}$ associated with a meshsize Δx : $T_d = P_{\Delta x} T P_{\Delta x}$ where $P_{\Delta x}$ is the projection onto $V_{\Delta x} = \text{Span} \{ \sqrt{1/\Delta x} \varphi(x/\Delta x - k) \}$. Thus we obtain an expansion

$$P_{\Delta x} f = \sum_k f_{\Delta x, k} \varphi_{\Delta x, k}$$

and

$$g_{\Delta x, k} = f_{\Delta x, k} * t_{\Delta x} \quad (16)$$

where

$$t_{\Delta x, k} = \langle \varphi_{\Delta x, 0}, T \varphi_{\Delta x, k} \rangle.$$

Thus the wavelet-Galerkin discretization of T acts as a discrete convolution on the expansion coefficients of f_d . It is proved in [11] that

- If a function f can be well-approximated locally by polynomials of degree less than or equal to n , then the action of the operator T is well-approximated by convolution of the *samples* of f with the kernel t_k that acts on the expansion coefficients.
- If the wavelets being used in this approximation procedure have moments vanishing to order M , then differentiation of order $p \leq 2m$ is well approximated by the wavelet-Galerkin discretization

Heller [15] has investigated the effect of multirate filtering (convolution followed by decimation) upon linear convolution. As the core operation of linear time-invariant systems, convolution is perhaps the most significant operation of signal processing. The Fourier transform is important precisely because it *diagonalizes* convolution, and yet in doing so it loses all time-domain information. Multirate filter banks provide both time and frequency information in their output, yet lose the precision of the Fourier transform in dealing with convolution. Heller's work in [15] is a first step in understanding the effect of convolution and decimation on linearly convolved inputs.

Resnikoff and Burrus [39] have discovered a set of formulae relating the Fourier expansion of a periodic signal with its wavelet expansion. Suppose that $g(t)$ is a periodic function on the real line (i.e. $g(t) = g(t + 1)$) whose Fourier expansion is

$$g(t) = \sum_{n=-\infty}^{\infty} b(n)e^{2\pi int}$$

with coefficients

$$b(n) = \int_0^1 g(t)e^{-2\pi int} dt ,$$

Analogously, the wavelet expansion of g is

$$g(t) = \sum_{l=-\infty}^{\infty} c(l)\varphi_l(t) + \sum_{j=0}^{\infty} \sum_{k=-\infty}^{\infty} d(j,k)\psi_{j,k}(t) \quad (17)$$

where

$$\psi_{j,k}(t) = 2^{j/2}\psi(2^j t - k)$$

and the family $\{\varphi_l, \psi_{j,k}\}$ form an orthonormal basis for $L^2(\mathbf{R})$ as described in [21].

Resnikoff and Burrus use the properties of the scaling function φ and wavelet ψ in combination with the periodicity of g to derive the facts that

$$c(l) = c(0) = c \text{ for all } l .$$

They then express the Fourier coefficients $b(n)$ in terms of the wavelet coefficients and the Fourier transform of the wavelet ψ :

$$b(n) = \begin{cases} c & \text{if } n = 0 \\ \sum_{j=0}^{\infty} \sum_{k=0}^{2^j-1} d(j,k)\hat{\psi}_{j,k}(n) & \text{if } n \neq 0 \end{cases} \quad (18)$$

Conversely, they find that the wavelet coefficients of g in terms of the Fourier coefficients:

$$d(j, k) = \sum_{-\infty}^{\infty} b(n) \hat{\psi}_{j,k}(-n), \text{ and} \quad (19)$$

$$c(l) = c = b(0). \quad (20)$$

Resnikoff [36] has developed and investigated the notion of wavelet phase space – the space of wavelet coefficients which provides a time-frequency picture of a function. In particular, suppose we are given a rank 2 wavelet system $\{a_k\}$ and the associated scaling function φ and wavelet ψ , so that an L^2 function $f(x)$ has the expansion

$$f(x) = \sum_{l \in \mathbf{Z}} c_l \varphi_l(x) + \sum_{j \in \mathbf{Z}_+} \sum_{k \in \mathbf{Z}} c_{jk} \psi_{jk}(x). \quad (21)$$

Alternatively, we can omit the scaling function part and use the full wavelet expansion

$$f(x) = \sum_{j \in \mathbf{Z}} \sum_{k \in \mathbf{Z}} c_{jk} \psi_{jk}(x). \quad (22)$$

Whereas a Fourier transform analyzes a signal in terms of its frequencies, a wavelet transform breaks the information content of a signal into *scale* and *time* components. The index j determines the scale while the index k represents time (or spatial) translation within that scale. The collection of wavelets $\{\psi_{jk}\}_{j \text{ fixed}}$ form an orthonormal basis for the information (or detail) at scale j ; The detail over all scales j with $j \leq 0$ is amalgamated into the set of scaling functions $\varphi_l(x) = \varphi(x - l)$ in the expansion (21).

We can now *plot* the magnitudes of the coefficients c_{jk} , with the x axis as the k or time index and the y axis as the j or scale index, providing a time-scale representation of the energy in the signal f . Several examples are worked out in detail in [36]; we describe one of them, the Dirac delta function, here.

The Dirac distribution has the full wavelet expansion

$$\delta(x) = \sum_{j \in \mathbf{Z}} \sum_{k \in \mathbf{Z}} 2^{j/2} \psi(-k) \psi_{jk}(x);$$

the magnitudes of these coefficients for a fixed basis $\{\psi_{jk}\}$ are shown in figure 6. The magnitudes of the coefficients grow exponentially with j even as the

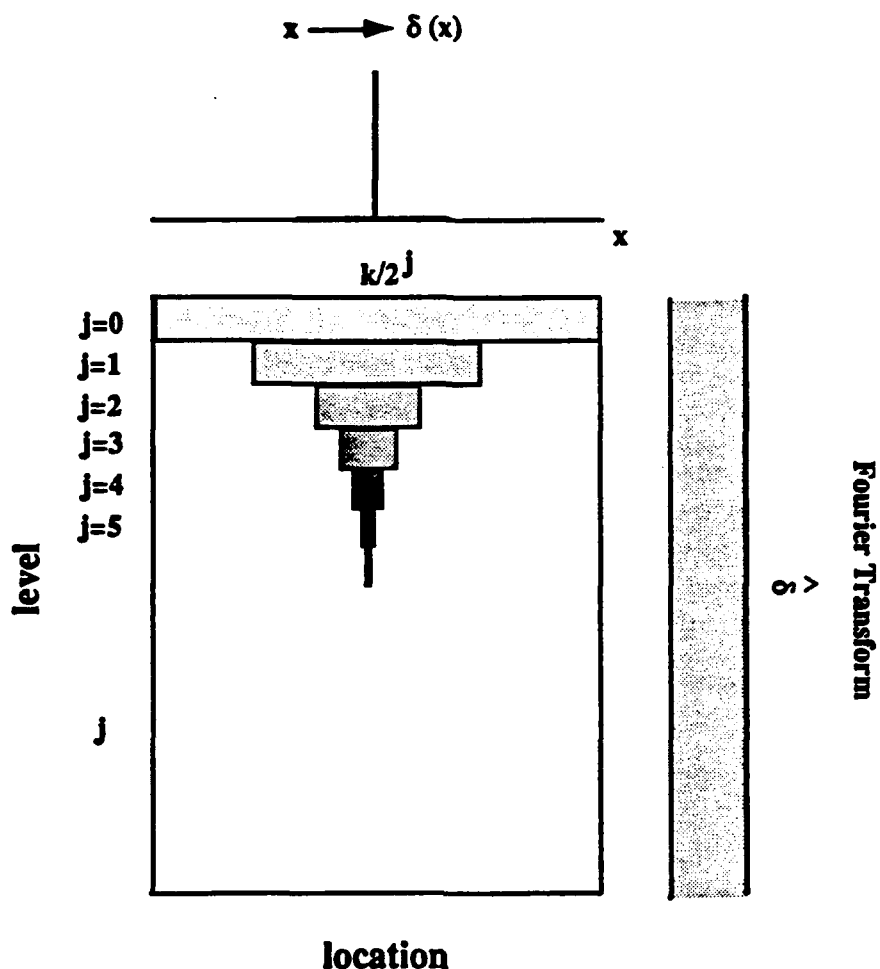


Figure 6: Wavelet phase space plot of the Dirac distribution

support width in k is shrinking. A finite approximation of the graph of the Dirac distribution is shown above the phase space plot, while a plot of the magnitude of the Dirac's Fourier transform is shown at the right. Notice that the wavelet phase space representation accurately describes the location of the Dirac, which the Fourier representation is unable to do.

4 Wavelets and the Numerical Solution of Partial Differential Equations

We have applied wavelet based numerical methods to the solution of partial differential equations [6, 18, 19, 33, 34, 35, 54]. Specifically, we compare the Wavelet-Galerkin method to standard numerical methods for the numerical solution of

- The Euler equations of a two-dimensional, incompressible fluid in a periodic domain.
- The Biharmonic Helmholtz equation and the Reduced Wave equation in nonseparable, two-dimensional geometry.
- The Euler and Navier-Stokes equations in nonseparable, two-dimensional geometry.

The wavelet methods have significant advantages with regard to stability, accuracy, and rate of convergence.

We numerically resolve the two-dimensional Euler equations and study the phenomena of two-dimensional turbulence. The compactly supported wavelets of Daubechies provide an orthogonal basis for the square integrable functions on the line or circle. These have several advantages for the numerical approximation of solutions of differential equations, including exact representation of polynomials of certain degrees and compact-support. For nonlinear systems (Euler equations) with solutions that may develop sharp gradients the primary advantage seems to be that wavelets can accurately approximate the smooth component to a solution while correctly resolving the components associated with strong gradients [54]. The reason for this is that wavelets are less smooth than their order of approximation and therefore are less *stiff* than other higher order methods, i.e. Fourier or spline bases. For instance, the six term Daubechies scaling function (D6) can exactly represent polynomials through the second degree. However, the actual scaling function has only a continuous 1.06 derivative.

We apply the Daubechies scaling function (translates of) with the standard Galerkin technique to define the wavelet-Galerkin method. We find it possible, with appropriate implicit time differencing, to develop numerical methods for the inviscid Euler equations. We also develop solutions that use implicit time differencing and the standard hyperviscosity.

For the inviscid calculations the numerical solutions develop a locally oscillatory structure. However, a simple three term smoothing removes the oscillations and produces a smooth approximation. The hyperviscosity regularized solutions are already smooth. We compare the results of these calculations by integrating over very long times. The similarities and differences suggest several interesting consequences for two-dimensional turbulence [54, 35].

Basically, the inviscid calculations over a long time preserve certain hyperbolic structures that are not preserved by the regularized calculations, and seem to better capture the limiting inviscid behavior.

We have presented a series of numerical experiments that illustrate several phenomena of possible relevance to two-dimensional turbulence and its' numerical resolution [54].

We use compactly supported wavelets as a Galerkin basis and develop a wavelet-Capacitance Matrix method to handle boundary geometry. We have developed an extension of the standard Capacitance matrix method that greatly reduces the numerical residual errors [33, 34]. In contrast with the standard method, our method shows fast, even spectral, convergence at relatively coarse levels of discretization. Furthermore, for comparable levels of discretization the rates of convergence appear to be independent of the geometry. For several geometries we have made a detailed comparison of methods, examining accuracy and rates of convergence. We have also developed Least-Square versions of our algorithm for the Helmholtz equation in nonseparable geometries and examined the accuracy and convergence of these methods.

In summary, our numerical study of the Helmholtz equation shows that:

- the Wavelet-Galerkin/Capacitance Matrix method (The Wavelet-Capacitance Matrix Method) is stable and *spectrally* accurate. These results apply to general nonseparable domains and all ranges of the parameters.
- The Wavelet algorithm is found to obtain accurate results for problems where, for instance, finite difference methods do not converge, or converge slowly, and where Fourier Spectral methods do not apply.
- For a fixed level of discretization, increasing the order of the wavelet basis spectrally decreases the error.
- The rates of convergence in sup norm appear to depend on the wavelet basis, DN , and discretization, δx , as $(\delta x)^{N-5}$.
- The rates of convergence in sup norm appear to be independent of the domain shape.

- Least-Square versions of the wavelet algorithm can preserve accuracy and decrease the computation by more than a factor of four. The finite difference algorithms would not allow effective least-squares implementations.

Furthermore,

- All errors (accuracy and convergence) are measured in the pointwise sup norm.
- Our implementation is fast, since it is based on fast (FFT) evaluations for periodic geometry adapted to nonseparable geometry.
- The basic algorithm applies to one, two and three space dimensions, without essential modification.
- For the Euler and Navier-Stokes equations fast wavelet algorithms have been developed for flow in nonseparable domains.

5 Channel Coding

Tzannes and others at Aware [42, 43] have developed innovative applications of wavelets to error correcting codes in communications channels. In particular, the wavelet channel coding algorithm presented in [42] provides error correction in additive white Gaussian noise burst noise and flat fading channels. We have carried out simulations which verify these performance gains.

References

- [1] A. Cohen, I. Daubechies, and J.-C. Feauveau, "Biorthogonal bases of compactly supported wavelets," AT&T Bell Laboratories, preprint, 1991.
- [2] I. Daubechies, "Orthonormal bases of compactly supported wavelets," *Comm. Pure Appl. Math.*, vol. 41, pp. 909-996, 1988.
- [3] I. Daubechies and J. Lagarias, "Two-scale difference equations I: existence and global regularity of solutions," *SIAM J. Math. Anal.*, vol. 22, pp. 1388-1410, 1991.
- [4] I. Daubechies and J. Lagarias, "Two-scale difference equations II: local regularity, infinite products of matrices and fractals," AT&T Bell Laboratories, preprint, 1989.
- [5] Z. Doganata, P. P. Vaidyanathan, T. Nguyen, "General Synthesis Procedures for FIR Lossless Transfer Matrices, for Perfect-Reconstruction Multirate Filter Bank Applications", *IEEE Trans. Acoust., Speech, and Signal Processing*, vol. 36, pp. 1561-1574, October 1988.
- [6] R. Glowinski, W. Lawton, M. Ravachol and E. Tenenbaum, *Wavelet Solution of Linear and Nonlinear Elliptic, Parabolic and Hyperbolic Problems in One Space Dimension*, in Proceedings of the 9th International Conference on Numerical Methods in Applied Sciences and Engineering SIAM, Philadelphia (1990)
- [7] R. A. Gopinath, "Rate vs. Distortion," Aware Technical Report AD8901004.
- [8] R. A. Gopinath and C. S. Burrus, "Efficient Computation of the wavelet transform," *Proc. IEEE ICASSP '90*, Albuquerque, NM, 1990.
- [9] R. A. Gopinath and C. S. Burrus, "Wavelet transforms and filter banks," pp. 603-654 in *Wavelets: A Tutorial in Theory and Applications*, C. K. Chui, ed., Academic Press, 1992.

- [10] R. A. Gopinath and C. S. Burrus, "State space approach to multiplicity M orthonormal wavelet bases," CML Report TR 91-22, Rice University E & CE Dept., 1992.
- [11] R. A. Gopinath, W. M. Lawton, and C. S. Burrus, "Wavelet-Galerkin approximation of linear translation-invariant operators," *Proc. IEEE I-CASSP '90*, Toronto, 1990.
- [12] P. N. Heller, "A Construction of Higher Multiplier Wavelet Matrices," Aware Technical Report AD910824, Cambridge, MA, 1991.
- [13] P. N. Heller, "Higher rank Daubechies wavelets - preliminary report," Aware Technical Report AD911204, Cambridge, MA, 1991.
- [14] P. N. Heller, "Regular M -band wavelets," Aware Technical Report AD920608, Cambridge, MA, 1992.
- [15] P. N. Heller, "Quarterly Tech Report #8, DARPA Wavelet Contract," Aware, Inc., March 1992.
- [16] P. N. Heller and H. L. Resnikoff, "Polynomials are generalized eigenfunctions of the wavelet transform," Aware Technical Report AD910908, Cambridge, MA, 1991.
- [17] P. N. Heller, H. L. Resnikoff, and R. O. Wells, Jr., "Wavelet matrices and the representation of discrete functions," pp. 15-50 in *Wavelets: A Tutorial in Theory and Applications*, C. K. Chui, ed., Academic Press, 1992.
- [18] A. Latto, H. L. Resnikoff and E. Tenenbaum, *The evaluation of connection coefficients of compactly supported wavelets*, Aware Technical Report AD910708 (July 1991) and the Proceedings of the French - US-A Workshop on *Wavelets and Turbulence*, Princeton University, June 1991, Editor, Y. Maday, Springer - Verlag (1992).
- [19] A. Latto and E. Tenenbaum, *Les ondelettes à support compact et la solution numérique de l'équation de Burgers*, *C. R. Acad. Sci. Paris 311* pp 903-909 (1990).

- [20] W. M. Lawton, "Tight frames of compactly supported affine wavelets," *J. Math. Physics*, vol. 31, pp. 1898-1901, 1990.
- [21] W. M. Lawton, "Necessary and sufficient conditions for constructing orthonormal wavelet bases," *J. Math. Physics*, vol. 32, pp. 57-61, 1991.
- [22] W. M. Lawton, "Multiresolution properties of the wavelet-Galerkin operator," *J. Math. Physics*, vol 32, pp XX-YY, 1991.
- [23] W. M. Lawton, "Wavelet discretization methods for surface reconstruction," Proc. SPIE 1990.
- [24] W. M. Lawton and H. L. Resnikoff, "Multidimensional wavelet bases," Aware Technical Report, Aware, Inc., Cambridge, MA 1991.
- [25] S. G. Mallat, "A Theory for multiresolution signal decomposition: the wavelet representation," *IEEE Trans. Pattern Analysis and Machine Intelligence*, vol. 11, pp. 674-693, 1989.
- [26] D. Pollen, " $SU_I(2, F[z, 1/z])$ for F a subfield of C ," *J. Am. Math. Soc.*, vol. 3, no. 3, July 1990.
- [27] D. Pollen, "Parametrization of Compactly Supported Wavelets," Aware Technical Report AD890000, Aware, Inc., Cambridge, MA, 1989.
- [28] D. Pollen, "Linear One-Dimensional Scaling Functions," Aware Technical Report AD900101.
- [29] D. Pollen, "Daubechies Scaling Function on $[0, 3)$ ", in in *Wavelets: A Tutorial in Theory and Applications*, C. K. Chui, ed., Academic Press, 1992.
- [30] D. Pollen and D. Linden, "Real quadratic two-dimensional scaling coefficients," Aware Technical Report AD900212, 1990.
- [31] G. Polya and G. Szegő, *Problems and Theorems of Analysis*, Springer, New York, 1972.
- [32] D. A. Pennebaker, W. W. Shurtleff, et. al. "Q Coder", *IBM J. Res. and Development*, 1989.

- [33] S. Qian and J. Weiss, *Wavelets and the Numerical Solution of Boundary Value Problems*, *Applied Mathematics Letters*, accepted for publication (1992).
- [34] S. Qian and J. Weiss, *Wavelets and the Numerical Solution of Partial Differential Equations*, *Journal of Computational Physics*, accepted for publication (1992).
- [35] S. Qian, H. Resnikoff, J. Weiss and W. Lawton, *Wavelets, Turbulence and Boundary Value Problems for Partial Differential Equations*, Aware Technical Report AD921005, to appear in *Wavelets: Mathematics and Applications*, J. Benedetto and M. frazier, Eds. CRC Press, (1993).
- [36] H. L. Resnikoff, "Phase Space Representation for Compactly Supported Wavelet Transforms," Aware Technical Report AD900407.
- [37] H. L. Resnikoff, "Wavelet-based image compression", Aware Technical Report AD900212.
- [38] H. L. Resnikoff, "Weierstrass functions and compactly supported wavelets," Aware Technical Report AD900810, Cambridge, MA, 1990.
- [39] H. L. Resnikoff and C. S. Burrus, "Relationships Between the Fourier transform and the wavelet transform," , *Proc. SPIE*, v. 1348, pp 291-300.
- [40] G. Strang, "Wavelets and dilation equations: a brief introduction," *SIAM Review*, vol. 31, pp. 614-627, 1989.
- [41] G. Strang and G. Fix, "A Fourier analysis of the finite element variational method," *CIME Constructive Aspects of Functional Analysis*, pp. 793-840, Rome, Edizioni Cremonese, 1973.
- [42] M.A. Tzannes and M.C. Tzannes, "Bit-by-bit Channel Coding Using Wavelets," Aware Technical Report AD920629, Aware, Inc., Cambridge, MA, 1992.
- [43] M.A. Tzannes and M.C. Tzannes, "Block Biorthogonal Channel Coding Using Wavelets," Aware Technical Report AD920622, Aware, Inc., Cambridge, MA, 1992.

- [44] P. P. Vaidyanathan, "Quadrature mirror filter banks, M -band extensions and perfect-reconstruction techniques," *IEEE ASSP Mag.*, vol. 4, pp. 4-20, July 1987.
- [45] P. P. Vaidyanathan, "Multirate digital filters, filter banks, polyphase networks, and applications: a tutorial," *Proc. IEEE*, vol. 78, pp. 56-93, January 1990.
- [46] P. P. Vaidyanathan, *Multirate Systems and Filter Banks*, Englewood Cliffs, NJ, Prentice Hall, to appear 1992.
- [47] P. P. Vaidyanathan, Hoang, "Lattice Structures for optimal design and robust implementation of two-channel perfect reconstruction QMF banks," *IEEE Trans. on ASSP*, vol 36, pp. 81-93, January 1988.
- [48] P. P. Vaidyanathan, T. Nguyen, Z. Doganata, and T. Saramaki, "Improved Technique for Design of Perfect Reconstruction FIR QMF Banks with Lossless Polyphase Matrices", *IEEE Trans. Acoust., Speech, and Signal Processing*, vol. 37, pp. 1042-1056, July 1989.
- [49] M. Vetterli, "A theory of multirate filter banks," *IEEE Trans. Acoust., Speech, Signal Processing*, vol. 35, pp. 356-372 March 1987.
- [50] M. Vetterli, "Wavelets and filter banks for discrete-time signal processing," pp. 17-52 in *Wavelets and their applications*, M. B. Ruskai, ed., Jones and Bartlett, Boston 1992.
- [51] M. Vetterli and C. Herley, "Wavelets and filter banks: theory and design," to appear, *IEEE Trans. Signal Processing* Sept. 1992.
- [52] M. Vetterli and D. LeGall, "Perfect reconstruction FIR filter banks: some properties and factorizations," *IEEE Trans. Acoust., Speech, Signal Processing* vol. 37, pp. 1057-1071, July 1989.
- [53] M. Vetterli and O. Rioul, "Wavelets and Signal Processing," *IEEE ASSP Mag.*, October 1991.
- [54] J. Weiss, *Wavelets and the Study of Two Dimensional Turbulence*, in the Proceedings of the French-USA Workshop on *Wavelets and Turbulence*, Princeton University, June 1991. Y. Maday, Ed., Springer-Verlag, NY, (1992).

- [55] R. O. Wells, Jr., "Parametrizing smooth compactly supported wavelets," submitted to *Trans. Amer. Math. Soc.*, 1991.
- [56] W. R. Zettler, J. Huffman, and D. Linden, "The application of compactly supported wavelets to image compression," *Proc. SPIE*, vol. 1244, pp. 150-160, 1990.
- [57] H. Zou and A. H. Tewfik, "A Theory of M -band orthogonal wavelets," submitted to *IEEE Trans. Circuits and Systems*, 1992.

6 Appendices

6.1 About Aware, Inc.

Aware, Inc. is a mathematical engineering company that designs and sells software and chipset products for bandwidth management. Aware's products organize and compress signals such as images and video, audio and speech, for storage and communications applications. Based on the powerful new wavelet mathematics, which provides superior signal representation and hierarchical data structures, Aware accomplishes this by compressing the amount of computation and storage needed to represent the signal, and managing the compressed data stream to create breakthrough products for satellite communications, teleconferencing, video editing and distribution, computer multimedia systems, mobile radios, cellular telephones, and secure communications.

The Changing Communications Environment

A revolution in information processing has been made possible by new telecommunications and computing technology. Digital formats enable computer generated pictures and sound, and conventionally generated photographs, video, audio and speech communications to be modified by computer editing and to interchangeably share the same storage media and communications channels. The boundaries between markets that were once distinct and independent are blurring, and product lines are overlapping. Companies are evolving new types of organization and skills to respond to the new communication synthesis.

Bandwidth Management

The common denominator of digital computing and digital telecommunications is bandwidth. Bandwidth is the measure of how much information can be transmitted or stored by an information system. It is the fundamental scarce resource whose value is reflected in technology trends and product pricing. The need for more communications, more information storage, and more computing resources in business and consumer products is pressing against bandwidth scarcity. Bandwidth management is the key tool for enabling new products, and for achieving higher productivity and profits

from existing systems.

Bandwidth can be increased by using more expensive technology: supercomputers, large disk drives, higher frequency communications carrier signals. Each of these methods increases the amount of usable bandwidth. Or, the available bandwidth can be used more efficiently by compressing the source information.

Compression reduces the amount of bandwidth required to do the task. Compression doesn't depend on the technology of computers or storage media or communications equipment: it just reorganizes the information that the customer uses in a much more efficient way.

6.2 Government contracts related to this contract

During the period of this contract, other DoD contracts that depend on it were awarded to Aware. They include:

- Spread Spectrum: Subcontract to Atlantic Aerospace Electronics Corp., based on Aware's wavelet channel coding technology (Contract No. AAEC-1214.046-91-001).
- ONR Wavelet Transform Chip: Design and fabricate a wavelet transform processor chip to demonstrate VLSI wavelet technology (Contract No. N00014-90-C-0167).
- ONR Partial Differential Equations Research: (Contract No. N00014-91-C-0086).

6.3 Aware reports and presentations supported in part by this contract

6.3.1 Reports and publications supported in part by this contract

The following is a list of technical reports whose preparation was supported in part by this contract.

- R. Glowinski, "Note on a Multiplier-Fictitious Domain Method for the Numerical Solution of the Dirichlet Problem," Aware Technical Report (1990)

- R. Glowinski, W. Lawton, M. Ravachol and E. Tenenbaum, "Wavelet Solution of Linear and Nonlinear Elliptic, Parabolic and Hyperpolic Problems in One Space Dimension." in Proceedings of the *9th International Conference on Numerical Methods in Applied Sciences and Engineering* SIAM, Philadelphia (1990)
- Heller, P. N. "Higher multiplier Daubechies wavelets," Aware Technical Report AD910614 (1991).
- Heller, P. N. "A construction of higher multiplier wavelet matrices", Aware Technical Report AD910728 (1991).
- Heller, P. N. "Polynomials are generalized eigenfunctions of the wavelet transform," Aware Technical Report AD910912 (1991).
- Heller, P. N. "Polynomials are generalized eigenfunctions of the wavelet transform," Aware Technical Report AD910912 (1991).
- Heller, P. N., Resnikoff, H. L., and Wells, R. O. Jr., "Wavelet matrices and the representation of discrete functions", to appear in *Wavelets: a tutorial*, C.K. Chui, ed., Academic Press, 1991.
- Heller, P. and Resnikoff, H. L., "Polynomials are generalized Eigenfunctions of the wavelet transform," Aware Technical Report AD910912.
- Heller, P., "Higher rank Daubechies wavelets - Preliminary report," Aware Technical Report AD911204.
- Huffman, J. C., Zettler, W. and Linden, D. C. P., "Applications of compactly supported wavelets to image compression," *Proc. SPIE*, vol. 1244, pp. 150-160, (1990).
- Jagler, K. B. and Morrell, W., "The application of multiresolution wavelet techniques to interference cancellation problems", Report to MRJ (1991).
- Lawton, W., "Tight frames of compactly supported affine wavelets", Aware Technical Report AD891012.

- Latto, A. and Tenenbaum, E., "Compactly supported wavelets and the numerical solution of Burgers' equation," *C. R. Acad. Sci. France, Série I*, pp. 903-909 (1990).
- Lawton, W., "Necessary and sufficient conditions for constructing orthonormal wavelet bases," *J. Mathematical Physics*, vol. 32, pp. 57-61 (1991).
- Lawton, W., "Tight frames of compactly supported affine wavelets", Aware Technical Report AD891012, (1989).
- Lawton, W. and Resnikoff, H. L., "Multidimensional wavelet bases," Aware, Inc., Technical Report No. AD910130 (1991).
- Pollen, D., " $SU_1(2, F[z, \frac{1}{z}])$ for F a subfield of C ," *J. of the Amer. Math. Soc.*, vol. 3, pp. 611-624, (1990).
- Pollen, D., "Parametrization of compactly supported wavelets", Aware Technical Report AD890503.4.1 (1989).
- Pollen, D., "Linear one-dimensional scaling functions", Aware Technical Report AD900104 (1990).
- Pollen, D. and Linden, D., "Quadratic one-dimensional
- Resnikoff, H. L., "Wavelets and adaptive signal processing," *to appear in SPIE International Symposium Proceedings, Vol. 1565, Adaptive signal processing*, October, 1991.
- Resnikoff, H. L., "Wavelets and adaptive signal processing," *Optical Eng.* 31(6), June, 1992.
- Resnikoff, H. L. and Wells, R. O., "Wavelet analysis and the geometry of Euclidean domains", *J. of Geometry and Physics*, vol. 8, pp. 273-282 (1992).
- Weiss, J., "Wavelets and the dynamics of enstrophy transfer in two dimensional hydrodynamics," Aware Technical Report, in progress, (June, 1990).

- Weiss, J., "The long term limit of two-dimensional Euler flow," Aware Technical Report AD911029.
- J. Weiss, "Wavelets and the Study of Two Dimensional Turbulence," in the Proceedings of the French-USA Workshop on *Wavelets and Turbulence*, Princeton University, June 1991. Y. Maday, Ed. Springer-Verlag, NY.

6.3.2 Related reports

The following report was largely prepared by Aware under subcontract to Martin-Marietta. It reports work based on research supported by the contract for which present document is the Final Report.

- Stirman, C., "Applications of wavelets to radar data processing," Final Technical Report under DARPA Order No. 7450 monitored by AFOSR under contract No. F49620-90-C-0050. Martin-Marietta Electronics, Information, and Missiles Group, July 1991.

6.4 Wavelet technology in the popular press

Articles on wavelet technology that have mentioned Aware's contributions based on work supported by Darpa include:

Business Week, Dr. Dobbs Journal, EE Times, Radio-Electronic Times, Science, Scientific American, The Boston Globe, The Economist, The Los Angeles Times.

6.5 Lectures and presentations supported in part by this contract

The following is a selection of presentations made with partial support from this conytract:

P. N. Heller:
W. Lawton:

H. L. Resnikoff:

R. Tolimieri:

John Weiss:

Michael Tzannes

International Symposium on Circuits and Systems, " On a Relation between the Principle MILCOM '92, "Block Biorthogonal Coding Using Wavelets," To be presented, October '92 Globecom '92, "Bit-by-bit Channel Coding Using Wavelets," To be Presented, 'December '9

6.6 Academic relationships

6.6.1 Affiliated consultants

- C. S. Burrus (Rice Univ.)
- R. Glowinski (Univ. of Houston and Rice Univ.)
- M. Godfrey (Imperial College and Stanford Univ)
- J. Proakis (Northeastern Univ.)
- G. Strang (M.I.T.)
- R. O. Wells (Rice Univ.)

6.6.2 Student internships

- R. Gopinath (Rice)

- David Pollen (Princeton Univ)

- Brian Usevitch (Illinois at Urbana)

- Marcos Tzannes (U. C. Berkeley)

The Scalable Structure of Information:
An Essay on Wavelet Technology
and its
Application to Bandwidth Management

H. L. Resnikoff

October 19, 1992

Aware, Inc.

One Memorial Drive

Cambridge, MA 02142

617-577-1700 617-577-1710 FAX

AD921018

This work was supported in part by the Defense Advanced
Research Projects Agency Order No. 7092 and AFOSR
Contract No. F49620-89-C-0125.

Copyright © 1992 by Aware, Inc.

No part of this book may be reproduced by any mechanical, photographic, or electronic process, or in the form of a phonographic recording, nor may it be stored in a retrieval system, transmitted, or otherwise copied for public or private use, without written permission from Aware, Inc.

Preface

This monograph is intended to provide the reader interested in mathematical engineering with an informal tour of the theory of compactly supported wavelets, its applications, and what it tells us about the relationship between the discrete and the continuous in mathematical models of physical systems.

Its content is largely based on the work of my present and past colleagues at Aware, who are in large measure responsible for the many results it contains. I of course assume all responsibility for errors (of omission as well as commission) but in this instance I could not have made some of those errors without their help! The book also is indebted to other explorers of the vast new territory that the concept of compactly supported wavelets has revealed. I have acknowledged their contributions where they have played a part in the story I have to tell.

I am pleased to express my appreciation to my former colleagues Wayne Lawton, David Pollen, David C. Plummer (Linden) and Eric Tenenbaum, whose early and fundamental contributions to the development of wavelet theory at Aware have profoundly influenced the way I think about the subject, and to Ramesh Gopinath and Professors C. S. Burrus and Roland Glowinsky for their insights and stimulation during their extended visits to the company. Discussions with Professor Louis Auslander during a period of more than three years stimulated the author's mathematical imagination and introduced Aware to the potential of wavelets for channel coding.

Special thanks are due to Jonathan Devine, Peter Heller, John Huffman, Karl Jagler, William Morrell, Richard Tolimieri, Michael Tzannes, John Weiss, and Bill Zettler, and to my friend and colleague Ronny Wells, all of whom will recognize their hands (and heads) throughout this book, and to the rest of the staff of Aware whose contributions to this book have been considerable even though they may be less visible.

I am particularly grateful to Christina Gorecki who kept the unruly team of *TeX*,[©] *Mathematica*,[©] and the Macintosh operating system hitched together and more or less pulling in a common direction as a sideline while she performed her real duties.

Aware, Inc. is indebted to the Defense Advanced Research Projects Agency for its far-sighted support which enabled Aware to explore fundamental issues at the interface of mathematics and computation in the

context of developing practical solutions to difficult and important problems. We believe that this partnership of common interests between small commercial companies and government agencies, between mathematicians and engineers, and between theory and practice will be the paradigm for developing advanced technology in the twenty first century.

Collected below are certain symbols used in the text.

Z	The <i>integers</i> $\mathbf{Z} := \{\dots, -2, -1, 0, 1, 2, \dots, n \dots\}$.
Q	The <i>rational numbers</i> $\mathbf{Q} := \{m/n \text{ where } m, n \in \mathbf{Z} \text{ and } n \neq 0\}$.
D	The <i>dyadic rationals</i> $\mathbf{D} := \{q/2^n : q \in \mathbf{Z} \text{ an odd integer and } n \in \mathbf{Z}\}$.
R	The <i>real numbers</i> .
C	The <i>complex numbers</i> .
$L^2(\mathbf{R})$	The space of finite energy signals on \mathbf{R} .
$L^2([0, 1])$	The space of finite energy signals on the interval $[0, 1]$.
$\lg x$	The base 2 logarithm of x .

The imaginary unit is $i := \sqrt{-1}$.

Figure 1: Aware's logo. The square is a map of the two dimensional pinched torus parameter space of six coefficient wavelet matrices. The curves are the loci of wavelet matrices that correspond to wavelet bases that are formally differentiable of order 1.



Contents

I	Background	19
1	The New Mathematical Engineering	21
1.1	Trial and Error in the 21st Century	21
1.2	Mathematical Engineering	22
1.2.1	Active Mathematics	22
1.2.2	The Three Types of Bandwidth	23
1.2.3	Communications Bandwidth: Mathematical Engineering for Channel Coding	25
1.2.4	Information Storage Bandwidth: Mathematical Engineering for Compression	27
1.2.5	Computational Bandwidth: Mathematical Engineering for Manufacturing	28
1.3	Are Breakthroughs on the Way?	30
2	Good Approximations	31
2.1	Approximations and the Perception of Reality	31
2.1.1	Efficient Mathematical Models	34
2.1.2	Computational Complexity	35
2.2	Information Gained from Measurement	36
2.2.1	Digital Computers and Measurement	37
2.2.2	Uncertainty and Natural Philosophy	39
2.2.3	Axioms for Measures of Information Gain	41
3	Wavelets: a Positional Notation for Functions	47
3.1	Multiresolution Representation	47
3.2	The Democratization of Arithmetic: Positional Notation for Numbers	49
3.3	Music Notation as a Metaphor for Wavelet Series	52
3.4	Wavelet Phase Space	52

II	Theory	59
4	Wavelet Theory	61
4.1	Comparison with the Fourier Transform	61
4.1.1	The Continuous Transform	62
4.1.2	The Discrete Transform	63
4.1.3	The Finite Transform	63
4.2	Mathematical Definition	64
4.2.1	The Basic Ingredients	64
4.2.2	Ways to Increase Spectral Resolution	66
4.2.3	Rank m Wavelet Matrices	68
4.3	Examples of Wavelet Matrices for $m = 2$	71
4.3.1	The sinc Wavelet Matrix ($m = 2, g = \infty$)	71
4.3.2	Real Wavelet Matrices for ($m = 2, g = 2$) and ($m = 2, g = 3$)	72
4.4	Orthonormal Bases of Wavelet Matrices.	73
4.4.1	Wavelet Expansion of Discrete Functions	73
4.4.2	Infinite Rank Smooth Wavelet Matrices	75
4.5	Orthonormal Bases of Compactly Supported Wavelets.	76
4.5.1	The Wavelet Basis	76
4.5.2	Representation of Functions by Wavelet Series	77
4.5.3	Daubechies Wavelets	78
4.5.4	Complex Wavelet Matrices and Wavelets	79
4.5.5	Wavelet Matrix Pairs and Biorthogonal Wavelets	80
4.6	Fourier Transform of Wavelets	81
4.6.1	1-Dimensional Scaling Functions	81
4.6.2	2-Dimensional Scaling Functions	81
4.7	Calculus of Wavelets	84
4.7.1	Exact Calculation of Wavelet Function Values	84
4.7.2	Integration	85
4.7.3	Formal Derivatives	85
4.7.4	Connection Coefficients for Numerical Differentiation	87
5	A Bestiary of Wavelets	93
5.1	Five Fundamental Examples	93
5.1.1	sinc Wavelets	93
5.1.2	<i>Haar</i> Wavelets	94
5.1.3	<i>CarAlarm</i> Wavelets	96
5.1.4	<i>NonNegative</i> Wavelets	98
5.1.5	<i>Daubechies</i> Wavelets	104
5.2	Real Orthogonal Wavelets	109
5.2.1	A wavelet basis of genus $g = 2$	109

5.2.2	<i>Hat</i> Wavelets	113
5.3	Flat Wavelets	113
5.4	Complex Orthogonal Wavelets	117
5.4.1	<i>Lauton-Resnikoff</i> Wavelets	117
5.5	Biorthogonal Wavelets	124
5.5.1	<i>Cohen-Daubechies-Feauveau</i> Wavelets	124
5.5.2	<i>Heller</i> Wavelets	127
5.6	Negative Multiplier <i>Daubechies</i> Wavelets	129
5.7	Higher Rank Wavelets	131
5.7.1	<i>Pollen-Plummer</i> Higher Rank Wavelets	131
5.8	Higher Dimensional Wavelets	136
5.8.1	Irreducible Two-Dimensional Wavelets	136

III Applications of Wavelet Technology to Bandwidth Management 143

6	Bandwidth Compression	145
6.1	Image Compression	145
6.1.1	Imagery	145
6.1.2	Measures of Image Quality	145
6.2	Transform Image Compression Systems	148
6.2.1	System Block Diagram	148
6.2.2	Conventional Block Transform Image Compression	151
6.3	Wavelet Image Compression	152
6.3.1	Comparison of Conventional and Wavelet Image Compression	160
6.4	Multiresolution Audio Compression	166
6.4.1	Audio Signals	166
7	Channel Coding	173
7.1	Relation to Shannon's Channel Coding Theorem	173
7.2	Wavelet Channel Coding	175
7.2.1	Modulation	177
7.3	The Wavelet Channel Coding Algorithm	181
7.3.1	The Basic Idea: Trellis WC Message Coding for $m = 2$	181
7.3.2	Recovery of a Trellis WC Coded Message for $m = 2$	182
7.3.3	The Simplest Case: Block WC Message Coding with $m = 2$	183
7.3.4	Code Rate and Channel Rate for Arbitrary Overlap Signalling	184
7.3.5	Distribution of WCC Symbols	185

7.4	Wavelet Channel Coding and Digital Modulation Techniques	186
7.4.1	Wavelet Channel Coding and M-ary Pulse Amplitude Modulation	186
7.4.2	Wavelet Channel Coding and M-ary Phase Shift Keying	186
7.4.3	Wavelet Channel Coding and M-ary Frequency Shift Keying	187
7.5	Performance of Wavelet Channel Coding	188
7.5.1	Introduction	188
7.5.2	Performance of WCC in Additive White Gaussian Noise	188
7.5.3	Performance on Pulsed Interference Channels	190
8	Numerical Solution of Partial Differential Equations	193
8.1	Understanding PDE	193
8.2	Wavelet numerical solutions for differential equations	194
8.3	Summary of Current Results	197
8.3.1	Advantages of wavelets for the numerical Solution of PDE.	197
8.3.2	Principal Results	197
8.4	A One Dimensional Example: Burgers Equation	198
	References	205

List of Tables

1.1	Spectrum allocation in the United States	24
4.1	Three types of Fourier Transform	61
4.2	Three types of Wavelet Transform	64
4.3	Conventional digital signal processing transforms within the framework of the arbitrary rank wavelet theory (m =rank, g =genus of wavelet transform and Dg =Daubechies' wavelets of genus g).	69
7.1	Example of Wavelet Channel Coding	191

List of Figures

1	Aware's logo. The square is a map of the two dimensional pinched torus parameter space of six coefficient wavelet matrices. The curves are the loci of wavelet matrices that correspond to wavelet bases that are formally differentiable of order 1.	3
2	One dimensional row-transformed <i>Lenna</i> image employing the <i>D3</i> wavelet basis. <i>Lenna</i> was the centerfold in the November 1972 issue of <i>Playboy</i> . This image, digitized from the original, has become a standard in the image processing community, which usually, but incorrectly, identifies it as "Lena." Today <i>Lenna</i> is also known as "NITF-6" in the National Image Transmission Format test image suite.	17
2-1	Continuous ramp transient.	32
2-2	Fifty-five point ramp transient: 27 term Fourier series approximation.	33
2-3	Fifty-five point ramp transient: 27 term <i>D3</i> wavelet series low pass approximation.	33
3-1	The basic step of a multiresolution analysis	48
3-2	Mallat tree of cascaded filters for $m = 2$	49
3-3	Complete binary tree of cascaded filters for $m = 2$	50
3-4	Diagram of wavelet phase space with keyboard.	53
3-5	Music notation, with appreciation to J. S. Bach.	53
3-6	Wavelet phase space.	55
3-7	Phase space representation of an impulse function; Energy for <i>D3</i> wavelet transform.	56
3-8	Modulus of the Fourier transform of the scaling function for the non-separable 2-dimensional Novon Haar wavelet matrix.	57
4-1	The <i>D2</i> scaling function φ ($m = 2, g = 3$).	65

4-2	The $D2$ wavelet ψ ($m = 2, g = 3$).	66
4-3	Typical transform application domains within framework of the arbitrary rank wavelet theory ($m = \text{rank}$ and $g = \text{genus}$ of wavelet transform.	70
4-4	The Daubechies scaling function of genus 2 for $m = 2$ and the analogous scaling function of genus 2 for $m = 5, 8$	75
4-5	A complex orthogonal scaling function φ ($m = 2, g = 3$). . .	80
4-6	Heller's complex biorthogonal scaling function ($m = 2, g = 3$). . .	81
4-7	Zeros of the Fourier transform of the "Rectangle" Haar scaling function.	82
4-8	Zeros of the Fourier transform of the "Twindragon" Haar scaling function.	83
4-9	Zeros of the Fourier transform of the "Novon" Haar scaling function.	83
4-10	Formal derivative of order 1 of the $D2$ scaling function ($m=2, g=2$).	87
4-11	Formal derivative of order 0.5500 . . . of the $D2$ scaling function ($m=2, g=2$).	88
4-12	Formal derivative of order 2.44998 . . . - $i4.53236$. . . of the $D2$ scaling function ($m = 2, g = 2$).	88
4-13	Formal derivatives of the $D3$ scaling function ($m=2, g=3$). . .	89
5-1	The sinc scaling function has non-compact support.	94
5-2	Standard <i>Haar</i> scaling function with compact support.	95
5-3	Standard <i>Haar</i> wavelet with compact support.	95
5-4	<i>Haar</i> scaling function with noncompact support.	96
5-5	<i>Haar</i> scaling function with noncompact support (Zoomed).	97
5-6	<i>CarAlarm2</i> scaling function; $J = 4$	97
5-7	<i>CarAlarm2</i> wavelet; $J = 4$	98
5-8	Modulus of the Fourier transform of the <i>CarAlarm2</i> scaling function, in dB.	99
5-9	Geometry of the eigenvalues of $A(0)$ for <i>CarAlarm15</i>	99
5-10	<i>CarAlarm3</i> scaling function; $J = 4$	100
5-11	<i>CarAlarm3</i> wavelet; $J = 4$	100
5-12	Modulus of the Fourier transform of the <i>CarAlarm3</i> scaling function, in dB ($m = 2, g = 3$).	101
5-13	The scaling function <i>NonNegative</i> ($m = 2, g = 2; J = 6$).	102
5-14	The same <i>NonNegative</i> scaling function: only computed points are shown. ($m = 2, g = 2; J = 6$).	102
5-15	The <i>NonNegative</i> wavelet ($m = 2, g = 2; J = 6$).	103
5-16	Modulus of the Fourier transform of the scaling function <i>NonNegative</i> , in dB.	103

5-17	Argument of the Fourier transform of the scaling function <i>NonNegative</i>	104
5-18	The scaling function <i>NonNegative(a)</i> ; only computed points are shown. ($m = 2, g = 2; J = 6$).	105
5-19	The <i>NonNegative(a)</i> wavelet ($m = 2, g = 2; J = 6$).	105
5-20	Modulus of the Fourier transform of the scaling function <i>NonNegative(a)</i> , in dB.	106
5-21	Argument of the Fourier transform of the scaling function <i>NonNegative(a)</i>	106
5-22	Modulus of the Fourier transform of the <i>D1</i> scaling function, in dB. i.e. $ \text{sinc}(\pi x) $	107
5-23	Modulus of the Fourier transform of the <i>D2</i> scaling function, in dB.	107
5-24	Argument of the Fourier transform of the <i>D2</i> scaling function.	108
5-25	Modulus of the Fourier transform of the <i>D3</i> scaling function, in dB.	108
5-26	Daubechies scaling function <i>D5</i> ($m = 2, g = 5$).	109
5-27	Daubechies wavelet <i>D5</i> ($m = 2, g = 5$).	110
5-28	Modulus of the Fourier transform of the <i>D5</i> scaling function, in dB.	110
5-29	Daubechies scaling function <i>D15</i> ($m = 2, g = 15$).	111
5-30	Daubechies wavelet <i>D15</i> ($m = 2, g = 15$).	111
5-31	Formally differentiable scaling function <i>Rt2</i> ($m = 2, g = 2$).	112
5-32	The wavelet <i>Rt2</i> ($m = 2, g = 2$).	112
5-33	The scaling function <i>Hat</i> ($m = 2, g = 3$).	113
5-34	The wavelet <i>Hat</i> ($m = 2, g = 3$).	114
5-35	Modulus of the Fourier transform of the scaling function φ for <i>Hat</i> ($m = 2, g = 3$).	114
5-36	The scaling function for a flat wavelet ($m = 2, g = 4$).	115
5-37	The modulus of the Fourier transform of the previous scaling function, in dB ($m = 2, g = 4$).	115
5-38	The argument of the Fourier transform of the previous scaling function, in dB ($m = 2, g = 4$).	116
5-39	The wavelet for the same flat wavelet matrix ($m = 2, g = 4$).	116
5-40	The scaling function for a flat wavelet ($m = 2, g = 16$).	117
5-41	The modulus of the Fourier transform of the previous scaling function, in dB ($m = 2, g = 16$).	118
5-42	The argument of the Fourier transform of the previous scaling function, in dB ($m = 2, g = 16$).	118
5-43	The wavelet for the same flat wavelet matrix ($m = 2, g = 16$).	119
5-44	Geometry of the eigenvalues for a real flat wavelet matrix of rank $m = 2$ and genus $g = 16$	119

5-45	The real part of the <i>Lawton-Resnikoff</i> complex scaling function, $m = 2, g = 3$.	120
5-46	The imaginary part of the <i>Lawton-Resnikoff</i> complex scaling function, $m = 2, g = 3$.	121
5-47	The real part of the <i>Lawton-Resnikoff</i> complex wavelet, $m = 2, g = 3$.	122
5-48	The imaginary part of the <i>Lawton-Resnikoff</i> complex wavelet, $m = 2, g = 3$.	123
5-49	Modulus of the Fourier transform of the <i>Lawton-Resnikoff</i> scaling function, $m = 2, g = 3$.	123
5-50	<i>Cohen-Daubechies-Feauveau</i> left biorthogonal scaling function ($m = 2, g = 4$).	124
5-51	<i>Cohen-Daubechies-Feauveau</i> left biorthogonal wavelet ($m = 2, g = 4$).	125
5-52	$\varphi_L - \varphi_R$ for Cohen-Daubechies-Feauveau biorthogonal wavelet ($m = 2, g = 4$).	125
5-53	φ_L for a biorthogonal wavelet matrix of genus $g = 8$. ($m = 2, g = 8$).	126
5-54	ψ_L for a biorthogonal wavelet matrix of genus $g = 8$ ($m = 2, g = 8$).	126
5-55	$\varphi_L - \varphi_R$ for a biorthogonal wavelet matrix pair of genus $g = 8$ ($m = 2, g = 8$).	127
5-56	Real part of the 6-coefficient <i>Heller</i> biorthogonal scaling function φ_L .	128
5-57	Imaginary part of the 6-coefficient <i>Heller</i> biorthogonal scaling function φ_L .	128
5-58	Modulus of the Fourier transform of the <i>Heller</i> scaling function, $m = 2, g = 3$.	129
5-59	Real part of the 6-coefficient <i>Heller</i> biorthogonal scaling function ψ_L .	130
5-60	Imaginary part of the 6-coefficient <i>Heller</i> biorthogonal scaling function ψ_L .	130
5-61	<i>Daubechies</i> wavelet with negative multiplier ($m = -2, g = 2$).	131
5-62	Formal derivative of <i>Daubechies</i> wavelet with negative multiplier ($m = -2, g = 2$).	132
5-63	Previous figures on a common scale.	133
5-64	<i>Daubechies</i> scaling function with negative multiplier ($m = -2, g = 3$).	134
5-65	<i>Daubechies</i> scaling function with negative multiplier ($m = -2, g = 5$).	134
5-66	<i>PPD</i> (3,2) scaling function ($m = 3, g = 2$).	135
5-67	<i>PPD</i> (5,2) scaling function ($m = 5, g = 2$).	135

5-68	<i>PPD(inf, 2)</i> scaling function ($m = \infty, g = 2$).	136
5-69	One-dimensional to two-dimensional mapping for the <i>Rectangle Haar</i> scaling function $\varphi(z)$ ($m = 2, g = 1$).	138
5-70	<i>Novon Haar</i> scaling function $\varphi(z)$ ($m = 2, g = 1$).	138
5-71	One-dimensional to two-dimensional mapping for the <i>Novon Haar</i> scaling function $\varphi(z)$ ($m = 2, g = 1$).	139
5-72	<i>Twindragon Haar</i> scaling function $\varphi(z)$ ($m = 2, g = 1$).	139
5-73	Two dimensional row and column transformed image <i>Lenna</i> image employing the <i>D3</i> product basis.	141
6-1	Simultaneous contrast enhances edges.	146
6-2	Trade-off between compression ratio and image size for three fixed levels of quality for Aware's compression.	147
6-3	Diagram of a transform image compression system.	149
6-4	Discrete cosine transform ("DCT") matrix for JPEG: $m = 8, g = 1$	151
6-5	Hadamard transform matrix: $m = 8, g = 1$	152
6-6	<i>Daubechies</i> scaling function φ for <i>D3</i> ($m = 2, g = 3$).	153
6-7	<i>Daubechies</i> wavelet ψ for <i>D3</i> ($m = 2, g = 3$).	153
6-8	Stereogram of the product of scaling functions $\varphi(x)\varphi(y)$ for <i>D3</i> . (The origin of coordinates is at the lower right.)	154
6-9	Stereogram of the product of wavelet functions $\psi(x)\psi(y)$ for <i>D3</i> . (The origin of coordinates is at the lower right.)	155
6-10	Two-dimensional low-low product wavelet basis function built from <i>D3</i> : $\varphi(x)\varphi(y)$	156
6-11	Two-dimensional low-high pass product wavelet basis function built from <i>D3</i> : $\varphi(x)\psi(y)$	157
6-12	Two-dimensional high-low pass product wavelet basis function built from <i>D3</i> : $\psi(x)\varphi(y)$	158
6-13	Two-dimensional high-high pass product wavelet basis function built from <i>D3</i> : $\psi(x)\psi(y)$	159
6-14	<i>Lenna</i> eye source image.	161
6-15	<i>Lenna</i> eye decompressed at 32-to-1 via <i>D1</i> ($m = 2, g = 1$).	161
6-16	<i>Lenna</i> eye decompressed at 32-to-1 using <i>D2</i> ($m = 2, g = 2$).	162
6-17	<i>Lenna</i> eye decompressed at 32-to-1 using <i>D3</i> ($m = 2, g = 3$).	162
6-18	<i>Lenna</i> eye decompressed at 32-to-1 using <i>D4</i> ($m = 2, g = 4$).	163
6-19	<i>Lenna</i> eye decompressed at 32-to-1 using the DCT ($m = 8, g = 1$).	164
6-20	<i>Lenna</i> eye decompressed at 32-to-1 using the "wavelet'ed" DCT ($m = 8, g = 2$).	164
6-21	<i>Lenna</i> eye decompressed at 32-to-1 using the Hadamard transform ($m = 8, g = 1$).	165

6-22	<i>Lenna</i> eye decompressed at 32-to-1 using the "waveletized" Hadamard transform ($m = 8, g = 2$).	165
6-23	Original NITF6 <i>Lenna</i> image.	167
6-24	<i>Lenna</i> decompressed at 32-to-1 using the <i>D3</i> wavelet transform with quantization ($m = 2, g = 3$).	168
6-25	Schematic representation of the audio masking threshold function.	169
6-26	Energy density as a function of time and frequency for an audio signal.	170
6-27	Psychoacoustic map of the same audio signal showing effect of the masking threshold.	171
7-1	Shannon's channel coding theorem.	174
7-2	Wavelet channel coding performance in a channel with 5% burst noise.	179
7-3	Wavelet channel coding performance in fading channels. . .	180
7-4	Wavelet channel coding performance in flat Rayleigh channels. .	181
8-1	Initial condition for the solution of Burgers equation.	199
8-2	Evolution of the numerical solution of Burgers equation employing unsmoothed de-aliased spectral method.	201
8-3	Evolution of the numerical solution of Burgers equation employing smoothed de-aliased spectral method.	202
8-4	Evolution of the numerical solution of Burgers equation employing unsmoothed Wavelet-Galerkin method.	203
8-5	Evolution of the numerical solution of Burgers equation employing smoothed Wavelet-Galerkin method.	204

Figure 2: One dimensional row-transformed *Lenna* image employing the *D3* wavelet basis. *Lenna* was the centerfold in the November 1972 issue of *Playboy*. This image, digitized from the original, has become a standard in the image processing community, which usually, but incorrectly, identifies it as "Lena." Today *Lenna* is also known as "NITF-6" in the National Image Transmission Format test image suite.



Part I
Background

Chapter 1

The New Mathematical Engineering

1.1 Trial and Error in the 21st Century

A fundamental break with the past occurred during the last forty years. Each of us is now dependent on technology for sustaining not only our style of life but possibly our life itself. Today nations and corporations undertake projects whose scale and complexity were undreamt merely a generation ago. People depend on products their grandparents would have called miracles, and they expect the marketplace to provide levels of performance, safety, and affordability that require advances all along the convoluted frontier of science and technology.

Before this break with the past, most large undertakings differed in degree, but not in kind, from what had previously been tried and mastered. New products were *tested in the laboratory* and industrial processes were *scaled up* from laboratory trials.

Improvement by trial and error served past generations well, but it cannot serve the future. Today, design and manufacturing antecedents that provide insight into the long term consequences of large scale projects are usually lacking. The trans-Alaskan pipeline, landing explorers on the moon and bringing them home, assessing the crashworthiness of new automobiles, and finding the optimal shape for the wing of a jet transport are problems that cannot be solved by trial and error or by scaling up the results of affordable small scale tests.

Today, testing the real thing is often too costly, too time-consuming, or just too complicated to be practical. More and more often, when a project

involves human health, or the interdependence of human well-being and the well-being of the environment, testing the real thing may not be possible.

Development by trial and error was suited to the time when technology was in its infancy. That approach is no longer adequate. The need to predict performance and consequences, and to *optimize* design for safety, quality, and cost have become key competitive and social factors for industrial economies. These factors call for new tools suited to these new problems. One important new tool for predicting performance and optimizing design is *mathematical engineering*.

1.2 Mathematical Engineering

1.2.1 Active Mathematics

Traditionally, mathematics only played a role in the earliest stages of engineering design. Mathematics was used, for example, to prescribe the arrangement and strength of the parts of a structural bridge design, or the shape and size of a wing that would meet the design objectives for lift, or to test the electrical characteristics of a layout for a VLSI chip design. Once the design was complete, the role of mathematics was played out.

Today, the digital computer and the VLSI chip have created a new role for mathematics in technology. Mathematical algorithms can now be directly embodied in products, so that every time the product is used, the algorithm is working. This *active mathematics* enables totally new classes of products, from the cellular telephone, where an algorithm in the form of channel coding protects the message from the distortions of noisy channels, to compact audio discs, where error correction coding insures the fidelity of music despite dust and imperfections of the recording medium. This new kind of use of mathematics will have an increasingly profound impact on adaptive process controls in manufacturing and on real-time dynamic controls in products - from automobiles and airliners to electronic pocket organizers - that are used by everyone.

Active mathematics calls for a new approach to the use of mathematics in engineering - a new *mathematical engineering* - that employs a systems approach to problems where mathematical process models, efficient algorithms for computer numerical solutions, and area-efficient VLSI implementations for portable and computation-intensive real-time applications are efficiently combined to yield an integrated solution.

1.2.2 The Three Types of Bandwidth

Communications Bandwidth

Bandwidth is usually thought of in the context of broadcast communications, where it is the physical means by which a radio or television signal carries information. In the United States, the available spectrum is allocated by the Federal Communications Commission (FCC) for signals that propagate through the atmosphere. Although bandwidth is an abstract concept that many people find difficult to understand, from an economic point of view bandwidth acts like a commodity. Like any other commodity, bandwidth can be plentiful or scarce relative to the need for it. With the growth of telecommunications and computing, communications and electronic storage bandwidth have become increasingly scarce commodities.

Information Storage Bandwidth

Information that is stored on a disk drive or any other storage medium also consumes bandwidth, but in this case the *storage bandwidth* that the device uses is built into the product in the form of the physical storage medium. For a fixed technology, the price of the product will generally increase with the storage bandwidth it provides. The user pays for the bandwidth.

Computational Processing Bandwidth

Every computer has a *computational bandwidth* which is roughly proportional to the number of operations it can perform per second. Computational bandwidth is really a measure of the amount of computation that a computer can perform per unit time. The difference between these two definitions depends on the efficiency of the algorithms that are employed. Processing bandwidth is not strictly independent of communications bandwidth and storage bandwidth because a computer combines logical processing operations, communication with its internal memory, and intermediate storage of information in registers as components of the computational process.

These three types of bandwidth - *communications bandwidth*, *information storage bandwidth*, and *computational processing bandwidth* - are three aspects of one fundamental concept.

Table 1.1: Spectrum allocation in the United States

Frequency Band (kHz)	Designation	Propagation Characteristics	Typical Uses
$3 \times 10^3 - 3 \times 10^4$	VLF		Submarine communications
$3 \times 10^4 - 3 \times 10^5$	LF		Long-range navigation; Marine communications
$3 \times 10^5 - 3 \times 10^6$	MF	Atmospheric noise.	AM broadcasting; Emergency frequencies; Maritime radio.
$3 \times 10^6 - 3 \times 10^7$	HF	Ionospheric reflection	Telephone; Facsimile; Aircraft and ship comm; International broadcasting; Military communications
$3 \times 10^7 - 3 \times 10^8$	VHF	Near line-of-sight; scattering.	VHF television; FM two-way radio; AM aircraft comm.
$3 \times 10^8 - 3 \times 10^{10}$	UHF	Line-of-sight.	UHF television; Radar; microwave links.
$3 \times 10^9 - 3 \times 10^{10}$	SHF	Line-of-sight; Rainfall attenuation.	Satellite communications Radar.
$3 \times 10^{10} - 3 \times 10^{11}$	EHF	Water vapor absorption.	Radar; Satellite communications
$10^{12} - 10^{16}$	Infrared, Visible Light, Ultraviolet		Optical communications.

1.2.3 Communications Bandwidth: Mathematical Engineering for Channel Coding

Digital signal processing for communication is one of the areas where wavelet technology is making a difference.

Communication always involves a sender, a receiver, and a "communications channel," which is a means for transmitting the signal. A conversation, a radio broadcast, a cable TV program, a person reading a book, a person typing on a computer keyboard, and a computer transferring information to a hard disk are all examples of communication. In each case, information is transmitted by modifying something physical that can interact with both the sender and the receiver. For instance, speaking causes small systematic pressure variations in the air between the speaker and the hearer, which the hearer's ear translates or "decodes" into a stream of nervous impulses that are transmitted to the brain. The pressure variation of air is the communications channel for transmitting the speech signal. The air between the speaker's mouth and the hearer's ear can be thought of as the "carrier" of the speech signal; the small pressure variation caused by speaking "modulates" the carrier to encode the information signal on it.

Channel

For broadcast radio and TV, the channel is the electrical variation of an electromagnetic wave broadcast from the transmitter tower. The electromagnetic wave is the carrier. The small electrical variations that represent the information signal modulate the carrier by changing its physical properties. Amplitude modulation, used for AM radio, modifies the energy of the electromagnetic carrier wave, while frequency modulation, used for FM broadcasts and TV, modifies its frequency.

Noise

While a signal is passing from the source to the receiver, it is at the mercy of the surrounding physical environment. A lightning flash will drown out an AM radio signal just as a drum roll will drown out speech. The information signal is still there, but it is masked by the larger signal and cannot be detected by the receiver, just as the ear cannot detect a softer tone masked by a nearby louder one. "Noise" is simply an unwanted modulation of the carrier whose presence interferes with detection of the desired signal. One person's noise is another person's signal. The boom boxer thinks the nearby conversation is noise. Other people's conversations audible on a telephone line are usually placed into the noise category. The telephone company calls this "co-channel interference."

Noise - interference - is always present in every communications channel, and it corrupts every communication. It causes the receiver to make errors in decoding the transmitted signal. These channel errors limit the efficiency of the communications system.

Channel Capacity

Every communications channel can transmit a certain amount of information but no more. The number of bits per second that a channel can transmit is called its channel capacity. Channel capacity decreases as the amount of noise increases, and it increases as the amount of energy used to modulate the carrier increases. For radio channels, the channel capacity is proportional to the channel's frequency bandwidth. *Bandwidth* is another name for channel capacity, and channel coding is an important part of a strategy for managing bandwidth efficiently.

The notion of channel capacity is very general and can be used to describe any communications system. Commercial airline traffic supplies an easily understood example. The travelers on the airplane represent the information bits and the aircraft is the carrier. The route through the sky is the channel. In regulated international air travel, airline routes are a valuable commodity. Increasing the number of flights between two airports is one way of increasing channel throughput to increase revenues. The capacity of the channel is determined by how many aircraft can occupy the route at the same time.

Channel Coding

We will pursue this example further. The number of airplanes that could occupy the routes between, for example, Boston and London, is much greater than the number that are permitted to fly, because government regulations require aircraft to maintain a minimum separation in both space and time. This minimum distance guarantees reliable air travel. It is a form of channel coding.

A communications link needs to be reliable. The importance of the information being transmitted determines how. Reliability is usually measured by the average bit error rate, i.e., the number of bit errors that, on the average, are tolerable for the application. For radio communications, links employing digital data, an error rate of one in every ten thousand bits may be acceptable. In the case of airplane travel, no error - no loss of life - is acceptable, so the distance between airplanes in flight is kept relatively large.

Cars traveling on a road maintain as great an inter-car distance as airplanes in flight. Less distance between them is required because the road channel is "less noisy" (events happen more slowly), and the consequences of an occasional error are usually not catastrophic. The distance between vehicles, although it wastes part of the channel capacity, is needed to maintain "reliable communications."

Channel coding is a sophisticated means of placing distance between information signals by putting *redundancy* in the information. This is the only way to avoid or correct errors that arise from channel noise.

1.2.4 Information Storage Bandwidth: Mathematical Engineering for Compression

There are two kinds of compression - "lossless" and "lossy".

Lossless Compression

Lossless compression is sometimes called "arithmetic coding" or "entropy coding" because it never destroys information. Lossless compression merely removes the redundancy in a signal. Since it never destroys information, the original signal can be exactly reconstructed from the losslessly compressed version. But most signals do not have very much redundancy. This limits the effectiveness of lossless compression which, for gray scale images, tends to produce compression ratios of only 2- or 3- to -1 [44].

Lossless compression is like compressing a gas in a cylinder by means of a piston: all the gas molecules are still there, and the gas returns to its original condition when the pressure is released by withdrawing the piston. The compressed gas requires a smaller volume to store the same number of gas molecules. The cost of compression and subsequent decompression when the gas is used is repaid by the savings that are byproducts of the reduced volume for shipment and storage.

Lossless compression of information works the same way. Information expressed in digital form as a sequence of bits can be reorganized so that the same information can be expressed in terms of fewer bits by removing the redundancy. The compressed format is usually not directly usable; when the information is used, it will be wanted in its uncompressed form. The cost of lossless compression and decompression must be repaid by the savings that are byproducts of the smaller amount of storage or transmission time required by the compressed information if lossless compression is to be commercially worthwhile. Lossless compression is used when it is important to be able to reconstruct the signal exactly; no errors are permitted. The use of lossless compression for financial data records is a typical application.

The critical difference between compressing a gas and compressing information is that there is a limit to how far information can be losslessly compressed. The amount of information in a signal is the number of bits that are needed to express the information in its most compressed form. If the signal is compressed further (e.g., by throwing away some of the remaining bits), then some information present in the original signal will be lost.

Lossy Compression

Lossy compression selectively discards less important information from the signal. This permits much higher compression ratios and often – it depends on the application – there will be little or no perceptible difference between the original signal and the signal constructed from the compressed version. Lossy compression for full color still images can be 30 times as great as lossless compression without producing significant distortion. This is possible because images typically contain “noise” and other details that are subliminal and therefore not perceived by the viewer. Speech, sound, and imagery can all be compressed by lossy compression to a far greater degree than by lossless compression.

Lossy compression discards “less important” information. The critical feature of a lossy compression method is the way it decides which information is important. The decision generally depends on the application, but for sensory data like speech, sound, and imagery, all of which are processed by people, there are similarities that make it possible to design compression algorithms that have a common general structure.

1.2.5 Computational Bandwidth: Mathematical Engineering for Manufacturing

Some of the most demanding applications for mathematical engineering are problems of manufacturing. Shortening product design cycles and improving the performance of manufactured products are necessary for economic competitiveness. They directly affect manufacturing costs and the ability to be responsive to changes in consumer taste, the two short-term factors that determine profitability. The health and safety effects of products will become increasingly important as products become ever more complex. Other things being roughly equal, economies and companies that are able to lead in these aspects will be more successful than those that cannot.

It is not easy to shorten design time and improve product performance because today’s manufactured products are much more complex than those

of just a few decades ago. From an inexpensive television set to a multimillion dollar gas turbine jet engine, most manufactured products are now too complicated for old fashioned design procedures. The old procedures cost too much; they take too long; and they are incompatible with interactive performance simulation that is necessary to optimize designs for reduced manufacturing cost and increased quality.

The traditional role of mathematics in engineering design and its new active role in product operation can be combined by interactively using computer-implemented mathematical simulations to analyze and improve product performance. Although the computer is already a principal tool in many industries, and has been used to make great strides in organizing and controlling manufacturing processes, its interactive use to optimize product design and reduce design cycle time is still untapped.

At the heart of the product design process is the ability to represent the operation of a product by a mathematical process model. The process model underpins the ability to simulate performance by "running" the mathematical model on a computer.

If a mathematical simulation is to be useful for design, it must be accurate and fast; if it is to be practical, it must run on inexpensive computers. Typically, the most difficult and costly part of mathematical simulation for manufacturing involves nonlinear processes, like combustion, fluid flow, and forming metals and plastics. In this context, the mathematical description usually consists of a collection of partial differential equations that model the physical properties of the product. The numerical solution of these equations describes the changes that occur as the product performs its function.

Although the speed of computers will continue to increase in the coming years, this, by itself, will not be sufficient to put the power of interactive simulation in the hands of every product design and manufacturing engineer who could benefit from it. Unless the product is very expensive or the number of units manufactured is very large, most companies cannot afford the cost of the powerful computer or supercomputer that would be needed to provide accurate and timely simulation results if the the current generation of simulation techniques are used. This means that in a period of increasing product customization, the vital "middle class" of the manufacturing sector that consists of medium sized engineering companies will not be competitive.

Affordable solutions to the interactive design problem are likely to be based on a combination of new and more accurate mathematical models for representing the product's operation, and more accurate and more stable numerical methods for solving the resulting differential equations quickly enough to support interactive design solutions. These advances would en-

able simulations that can reduce the time to solution, be applied to cases where conventional methods fail, and are interactive and economical.

1.3 Are Breakthroughs on the Way?

Is there a scientific basis for the breakthroughs that will be required to support active mathematics in complex products and for interactive design? We believe there is. The mathematical theory of compactly supported wavelets was discovered just a few years ago, but wavelet numerical solution of nonlinear differential equations has already demonstrated its potential, and wavelet-based active mathematics have already shown their ability to support dynamic bandwidth management for digital communication, storage, and high quality compression of audio and imagery.

Nonlinear and transient physical phenomena that exhibit nonlinear behavior such as combustion processes in an automobile engine, or air flow over a turbine blade in a jet engine are difficult to simulate. Systems like these exhibit shock behavior, with turbulence and detailed structure at many levels of resolution. Conventional numerical procedures require very fine meshes and very small time steps to insure the accuracy of numerical solutions, although they do not insure that the numerical procedures will be stable, or produce accurate results. Wavelet numerical solutions, however, are well suited to these types of problems. They are able to capture the behavior of complex, nonlinear dynamical systems with an accuracy and speed not possible with known alternative techniques.

In this book we introduce the reader to the ideas that lie behind the theory of compactly supported wavelets. We relate them to previously known methods in mathematics and engineering; show how they can be practically used in a digital signal processing and computing environment, and illustrate their potential for mathematical engineering by describing successful applications in bandwidth management.

Chapter 2

Good Approximations

“An addition to knowledge is won
at the expense of an addition to ignorance.”
—Arthur S. Eddington ¹

2.1 Approximations and the Perception of Reality

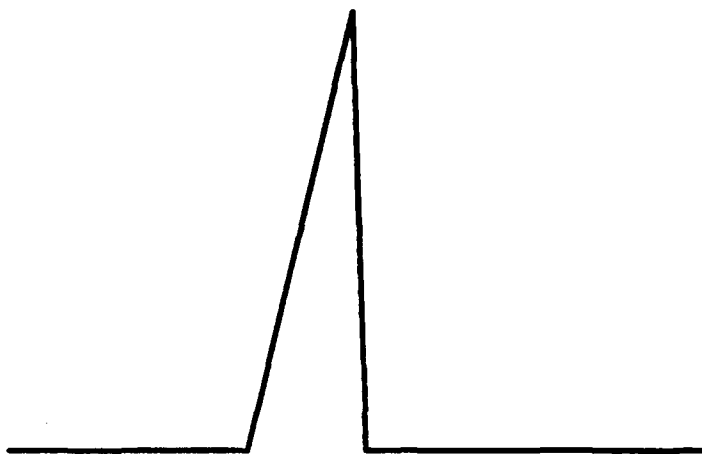
Every measurement, whether the naked result of an impression on the human eye or ear, or the result of a sophisticated measuring instrument, is merely an *approximation*. We can know, and our computing machines can know, only a finite number of decimal places in the numerical representation of a distance or a weight or a force or a temperature.² The eye has limited resolving power, the ear a limited frequency response, and this is true for all instruments whether biological or “mechanical.” This limitation is not merely due to poor “manufacturing technique;” as Heisenberg’s Uncertainty Principle tells us, it is inherent in the essence of things. Life and the universe depend on approximations. And so, too, does technology.

The certainty of error in every measurement and every physical interaction emphasizes the importance of knowing how accurate a particular approximation happens to be. If an approximate value is accurate enough for the purpose in hand, it is “good.” Other things being equal, a better approximation is preferred to a worse one. How good is a particular approximation? For a fixed expenditure of computational resources, measurements and analyses expressed in terms of *compactly supported wavelets*

¹[10]

²It follows that every measured or explicitly computed number is a rational number.

Figure 2-1: Continuous ramp transient.



give better approximations to speech signals, turbulence and other transient or localized phenomena than conventional methods. Here is a simple example: consider a time series that describes a quantity that is zero for a long time; ramps up linearly to a maximum value; and falls instantaneously to zero where it remains. Such a signal is shown as the smooth curve in figure 2-1.

Suppose this signal is sampled at 55 uniformly spaced times. The sample measurements can be used to construct a Fourier series expansion of the signal; if all 55 measurements are used, then the Fourier series will have 55 terms and it will perfectly reproduce the measured numbers. It will also interpolate values for unmeasured instants. However, if fewer than 55 terms are used, then the partial series will produce an approximation of the measured values. The figure shows the approximate values provided by a 27 term Fourier expansion. Figure 2-3 shows a 27 term wavelet series approximation. These figures display two important properties of wavelets: *Wavelet series approximate abrupt transitions much more accurately than Fourier series* and *Wavelet series perfectly reproduce constant measurements*. Wavelets produce better approximations but a wavelet approximation doesn't cost more to calculate than an ordinary approximation.

Figure 2-2: Fifty-five point ramp transient: 27 term Fourier series approximation.

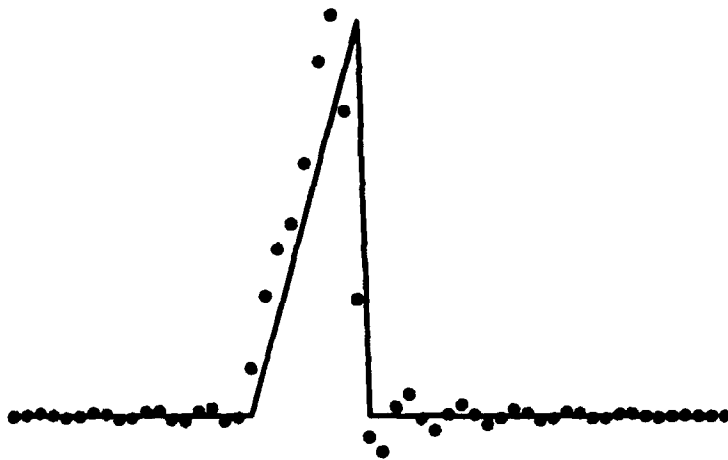
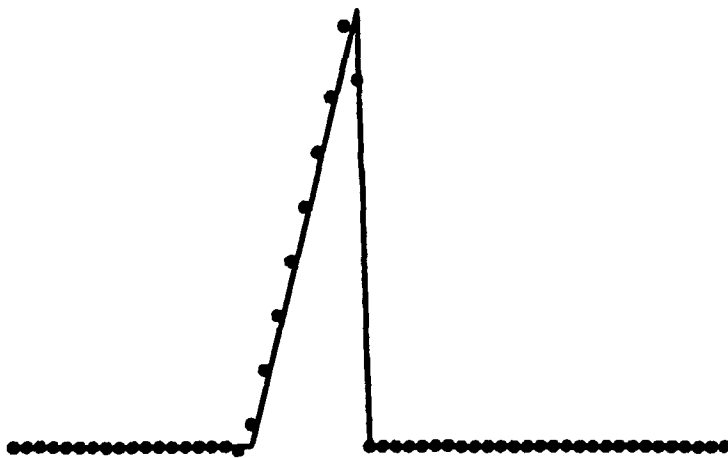


Figure 2-3: Fifty-five point ramp transient: 27 term D_3 wavelet series low pass approximation.



2.1.1 Efficient Mathematical Models

We can expect wavelets to provide better approximations when the data exhibit localized variations, but when the data vary regularly and smoothly other more traditional representations may be better. For instance, if a violin string is plucked, most of the energy will be concentrated near the plucked point for a short period of time – here, the wavelet series will provide an accurate and economical approximation. But as time passes, the energy of the pluck will spread along the string and be distributed among the normal modes of oscillation, which are sinusoidal. After a while, a Fourier series will provide a more economical approximation.

This example shows that it is important to know how to use wavelet approximations and traditional approximations in the same problem.

Compact support

One reason that wavelets provide good approximations for transient or localized phenomena is that each basis function – each term – in a wavelet series has *compact support* and, no matter how short an interval is, there is a basis function whose support is contained within that interval. The intuitive meaning of this property is that compactly supported wavelet basis functions can model local behavior efficiently because they are not constrained by properties of the data far away from the location of interest.

This feature of compactly supported wavelets also makes it easy to *concentrate computation where the activity is high*.

Compactly supported bases lead to inherently parallelizable algorithms. Aware's collaborators at Rice University recently demonstrated that wavelet methods for the numerical solution of a class of nonlinear partial differential equations could be run on a massively parallel computer with little change in the algorithm or program design. They led to an efficient use of the parallel computer, and an accurate solution of the problem.

Orthogonality

The terms in a wavelet series are *orthogonal* to one another, just like the terms in a Fourier series. This means that information carried by one term is independent of information carried by any other term: there is no redundancy in the representation.³ This is good because it means that

³More precisely, there is no redundancy with respect to the $L^2(\mathbb{R})$ norm in terms of which orthogonality is defined. There may be other types of relationships among the coefficients of a wavelet expansion that would permit a further reduction of redundancy, but they would lie outside the realm of square-integrable orthogonality. This is a general question that has nothing in particular to do with wavelets.

neither computing cycles nor storage are wasted as a result of coefficient redundancy when a wavelet series is calculated or stored.

Multiresolution representation

Biological sensory systems, such as vision, and many physical systems are organized into "levels" or "scales" of some variable, just like organizational and economic structures, and the positional notation of arithmetic. In this sense, a multiresolution or scalable mathematical representation may provide a simpler and more efficient representation than conventional mathematical representations. We delve more deeply into this basic concept in the next chapter.

2.1.2 Computational Complexity

Computational complexity is a measure of the number of elementary operations need to solve a computational problem. Computational complexity is indirectly a measure of time to solution for a given computing system as well as a measure of the cost of solution. Therefore the computational complexity of the numerical solution of a problem is a critical factor in deciding whether a proposed solution method can be practical.

Problems of design or active operation use measured data as an input. If the problem requires N data points, then the computational complexity of a solution must be at least $O(N)$, since reading the data into the computer is already an $O(N)$ operation; this is the best that can be done. Conventional mathematical operations, such as matrix multiplication or calculation of the finite Fourier transform, have been superseded by "fast" algorithms that make their use practical. Thus, the complexity of the fast Fourier transform is only $O(N \log N)$, compared with $O(N^2)$ for the conventional finite Fourier transform.

We shall see that wavelet transform operations are typically $- O(N) -$ asymptotically the best that could be hoped for.

It is possible to reduce computational cost without reducing computational complexity. If one method produces much better approximations than another, then fewer data points will be required to provide the desired solution accuracy. Reduction in the quantity of data is often a more important practical factor than the abstract complexity of a calculation.

2.2 Information Gained from Measurement

Immediately⁴ upon its invention, the digital computer was recognized as an entirely new kind of machine whose major influence would be on information-intensive activities — the life of the mind — rather than on energy-intensive activities, which had been the case for all previous machine inventions. In a prescient analysis in 1948 of the potential effect of computers on the social and economic structure, Norbert Wiener ([73], pp.27-28) drew attention to the distinctive and unprecedented role of this machine at the level of mind.

Today, the digital computer dominates the scene in psychology and biology as the principal metaphor for the operation of the brain⁵ and some physicists and computer scientists have argued that the physical universe itself can best be understood and modeled as an enormous digital computer whose evolution represents the working out of a program the source and purpose of which remain unknown.

Thus it is not surprising that the word *information* has taken on special meanings in all phases of everyday life as well as in science and philosophy: we speak of and hear about *information age*, *information glut*, *information management*, *information overload*, *information society*, *information technology*, *information theory*, and *information workers* without end. These modifications of vocabulary merely reflect the now universally recognized truth that information is a fundamental constituent of the world that interacts with such traditional and immediately physical constituents such as the mass and charge of material bodies, and space and time as the stage on which natural philosophy plays [49]. Nevertheless, philosophers and scientists no less than economists still have great difficulty in identifying exactly what information is, how it interacts with the other constituents of physical or societal reality, how to quantify it in the natural as well as the natural accounts, and even how to recognize it.

In this section we will examine the role of information at the fundamental level of *measurement*, which is the interface between science and experience, and *calculation*, which we think of as the interface between measurement and mind. We shall see that a *multiresolution* or *scaled* representation is the essential ingredient for extracting information from observations.

⁴This section is a modified version of [50].

⁵This metaphor has been implicitly adopted by art historians in their analysis of the role of the psychophysics of vision. A standard presentation is Gombrich [16].

2.2.1 Digital Computers and Measurement

A binary digital computer deals directly with dyadic rational numbers, that is, with numbers of the form

$$r = \pm \frac{q}{2^n}$$

where q is odd or zero and n is an integer. Moreover, any operation that a digital computer can perform can be thought of, or encoded as, a finite sequence of bits – of zeros and ones – and hence as a particular binary expansion of a dyadic rational number. Thus the entire realm of digital computers is limited to the ring D of dyadic rationals.⁶ Moreover, every reading produced by a measuring instrument is a rational number and, if the instrument is constrained so that the bits in the binary expansion of a measured value can be read off one by one, then the instrument only produces dyadic rationals.⁷ Thus, direct observation of the physical world can only produce numbers of exactly the sort that a digital computer can use.

Until recently, when one spoke of using *mathematics* to model natural phenomena, one meant *the calculus*. The ideas that underlie the calculus were systematically introduced in the late seventeenth century and the principal properties of derivatives and integrals were obtained by means of informal arguments that employed infinitesimal quantities. Leibniz recognized that the introduction of infinitesimals implied the existence of ideal infinitely small and infinitely large numbers that share the properties of the ordinary real numbers and, although mathematicians were unable to justify the use of these ideal numbers – indeed, the real numbers themselves were not fully understood until the late nineteenth century – infinitesimals were freely used in research and in mathematics education, as they still tend to be used in engineering and other branches of applied mathematics

⁶ A *ring* is a mathematical structure in which addition, subtraction and multiplication can be performed. If division by every non-zero element is also possible, mathematicians call the structure a *field*. The reader will note that a reciprocal of a dyadic rational is not in general a dyadic rational. This is why the numbers known to a computer do not form a field. A rational number is one of the form m/n where m and n are integers and $n \neq 0$. The set of all rational numbers, denoted Q , is the smallest infinite field and the ring D is contained within it.

⁷ This argument is not strictly correct. The computer can represent an integer by its finite binary expansion, which is a dyadic rational number. Therefore, an arbitrary rational number can be identified with the ordered pair of dyadic rational integers that are the numerator and denominator of the rational number in reduced form. Similarly, algebraic numbers such as $\sqrt{2}$, $\sqrt{17}$, etc., can be coded by finite sequences of integers, so they can also be expressed exactly in a digital computer. A measuring apparatus, however, cannot usually be arranged to measure the numerator and denominator of a rational number separately.

today. As Abraham Robinson [51] observed, "The idea of the infinitesimally small seems to appeal to our intuition." It was not until 1960 that infinitesimals were put on a sound logical basis by Robinson's introduction of non-standard analysis, which relies on the modern theory of models in mathematical logic to introduce a structure that extends the field \mathbb{R} of real numbers to include an infinite hierarchy of infinite and infinitesimal numbers in a way that insures the validity of first order predicates in the extended system; cf. [51]. This extension provides a kind of multiresolution analysis for infinite and infinitesimal quantities.

The kinds of numbers that seem to be needed for the theoretical mathematics of the calculus are evidently very different from the numbers that are produced by direct observation of the physical world: measurements are not unrestricted real numbers which, like the transcendental π , require infinitely many bits to specify their binary expansion, and they certainly are not one of Leibniz' and Robinson's infinitesimals. We appear to be faced with two unpleasant alternatives: either real numbers (and possibly infinitesimals) occur in the world but cannot be measured exactly (which introduces an inherent uncertainty in measurement and in all deductions based on measurements), or measurements reveal all that there is to know (so that our mental models, dependent upon the real numbers and perhaps even upon infinitesimals, are overdetermined: they contain far too many constraints to accurately reflect the phenomena).

These remarks recall Kronecker's century-old criticism of the "completed infinite," that nothing could be said to have mathematical existence unless it could actually be constructed in terms of a finite number of positive integers. In his view, the rational numbers exist since they can be represented as the ratio of two integers but transcendental numbers like π do not exist, since they require infinitely many fractions or operations for their representation. Kronecker is thus the mathematician in whom a digital computer can believe. He proposed a program to "arithmetize" mathematics and eliminate from it all "non-constructive" concepts.⁸ It is

⁸ "And if I can't do this," he said, "it will be done by those who come after me!" ([48], p. 26). Indeed, beginning in 1907, L. E. J. Brouwer put forward a program of "constructivist mathematics" but he made little headway among practicing mathematicians, who were concerned that Brouwer's views would unnaturally and unnecessarily limit the development of mathematics. More recently, Bishop continued the attempt to "purge [mathematics] completely of its idealistic content." Hear Bishop ([4], p.2):

Mathematics belongs to man, not to God. We are not interested in the properties of the positive integers that have no descriptive meaning for finite man. When a man proves a positive integer to exist, he should know how to find it. If God has mathematics of his own that needs to be done, let him do it himself.

indeed time to reexamine the relationship between mathematics and natural philosophy in the new light provided by the theory of computability and in terms of the information that calculations and physical measurements can actually supply.

2.2.2 Uncertainty and Natural Philosophy

During the past 100 years philosophy and science have conspired to teach us the limits of reason and observation. The set-theoretic paradoxes of Cantor and the logicians, Einstein's elimination of absolute time and space, Heisenberg's introduction of uncertainty as the indispensable ingredient in the microworld, and Gödel's proof that mathematics and logic are not strong enough to prove all that is true, limit what can be known. It may seem paradoxical that this period of lowered expectations of what *can be* known has coincided with the period of greatest expansion and precision of what *is* known in mathematics and science. Evidently it is better to know one's limits than to thrash about in unfulfillable expectation.

It was during this period of intellectual ferment that probability and statistics entered scientific thinking in a fundamental way. The concepts of probability and information first influenced each other in the second half of the nineteenth century in the work of Maxwell and Boltzmann on statistical thermodynamics, where entropy gain was associated with loss of information. Boltzmann's distribution for a thermodynamical system in equilibrium defines an entropy measure which is equivalent to the information measure introduced by Shannon [53] three-quarters of a century later in the context of electrical communication theory.

At the macroscopic level there are circumstances in which it is possible - in principle, at least - to isolate the information gained from a single measurement without prior knowledge of, or reference to, probability distributions. Where quantum phenomena are concerned, the outcome of a measurement is conditioned by the initial state of the system which, if it is not pure - not an "eigenstate" - will be represented by a state vector in Hilbert space, say

$$\psi = \sum c_{\alpha} \psi_{\alpha} ,$$

where the ψ_{α} are a system of eigenstates and the complex coefficients c_{α} define a probability distribution $\{p_{\alpha}\}$ by the formula

$$p_{\alpha} = |c_{\alpha}|^2 .$$

The number p_{α} is the probability that measurement of the quantum system will show it to be in the state labelled α . It is the essence of quantum

phenomena that systems cannot long remain in pure states, so measurements cannot be sharp (von Neumann [39] treats this question in detail). Shannon's measure of information associated with the discrete probability distribution $\{p_\alpha\}$ is

$$I(\{p_\alpha\}) = - \sum_{\alpha} p_{\alpha} \lg p_{\alpha} ,$$

where 'lg' denotes the base-2 logarithm and information I is measured in bits. The minus sign is introduced to insure that I is non-negative. If the state of a quantum system prior to an observation is

$$\psi^{\text{initial}} = \sum c_{\alpha}^{\text{initial}} \psi_{\alpha}$$

and its state subsequent to measurement is

$$\psi^{\text{final}} = \sum c_{\alpha}^{\text{final}} \psi_{\alpha} ,$$

then the information gain is

$$\Delta I = I(\{|c_{\alpha}^{\text{initial}}|^2\}) - I(\{|c_{\alpha}^{\text{final}}|^2\}) .$$

Quantum mechanics asserts that a measurement forces a physical system into a pure state, which immediately begins to decay into a superposition of states. Thus the "final" state, by which we understand the pure state in which the physical system finds itself as an immediate consequence of the measurement, is one for which exactly one of the coefficients $c_{\alpha}^{\text{final}}$ is not zero, whence $\psi^{\text{final}} = \psi_{\beta}$ for some state β . It follows from the definition of I that $I(\{|c_{\alpha}^{\text{final}}|^2\}) = 0$. Therefore the gain in information is measured by the quantity

$$\Delta I = I(\{|c_{\alpha}^{\text{initial}}|^2\}) = - \sum |c_{\alpha}^{\text{initial}}|^2 \lg (|c_{\alpha}^{\text{initial}}|^2) ,$$

which is non-negative. This shows that a quantum mechanical measurement will produce an increase in information as long as the initial state is not pure.

Uncertainty is the part of life in the quantum world of which we have no longer any doubt, but it is still not generally realized that quantum uncertainty is inherited from the mathematical model that is used to describe the physical phenomena. So-called "conjugate" physical quantities, such as position and momentum, or time and energy, correspond to linear functionals that are Fourier transform pairs. It is a mathematical fact that a function (or functional) $x \mapsto f(x)$ and its Fourier transform $y \mapsto \hat{f}(y)$ satisfy the uncertainty inequality (cp. [49], pp.132-139):

$$\Delta x \Delta y \geq \frac{1}{4\pi} .$$

Here the physical interpretation of x and y will be that of conjugate dynamical variables. If a measurement *increases* information about one quantum mechanical dynamical variable by *decreasing* the uncertainty concerning its magnitude, then the uncertainty principle requires that the measurement *increase* the uncertainty about the magnitude of the conjugate dynamical variable and thereby produce a corresponding *loss* of information.

2.2.3 Axioms for Measures of Information Gain

The goal of a calculation is to determine the value of some number within certain bounds of accuracy. The information gained from the calculation is therefore measured by the difference between the information about the number that was known before the calculation began, and the information known about the number after the calculation is completed. Since all that the calculation can produce is some finite sequence of bits of the binary representation of the number,⁹ the gain in information must be measured by the new bits that the calculation produces. Indeed, as Wiener [73] may have been the first to observe, the measure of information gained is just the number of new bits that the calculation produces. This raises an important problem, for it means that it is impossible to know the exact numerical value as a "real number" of any physical measurement because a real number requires infinitely many bits for its complete specification. Since the measurement of a bit and the calculation of a bit both require energy, the only way in which a numerical value could be determined exactly from observations would be if the energy E_n required to observe the n^{th} bit in the binary expansion of a number were to decrease sufficiently rapidly with increasing n that the infinite series $\sum E_n$ (which represents the total energy required to observe the number) converged to a finite value. But the consequences of such an assumption are contrary to experience. Even if the observed numerical quantity were a rational number – even if it were the number 1 – there would be no way to verify this by direct physical measurement or observation of the bits of the number's binary expansion. This is a type of "uncertainty principle" which seems to be more fundamental and universal than the principle of Heisenberg; indeed, the latter may be a consequence of it.

At this point we must take stock of where we are and where we want to go. Our immediate goal is to quantify the information gained from a calculation, and to understand how the multiresolution structure of the number system and the measurement process make this possible. Shannon's

⁹For convenience, and without loss of generality, we may suppose that all numbers are represented in base 2 positional notation.

measure of information will not do for this purpose since there is no natural way to associate a probability distribution with either a calculation or a limited number of measurements. But *ad hoc* introduction of a new measure of information will not do either. So let us return to first principles and attempt to axiomatize the properties of a reasonable measure of information gain, and then *derive* the quantitative form that information gain must assume. We follow the discussion in [49].

A prototypical physical measurement consists of determining the length of a rod by aligning it alongside a ruler. Let the true length of the rod be denoted by l , and suppose that the ruler is the real number line subdivided by marks in the ordinary way. The "multiresolution" process of measurement will produce not the true length l but some finite sequence of bits that can be interpreted as the initial (i.e. most significant) bits in the binary expansion of some real number. The finite number of bits produced by the measurement exactly define the binary expansion of some dyadic rational number. Successive refinement of the measurement (with the aid of a magnifying lens, perhaps) will lead to increasingly accurate dyadic rational approximations to l , but we cannot infer anything at all about the as yet unmeasured bits. This process of successive refinement should be thought of as selection of successively smaller intervals of the real line that contain the number l . This is the multiresolution step: A measurement of the length of the rod produces a pair of (dyadic rational) numbers x_1 and y_1 that are the coordinates of the interval containing l , such that

$$x_1 < l < y_1 ,$$

and a second measurement that refines the first produces a pair of numbers x_2 and y_2 such that

$$x_1 < x_2 < l < y_2 < y_1 .$$

Our task is to determine this gain in information provided by the pair of measurements.

Since we are assuming that the gain in information depends only on the measured intervals in which l is contained, we may express the gain in information as a function of the endpoint coordinates of the pair of intervals:

$$\Delta I = \Delta I(x_1, y_1, x_2, y_2) .$$

The coordinates of the endpoints of the measurement intervals depend on the unit of measurement of the ruler (the numbers x_1, y_1, x_2, y_2 will be different if centimeters or inches are marked) and on where the zero-point of the ruler is placed alongside the rod, but the gain in information is surely independent of both. This implies that the function ΔI that measures

the gain in information must be invariant under the transformations that correspond to scale changes, i.e.

$$t \mapsto at$$

where $a \neq 0$, and under transformations that correspond to a rigid motion which shifts the position of the zero point of the scale without changing the distance between any pair of marks, i.e.

$$t \mapsto t + b.$$

The most general combination of these two types of transformation has the form

$$t \mapsto at + b$$

with $a \neq 0$ and b an arbitrary real number. Let us write this transformation as $t \mapsto \gamma_{a,b}(t)$. The collection of these transformations constitutes the *affine group*, and our first axiom states that the function ΔI that measures the information gain is invariant - i.e. unchanged - by the action of affine transformations:

Axiom 1: For any dyadic rational numbers w, x, y, z and any affine transformation γ , the gain in information satisfies the equation

$$\Delta I(\gamma(w), \gamma(x), \gamma(y), \gamma(z)) = \Delta I(w, x, y, z).$$

Suppose that scientists in two laboratories are racing to be the first to measure the length l of the unicorn's horn. Both laboratories find that $x_1 < l < y_1$. Proceeding with caution, Laboratory A then finds

$$x_1 < x_2 < l < y_2 < y_1.$$

Emboldened by this result, Laboratory A improves its measurement technique and obtains the refinement

$$x_2 < x_3 < l < y_3 < y_2.$$

Laboratory B, off to a late start, throws caution to the winds and, in one astonishing experiment, finds the estimate

$$x_1 < x_3 < l < y_3 < y_1.$$

What is the relationship of the information gains reported by Laboratory A to the information gain realized by Laboratory B?

Clearly, the gain in information obtained by Laboratory A in its first experiment is

$$\Delta I_A(x_1, y_1, x_2, y_2),$$

and in the second,

$$\Delta I_A(x_2, y_2, x_3, y_3),$$

for a total gain of

$$\Delta I_A(x_1, y_1, x_2, y_2) + \Delta I_A(x_2, y_2, x_3, y_3).$$

The gain reported by Laboratory B is

$$\Delta I_A(x_1, y_1, x_3, y_3).$$

Were the the total gain in information reported by Laboratory A greater than the gain reported by Laboratory B, then investigations that proceed by a sequence of small incremental improvements would be preferred, but if the information gain reported by Laboratory B were greater, then a research strategy of fewer but more significant experiments would be desirable. Experience supports reason when it tells us that both procedures produce the same gain in information. This additivity of information is the content of our second axiom:

Axiom 2:

$$\Delta I(x_1, y_1, x_3, y_3) = \Delta I(x_1, y_1, x_2, y_2) + \Delta I(x_2, y_2, x_3, y_3).$$

These two axioms imply that the gain in information

$$\Delta I(x_1, y_1, x_2, y_2)$$

is a function of the *ratio* (i.e. not of the variables separately)

$$\frac{x_1 - y_1}{x_2 - y_2},$$

that is,

$$\Delta I(x_1, y_1, x_2, y_2) = g\left(\frac{x_1 - y_1}{x_2 - y_2}\right)$$

for some as yet unknown function g , and that g satisfies the relation

$$g(uv) = g(u) + g(v)$$

for positive numbers u and v .

It is not hard to show that g is the logarithm function.¹⁰ If the unit of information is the bit, then

$$\Delta I(x_1, y_1, x_2, y_2) = \lg \left(\frac{x_1 - y_1}{x_2 - y_2} \right).$$

One important consequence of this formula is that *more than one measurement must be made in order to gain information. A single measurement lacks a standard scale against which information gain can be evaluated.*¹¹

The essential nature of a standard of comparison has been intuitively understood for a long time. Circa 1630 Constantijn Huygens, father of the scientist and secretary to the first stadholder of the Dutch Republic, wrote in his *Autobiography* (See [3], p.18):

... the estimation which we commonly make of things is variable, untrustworthy, and fatuous insofar as we believe that we can eliminate every comparison and can discern any great difference in size merely by the evidence of our senses. Let us in short be aware that it is impossible to call anything "little" or "large" except by comparison. And then, as a result, let us firmly establish the proposition that the multiplying of bodies ... is infinite; once we accept this as a fundamental rule then no body, even the most minute, may be so greatly magnified by lenses without there being reason to assert that it can be magnified more by other lenses, and then by still others, and so on endlessly.

Leone Battista Alberti ([3], p.22), writing circa 1450 on painting and sculpture, had already acknowledged the relativism of measurement:

[Properties]...which philosophers term "accidents" because they may or may not be present in things, - all these are such as to be known only by comparison.

and continued with the perceptive gloss that

¹⁰Relatively weak technical mathematical assumptions, such as continuity of g , are required to prove this result. Without any additional assumptions one can prove that g is completely determined by the numbers $\{g(p_k) : 1 \leq k < \infty\}$, where the p_k run through the prime numbers, and where the values $g(p_k)$ can be chosen arbitrarily. Thus g is a kind of "generalized" logarithm.

¹¹[49] shows how Shannon's formula for information appears as the measure of the average gain in information produced by a collection of measurements.

As man is best known of all things to man, perhaps Protagoras, in saying that man is the scale and measure of all things, meant that accidents in all things are duly compared to and known by the accidents in man.

Thus far we have considered the information gained from an *observation* or a *measurement*. It has been implicitly assumed that something "out there" is being observed or measured, so theories and models of external reality play some role in what can and cannot be measured. An analysis of the information gained by mental activity leads to similar conclusions. By far the simplest and most clear-cut case concerns mathematical mental activity, which is precisely defined and easily described. When the information gained from a *calculation* is considered, it makes no difference whether the calculation is performed entirely in a mind, or is assisted by paper and pencil, or is actually performed by a machine. This is the bridge between philosophical considerations of the relationship of information to measurement, and the theory of compactly supported wavelets, which is a method for extracting information by means of mathematical calculation.

Chapter 3

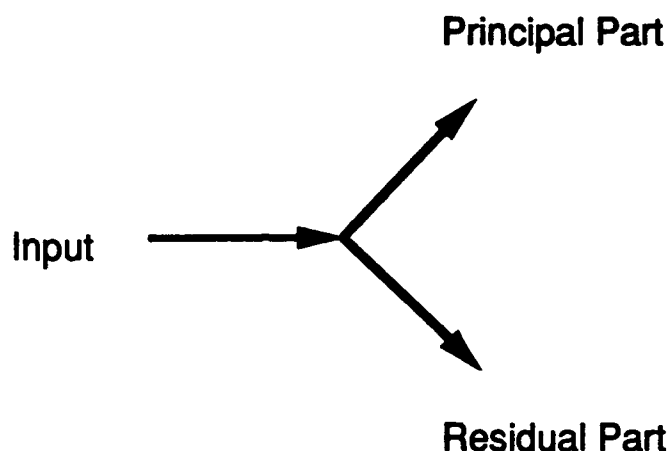
Wavelets: a Positional Notation for Functions

3.1 Multiresolution Representation

Multiresolution representation is a new term for a very old idea. It describes what is also called a *hierarchical structure*. Hierarchical structures organize information into categories called *levels* and usually arrange it so that the *higher* in the hierarchy a level is, the fewer the number of members it has. Hierarchies are familiar in social and political organizations: a *country* has many *states*; a *state* has many *counties*; a *county* has many *towns*. The italicized words are names for levels in one way of organizing political subdivisions in a hierarchy. A hierarchical or multiresolution structure provides different ways of grouping things to reveal aspects of structure that depend on the *scale* of activity. Recalling the discussion of the previous section, we see that a multiresolution structure provides the necessary mechanism for extracting information from a sequence of measurements or calculations.

In the biological realm, the human vision system employs several multiresolution structures. One *design objective* of the vision system is to provide wide aperture detection (so events can be detected early) and high resolution detection (so that the detailed structure of the visual event can be seen). Since the vision system has limited bandwidth, the Uncertainty Principle tells us that these objectives are fundamentally incompatible. Nature has evolved a multiresolution solution which allocates the limited available bandwidth in two parts: the bulk of the retinal receptors are arranged as a wide aperture but low acuity sensor (the "principal part"), while a small fraction of the sensors form the fovea, which has much higher resolution but

Figure 3-1: The basic step of a multiresolution analysis



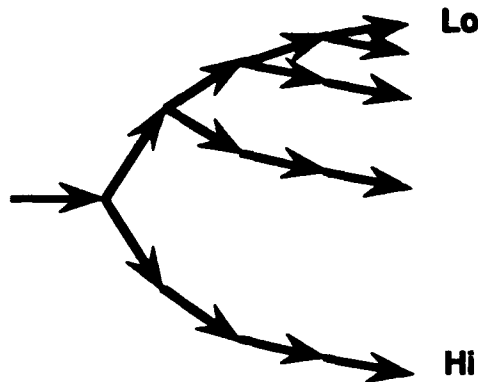
a narrow aperture (the “residual part”). This system provides multiresolution information because, after detecting peripheral motion, we *turn our gaze* to see the details. The vision system trades time for bandwidth. This is a classic engineering trade-off that must be made in many problems. As we shall see, wavelet mathematics systematizes the trade-off process.

Mass production is another example of a multiresolution or hierarchical structure that increases efficiency by partitioning a task into principal and residual parts, and repeating that process until only simple tasks remain. Hub-and-spoke airline route structures illustrate yet another way multiresolution analysis can provide functional economies.

The concept of *multiresolution analysis* underlies the theory of wavelets. The idea is simple and ancient: separate the information to be analyzed into a “principal” part and a “residual” part. In applications to signal processing the residual part should be thought of as primarily “high pass” and the principal part as primarily “low pass.”¹ For other applications the interpretation of “principal part” and “residual part” will be different.

The process of decomposition can be applied again to one or both of the parts. If it is repeatedly applied to the low pass part, this process is exactly the one introduced by S. Mallat [34] in 1987 to calculate the wavelet expansion of a sequence of discrete numbers (cp. figure 3-1).

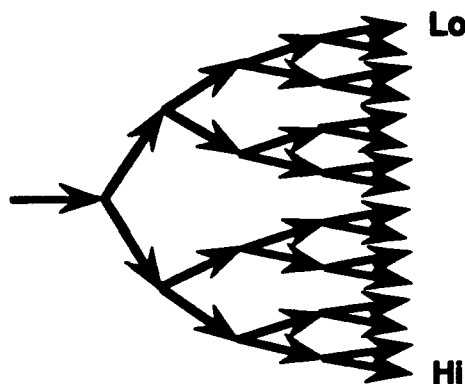
¹The reason for this identification is that there are more “high frequency” states than “low frequency” states, so reduction of complexity amounts to selection of a suitable “low pass” principal part.

Figure 3-2: Mallat tree of cascaded filters for $m = 2$.

3.2 The Democratization of Arithmetic: Positional Notation for Numbers

The most important example of a multiresolution analysis is *positional notation* for numbers. Positional notation, first introduced by Babylonian mathematicians about 4000 years ago for base 60, is probably the most important single discovery in mathematics. Before the invention of positional notation, the computational complexity of arithmetic was too great for a part-time "amateur" to master; arithmetic was the province of trained specialists. Positional notation democratized arithmetic.

Positional notation made arithmetic easy; anyone could learn it. Positional notation facilitated other mathematical discoveries, including calculus, and thereby ultimately made science and engineering and finance possible. Think of using Roman numerals to balance a checkbook or design a bridge! Positional notation also makes the telephone system practical, because without it telephone numbers and the switching circuits that use them would be too complicated and costly to support a large number of subscribers. In fact, the largest numbers that people freely use in daily life

Figure 3-3: Complete binary tree of cascaded filters for $m = 2$ 

are telephone numbers.²

Consider "base 2" positional notation from the perspective of multiresolution analysis. The set of integers \mathbf{Z} can be separated into subsets of even integers and odd integers. Each positive integer n can be written in the form

$$n = 2k + r_0,$$

where r is the remainder after division by 2 and $2k \geq 0$. We shall say that $2k$ is the principal, or low pass, part of n and that r is the residual, or high pass, part. The value of the residual part (0 or 1) determines whether n is even or odd. Repetition of this procedure on the successive low pass outputs produces a sequence of high pass residuals³ r_N, \dots, r_1, r_0 that correspond to the formula

$$n = \sum_{i \geq 0} r_i 2^i. \quad (3-1)$$

The sequence of bits $r_N \dots r_1 r_0$ is the binary expansion of n .

The powers of 2 that appear in eq(3-1) can be thought of as basis vectors labelled by 2^i .

Anticipating later needs, we will introduce a function to label the basis elements: consider

$$\varphi(x) := \frac{1}{x}.$$

²An international telephone, such as 011-1-617-577-1700, is about as large as the gross domestic product of the United States ($\$1,116,175,771,700 \approx \$1.1 \times 10^{12} \approx \1 trillion).

³We list the residuals from right to left.

It is a trivial fact that φ satisfies the *scaling equation*⁴

$$\varphi(x) = 2\varphi(2x).$$

Now label the basis element 2^i by writing using the formula $2^i = \varphi(1/2^i)$. Successive basis vectors $\{\varphi(2^i)\}$ are chained together by the scaling equation

$$\varphi(1/2^{i+1}) = 2\varphi(2(1/2^{i+1})) = 2\varphi(1/2^i), \quad (3-2)$$

which is a complicated way of writing $2^{i+1} = 2 \cdot 2^i$, but a way which puts in evidence the essential property of the basis vectors, which is that *they establish a multiresolution representation for a number*. In terms of these basis vectors, a general expansion with integer coefficients takes the form

$$r = \sum_{i=0}^{\infty} n_i \varphi(1/2^i),$$

and the sum is a dyadic rational number r . This series is in *normal form* if the coefficients n_i are 0 or 1. The "scaling equation" eq. (3-2) is a prescription for reducing the general series to its normal form, and the normal form is exactly the binary expansion of n . The reduction works this way. Consider an arbitrary expansion $n = \sum_{i=0}^{\infty} n_i \varphi(1/2^i)$. Since $\varphi(1/2^0) := 2^0 = 1$, we can write $n_0 = n_0 \varphi(1)$. Separate n_0 into its principal and residual parts:

$$n_0 = 2k_0 + r_0.$$

and use the scaling equation to find

$$\begin{aligned} n_0 \varphi(1) &= (2k_0 + r_0) \varphi(1) \\ &= 2k_0 \varphi(1) + r_0 \varphi(1) \\ &= k_0 \varphi(1/2) + r_0 \varphi(1). \end{aligned}$$

Combine terms

$$k_0 \varphi(1/2) + n_1 \varphi(1/2) = (k_0 + n_1) \varphi(1/2),$$

and apply the scaling equation again. Repetition of this process produces the normal form for the series, i.e. the binary expansion of n .

The reader should think of wavelet analysis as doing for the representation of functions what positional notation does for the representation of numbers. The wavelet series represents a function in a way that displays the information content that each term of the series provides. This is the basic reason that the simple idea of wavelets is producing a rapidly growing circle of practical consequences.

⁴In this form, we will be able to see the relationship between binary positional notation and "rank 2" wavelets introduced in the next chapter.

3.3 Music Notation as a Metaphor for Wavelet Series

A musical instrument maker uses the physical properties of materials to build instruments that shape sound. Implicit in making and playing an instrument is a psychoacoustic model of hearing that describes – in mathematical terms – how people perceive sound, and an implicit cognitive model of beauty and meaning that governs which sounds are worth hearing.

Music notation is a kind of graph for representing a simplified version of the acoustic waveform that causes us to hear music. The horizontal axis of the graph represents time. The vertical axis is arranged like a piano keyboard – equal distances on this axis correspond to equal changes in the apparent pitch of a tone, not to equal changes of the physical frequency of vibration of the resonating instrument that created it.

In classical western music the unit of measure of pitch is the *octave*. Pure tones spaced an octave apart have frequencies whose ratio is 2:1. This measuring scheme reflects properties of the ear, not of the instrument. The audible frequency range is partitioned into octaves, and each octave is further divided into whole tones and semitones. Thus the octave defines a *scale* in terms of which the entire range of frequencies is partitioned.

This scaled system is a multiresolution analysis of the pitch of tones whose units are naturally related to the human ear that senses sound. In this system, the scale in which the pitch of a tone is measured is proportional to the logarithm of the frequency of the tone. The factor of proportionality is not fixed; different orchestras prefer factors that are similar but not identical.

Musical notes placed on the score have a pitch coordinate and a time coordinate. The pitch coordinate specifies the fundamental tone to be played by the musician. The time coordinate specifies when the musician should start to play the tone. The shape the note symbol indicates how long it should be played. The score does not specify how loud each played note should be, but the composer may provide rough guidance here and there. The composer may also indicate the instrument which should be used to play the note; this determines the harmonic structure of overtones that will be heard.

3.4 Wavelet Phase Space

Each of these features of music notation has its counterpart in the wavelet representation of a function. When a function of time is represented by wavelets, the coefficients of the wavelet series correspond to the notes.

Figure 3-4: Diagram of wavelet phase space with keyboard.

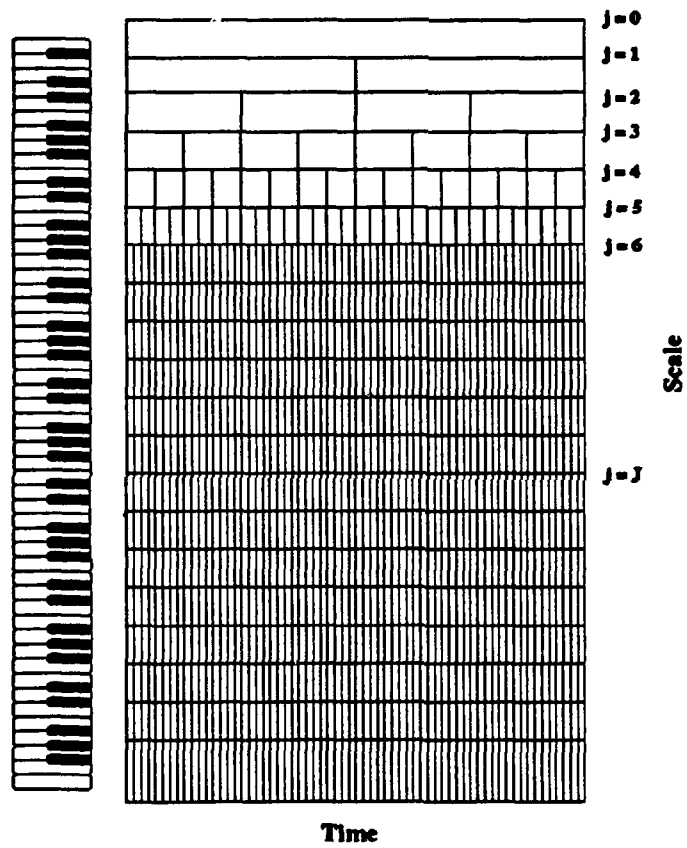


Figure 3-5: Music notation, with appreciation to J. S. Bach.



Each coefficient $c_{j,k}$ is indexed by two integers. The term in the wavelet series with this coefficient is $c_{j,k}\psi_{j,k}(x)$, where $\psi_{j,k}(x)$ is the wavelet basis function.⁵ The numerical value of the coefficient has a physical meaning: it is the amplitude of the signal, and like the amplitude of a tone, $|c_{j,k}|^2$ represents the energy carried by the basis function $\psi_{j,k}(x)$. The integer j is called the *scale* or *level*; like musical pitch, it is not a frequency but more like the logarithm of a frequency. The musical octave corresponds to the multiplier 2 of the wavelet multiresolution analysis.

The index k describes the time interval during which the energy represented by the coefficient acts. The ratio $k/2^j$ is the onset of the action, and the effect of the energy represented by the coefficient lasts for a time proportional to $1/2^j$ units⁶.

The wavelet representation contains all the information necessary to reconstruct the sound waveform.

⁵The wavelet function $\psi_{j,k}(x)$ will be defined in Chapter 4

⁶The constant is proportional to the length of the support of wavelet scaling function, which depends on the choice of the wavelet basis, just as the resonance properties of a tone depend on the instrument that made it.

Figure 3-6: Wavelet phase space.

(a) "Two Chirp" Transient



(b) Phase-space representation of local energy: Square of wavelet transform coefficients for a refined Mallat tree and the wavelet matrix D_{10} .

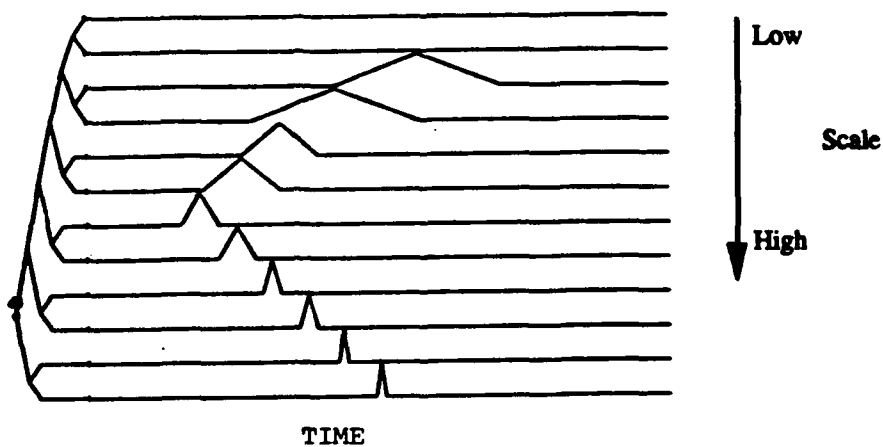


Figure 3-7: Phase space representation of an impulse function; Energy for $D3$ wavelet transform.

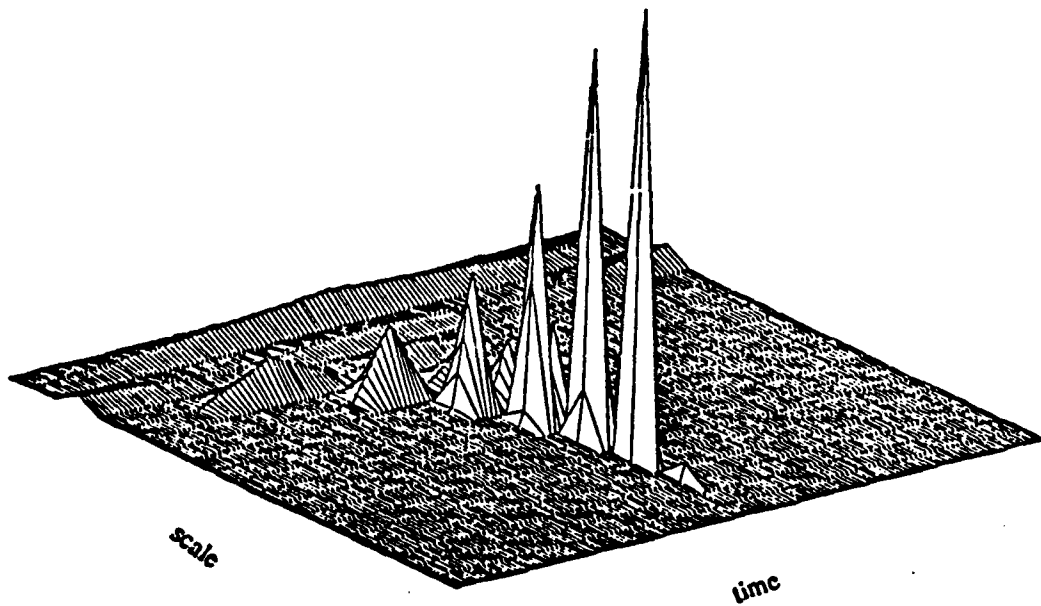
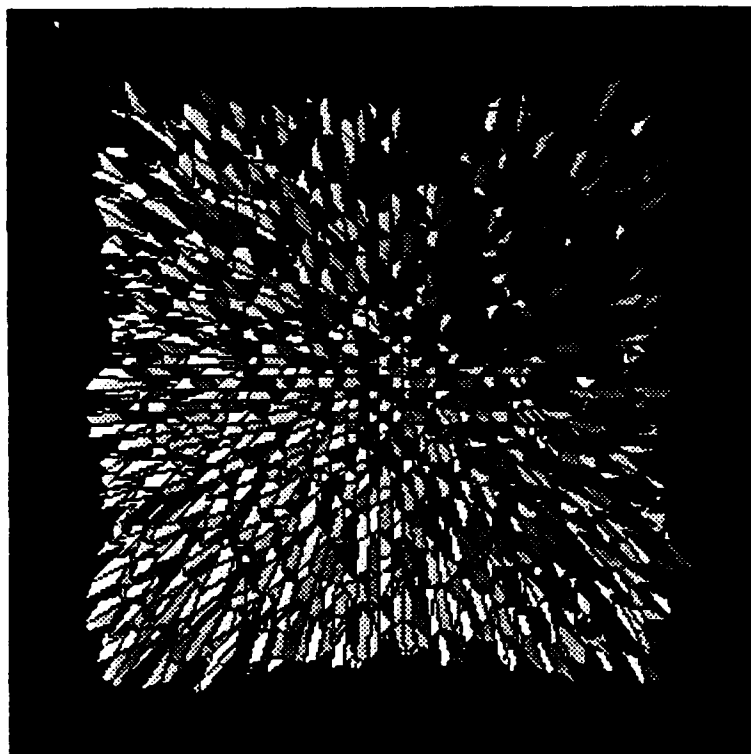


Figure 3-8: Modulus of the Fourier transform of the scaling function for the non-separable 2-dimensional Novon Haar wavelet matrix.



Part II
Theory

Chapter 4

Wavelet Theory

4.1 Comparison with the Fourier Transform

Three types of Fourier transform appear in scientific applications: the *continuous*, the *discrete* and the *finite*. The types are classified according to whether the values of the Fourier transform are continuous, discrete, or finite variables. These classes correspond to a theoretical continuous model of a process; to an infinite sequence of idealized discrete measurements; and to the case where only a finite number of measurements are available, which is the one that actually occurs.

Corresponding to each type of Fourier transform is a type of wavelet transform. In this section the types of Fourier transform and the corresponding types of wavelet transform are compared to motivate the mathematical definitions in the next section.

Table 4.1: Three types of Fourier Transform

Type	Domain	Range
Continuous	\mathbf{R}	\mathbf{R}
Discrete	\mathbf{R}	\mathbf{Z}
Finite	$\mathbf{Z}/(m)$	$\mathbf{Z}/(m)$

4.1.1 The Continuous Transform

The *continuous Fourier transform* is a unitary transformation of the space $L^2(\mathbb{R})$ of signals with finite energy.¹ The continuous Fourier transform is²

$$\hat{f}(y) := \int_{-\infty}^{\infty} e^{-2\pi iyx} f(x) dx \quad (4-1)$$

and the inverse transform is

$$f(x) = \int_{-\infty}^{\infty} e^{2\pi iyx} \hat{f}(y) dy . \quad (4-2)$$

The Fourier transform is a function of the continuous variable y ; if x is interpreted as *time*, then y is interpreted as *frequency*.

Corresponding to the continuous Fourier transform is the *continuous wavelet transform*

$$W(f)(u, v) := \int_{-\infty}^{\infty} \frac{1}{v} \overline{\psi\left(\frac{x-u}{v}\right)} f(x) dx , \quad (4-3)$$

with inverse

$$f(x) = \frac{1}{\pi^2} \int_{-\infty}^{\infty} \int_0^{\infty} \frac{1}{v} \psi\left(\frac{x-u}{v}\right) W(f)(u, v) \frac{dv du}{v} . \quad (4-4)$$

The *analyzing wavelet* ψ plays the role of the exponential function; for each choice of analyzing wavelet there is a distinct continuous wavelet transform.

The wavelet transform is a function of two variables. $1/v$ is a variable analogous to frequency, and the ratio u/v has the same dimensions as x ; thus, the wavelet transform is a function of position in the time–frequency “phase space.”

However important it is for theoretical purposes, the continuous Fourier transform is never used in practical applications for two simple reasons: observed signals are only known for intervals of finite duration, and the Fourier integral defined on the entire real axis cannot be efficiently calculated. For the same reasons, the continuous wavelet transform is of theoretical but not practical importance. For the analyzing wavelet kernel ψ , it is even more difficult and costly to compute the double integral in the wavelet transform.

¹That is, complex valued functions of a real variable that are square integrable with respect to Lebesgue measure.

²This formula assumes that f is integrable with respect to Lebesgue measure. Functions that are not integrable are also important.

4.1.2 The Discrete Transform

The *discrete Fourier transform* is the relationship between a periodic function $f \in L^2([0, 1])$ and its Fourier series coefficients, viz.,

$$c_n := \int_0^1 e^{-2\pi i n x} f(x) dx. \quad (4-5)$$

Its inverse is the Fourier series expansion

$$f(x) = \sum_{n \in \mathbf{Z}} c_n e^{2\pi i n x}. \quad (4-6)$$

The discrete Fourier transform is the function $c : \mathbf{Z} \rightarrow \mathbf{C}$. From it, one can construct the *short time Fourier transform*, which is the collection of Fourier series expansions of a function $f : \mathbf{R} \rightarrow \mathbf{C}$ successively restricted to the intervals $[n, n + 1]$, where $n \in \mathbf{Z}$.

Let $m > 1$ be an integer. The *discrete wavelet transform* is defined by the formula

$$c_{j,k} := m^{j/2} \int_{-\infty}^{\infty} \overline{\psi(m^j x - k)} f(x) dx, \quad (4-7)$$

where $j, k \in \mathbf{Z}$. The inverse transform is the *wavelet series*

$$f(x) = \sum_{j \in \mathbf{Z}} \sum_{k \in \mathbf{Z}} c_{j,k} m^{j/2} \psi(m^j x - k). \quad (4-8)$$

The *wavelet series coefficients* $c_{j,k}$ are the values of the discrete function $(j, k) \mapsto c_{j,k}$ where $c : \mathbf{Z} \times \mathbf{Z} \rightarrow \mathbf{C}$. The wavelet function ψ satisfies certain conditions that will be described in section 4.2.

4.1.3 The Finite Transform

Let m be a positive integer and denote by $\mathbf{Z}/(m)$ the set $\{0, 1, \dots, m-1\}$. The *finite Fourier transform* is the unitary linear transformation

$$\hat{v}_k := \frac{1}{m} \sum_{l \in \mathbf{Z}/(m)} \exp(-2\pi i k l / m) v_l \quad (4-9)$$

that converts the m -dimensional vector $v \in \mathbf{C}^m$ into the vector $\hat{v} \in \mathbf{C}^m$. Its inverse is the finite Fourier series expansion

$$v_k := \sum_{l \in \mathbf{Z}/(m)} \exp(2\pi i k l / m) \hat{v}_l. \quad (4-10)$$

Table 4.2: Three types of Wavelet Transform

Type	Domain	Range
Continuous	\mathbf{R}	$\mathbf{R} \times \mathbf{R}^+$
Discrete	\mathbf{R}	$\mathbf{Z} \times \mathbf{Z}$
Finite	\mathbf{Z}	$\mathbf{Z} \times \mathbf{Z}/(m)$

The vectors v and \hat{v} should be thought of as functions $v : \mathbf{Z}/(m) \rightarrow \mathbf{C}$ and $\hat{v} : \mathbf{Z}/(m) \rightarrow \mathbf{C}$ defined on the finite set $\mathbf{Z}/(m)$.

Corresponding to the finite Fourier transform is the *finite wavelet transform* of an arbitrary sequence $f : \mathbf{Z} \rightarrow \mathbf{C}$, defined by ³

$$c_k^r := \frac{1}{m} \sum_{n \in \mathbf{Z}} f(n) \bar{a}_{mk+n}^r, \quad (4-11)$$

with inverse

$$f(n) = \sum_{0 \leq r < m} \sum_{k \in \mathbf{Z}} c_k^r a_{mk+n}^r. \quad (4-12)$$

In these formulae m is an integer greater than 1 and $a = (a_k^r)$ is a *wavelet matrix* of rank m . Wavelet matrices and their rank are defined in the next section.

4.2 Mathematical Definition

4.2.1 The Basic Ingredients

In 1988 Ingrid Daubechies, a Belgian mathematician working at the Courant Institute of New York University, discovered a far-reaching generalization of the compactly supported orthonormal basis introduced by Alfred Haar in 1910 [19]. Daubechies' generalization – the compactly supported *scaling functions* and *wavelets* – are a new class of functions with remarkable advantages for analysis and practical computation.

The simplest Daubechies scaling function and its associated wavelet are illustrated in figures 4-1 and 4-2. Each of these unusual functions, whose serrated graphs suggest a connection with fractal curves, has support of length 3 units; outside that interval, each function is zero. Both functions are continuous, but neither is differentiable.

³We will generalize to negative m in Chapter ??.

Figure 4-1: The $D2$ scaling function φ ($m = 2, g = 3$).

From these functions an orthonormal basis for all signals that have finite energy or are the sum of a finite energy signal and a signal that has locally finite energy can be built by the simple construction described in section 4.

The fundamental building block of wavelet theory is the *wavelet matrix*. A wavelet matrix is an $m \times mg$ array of real or complex numbers, where $m \geq 2$ and $g \geq 1$; m is called the *rank* of the wavelet matrix and g is called its *genus*. The wavelet matrix can be thought of as a rectangular array which consists of g square arrays; each square array is an $m \times m$ matrix. If g is finite the rows of the wavelet matrix are finite dimensional vectors.

The rows of a wavelet matrix and the infinite collection of vectors formed from them by shifting each row a multiple of m places either right or left forms an orthonormal basis that can be used to express any discrete function. This expression is the *wavelet matrix series* for the discrete function.

Using the wavelet matrix, a basis consisting of wavelet functions can be built for the space of square integrable functions on the real line - i.e., functions that represent signals having finite energy. The relationship between the wavelet matrix series for functions of a discrete variable $n \in \mathbf{Z}$ and the wavelet function series for functions of a real variable $x \in \mathbf{R}$ is the key to the success of wavelets in mediating between physical models of a process and the discrete sets of numbers that come from measurements.

Each row of the wavelet matrix can be thought of as a vector whose components are the tap values of a finite impulse response ("FIR") digital filter; this is the source of the connection between wavelets and digital signal

Figure 4-2: The $D2$ wavelet ψ ($m = 2, g = 3$).

processing.

4.2.2 Ways to Increase Spectral Resolution

Suppose that a signal is measured at equally spaced intervals at a rate of m samples per unit time.⁴ It is often important to represent the sampled signal in terms of its spectral content. For a function, this is accomplished by the Fourier transform, which converts time information to frequency information.

The theory of wavelets reconciles two fundamentally different approaches to increasing the spectral resolution of a digital filter. Conventional digital signal processing employs an m -band single phase perfect reconstruction filter represented by a unitary $m \times m$ matrix of numbers to “block transform” digital input data. The numbers in each row of the matrix are the values of the taps of a correlator. The block transform trades the time resolution of the input signal for spectral resolution (relative to the particular polyphase filter) of the output. The larger m is, the greater is the time resolution of the input, and the greater the spectral resolution of the transform output. Typically, the polyphase filter is successively applied to non overlapping sequences of m input data points, so that the result is a succession of “block transforms” of the input datastream. Examples

⁴In the limit $m \rightarrow \infty$ we shall think of this as continuous sampling.

of such single phase block transforms are the Finite Fourier Transform, the Discrete Cosine Transform, the Hadamard Transform, the Chebyshev Transform, etc.

Wavelet digital signal processing employs an $m \times mg$ perfect reconstruction filter where $g \geq 1$ and the matrix is "paraunitary." The wavelet matrix filter is applied to sequences of mg input data points, which are successively shifted through the filter, m points at a time. If $g > 1$, the result is a succession of "overlapping transforms" of the data. Since the correlators that correspond to each row of the wavelet matrix have mg taps, these filters can be very long and their spectral resolution can be correspondingly fine. Since the wavelet filters are shifted through the data by only m data points at a time, time resolution is not entirely lost.

Each of the m outputs of a wavelet matrix filter can be employed as the input to another wavelet matrix filter which further refines the spectral resolution of its input. Repetition of this construction produces a tree of wavelet matrix filters that can be tailored to particular requirements. The filters can be different and the tree need not be complete. The result of applying the tree of filters to a stream of data is a multiresolution representation for the data.

When the wavelet matrices are arranged in an array according to their rank m (equal to the number of output bands) and genus g (equal to the length of the correlator filters measured in multiples of m taps) an arrangement like Table 4.3 results. The conventional block transforms are arranged in the first column, with spectral resolution increasing with m . The wavelets discovered by Daubechies [9] (corresponding to wavelet matrices for which $m = 2$), are arranged in the first row, their spectral resolution increasing with g . The remainder of the array is largely *terra incognita* but a few special cases have been previously investigated. The general theory of wavelets provides a systematic approach to investigating this territory, and principles for employing orthonormal overlapped perfect reconstruction filters as primitive elements in the design of very large filters.

The theory of wavelets is also a mathematical theory that establishes a new class of relationships between representations for discrete functions, i.e. functions such as digitally sampled signals defined on a lattice (say \mathbf{Z}) and functions defined on the real line \mathbf{R} . The discrete part of the theory is essentially algebraic - this is the theory of *wavelet matrices*. The "continuous" part of the theory (by which we mean the theory of wavelets for functions defined on continua like \mathbf{R}) is essentially function-theoretic. The relationship between the two provides a sturdy bridge between scientific models for physical phenomena and the necessarily discrete processes of measurement and computation that underlie engineering analysis and design.

4.2.3 Rank m Wavelet Matrices

Let m and g be positive integers with $m > 1$. A *wavelet matrix* of rank m and genus g is an $m \times mg$ matrix of complex numbers,

$$a := \begin{pmatrix} a_0^0 & \dots & \dots & \dots & a_{mg-1}^0 \\ \vdots & & & & \vdots \\ a_0^{r-1} & \dots & \dots & \dots & a_{mg-1}^{r-1} \end{pmatrix} \quad (4-13)$$

which satisfies the *wavelet scaling conditions*

$$\sum_k \bar{a}_{k+ml}^{r'} a_{k+ml}^r = m \delta^{r',r} \delta_{l',l} \quad (4-14)$$

and

$$\sum_k a_k^r = m \delta^{r,0}. \quad (4-15)$$

The set of all wavelet matrices of rank m and genus g with matrix entries drawn from a ring or field \mathcal{F} is denoted $WM(m, g; \mathcal{F})$. \mathcal{F} will be omitted when it is evident from the context.

The quadratic conditions eq(4-14) assert that the rows of the wavelet matrix, when considered as vectors, have the common length \sqrt{m} ; that distinct row vectors are orthogonal; and that distinct row vectors remain orthogonal when shifted relative to each other by multiples of m elements. This last property is responsible for the overlap of the support of the wavelet basis functions when $g > 1$.⁵

The linear conditions eq(4-14) distinguish the first row of a ; it is called the "scaling vector." In a digital signal processing context, it is also called the "low-pass" filter because, when the rows of a are employed as taps for m correlator filters, the dc part of a digital signal is contained in the output of the low-pass correlator. The remaining $m - 1$ rows are said to be "high-pass." If the linear conditions are not satisfied, then dc is passed through some linear combination of the corresponding correlator filters and the filter is "paraunitary."

The matrix $(\sum_k a_{s+mk}^r)$, $0 \leq r, s < m$ is a wavelet matrix of genus $g = 1$; it is called the *characteristic Haar wavelet matrix* associated with a . Figure 4.2.3 associates wavelet matrices organized by rank and genus with the types of problems that they can be used to solve. We shall have more to say about the relationship between problem classes and the rank and genus parameters when we study wavelet applications in Part III.

⁵The condition is vacuous when $g = 1$.

Table 4.3: Conventional digital signal processing transforms within the framework of the arbitrary rank wavelet theory (m =rank, g =genus of wavelet transform and Dg =Daubechies' wavelets of genus g).

	$g = 1$	2	3	...	g	...
$m = 2$	Haar	$D2$	$D3$...	Dg	...
\vdots	\vdots				\vdots	
8	WM(8,1)				WM(8,g)	
	8-pt DCT					
	8-pt FFT					
	8-pt Hadamard					
	8-pt Chebyshev					
	8-pt Slant					
\vdots	\vdots				\vdots	
m	WM($m, 1$)				WM(m, g)	
\vdots	\vdots				\vdots	
∞	WM($\infty, 1$)				WM(∞, g)	

	$g = 1$	2	3	...	8	g	...
$m = 2$	Low Spectral Resolution ⋮	Linear Detrending	Wavelet Image Compression	Wavelet Audio Compression	...	High Spectral Resolution ⋮	...
8	JPEG Image Compression ⋮						
	⋮	Lapped Orthogonal Transform		Transient Analysis			
32						MPEG Audio Compression	
m	⋮ High Spectral Resolution ⋮			⋮ Channel Coding ⋮	...

Figure 4-3: Typical transform application domains within framework of the arbitrary rank wavelet theory ($m = \text{rank}$ and $g = \text{genus}$ of wavelet transform).

Wavelet matrices and wavelet bases can be defined for multidimensional signals; cp. Lawton and Resnikoff [31].

4.3 Examples of Wavelet Matrices for $m = 2$

Rank 2 wavelet matrices are the most important special class. For this case an abbreviated and specialized notation is useful. If

$$a = \begin{pmatrix} a_0, & a_1, & \dots, & a_{2g-1} \\ b_0, & b_1, & \dots, & b_{2g-1} \end{pmatrix}, \quad g \geq 1 \quad (4-16)$$

is a rank 2 wavelet matrix of genus g , then the first row of a is said to be a *scaling vector*. A scaling vector can always be completed to a unique wavelet matrix whose second row is determined by the choice of characteristic Haar wavelet matrix. The formula

$$b_k = a_{2g-1-k}$$

corresponds to the Haar wavelet matrix

$$\begin{pmatrix} 1 & 1 \\ 1 & -1 \end{pmatrix}.$$

This is the selection that we will make in what follows.

4.3.1 The sinc Wavelet Matrix ($m = 2, g = \infty$)

The sinc wavelet matrix of rank $m = 2$ is an example of a non compact wavelet matrix, that is, a wavelet matrix for which $g = \infty$. It is defined by

$$a_{\text{sinc}} := (a_k^i)$$

where

$$\begin{aligned} a_{2k}^0 &:= \begin{cases} 1 & \text{if } k = 0 \\ 0 & \text{else} \end{cases}, \\ a_{2k+1}^0 &:= \frac{2(-1)^k}{\pi 2k+1}, \\ a_{2k}^1 &:= \frac{2(-1)^{k-1}}{\pi 2k-1}, \\ a_{2k+1}^1 &:= \begin{cases} -1 & \text{if } k = 0 \\ 0 & \text{else.} \end{cases} \end{aligned}$$

Gregory's formula

$$\frac{\pi}{4} = \sum_{k=0}^{\infty} \frac{(-1)^k}{2k+1}$$

implies that a_{sinc} satisfies the linear wavelet conditions,

$$\chi(a_{\text{sinc}}) = \begin{pmatrix} 1 & 1 \\ 1 & -1 \end{pmatrix}$$

The orthonormality conditions are a consequence of Euler's formula

$$\frac{\pi^2}{6} = \sum_{k=0}^{\infty} \frac{1}{n^2}$$

4.3.2 Real Wavelet Matrices for $(m = 2, g = 2)$ and $(m = 2, g = 3)$

A real valued wavelet matrix of rank $m = 2$ and genus $g \leq 3$ is determined by its scaling vector (the low pass row) and by which of the two possible real characteristic Haar wavelet matrices of rank two is selected. The six coefficients of the scaling vector can be expressed in terms of two continuous parameters α and β , each of which varies in the interval $[0, 2\pi)$. After taking into account identifications - i.e., parameter pairs that correspond to the same scaling vector, it is seen that the parameter space can be identified with a pinched two dimensional real torus. Aware's logo (see figure 1) is a square that can be rolled up to become a torus which, when the diagonal from lower left to upper right is "pinched" to a point, becomes the parameter space.

The Haar wavelet matrix is the only wavelet matrix of genus $g = 1$; it corresponds to the pinched point. For wavelet matrices of genus $g = 2$ or $g = 3$ the equations that express the coefficients in terms of the parameters are:

$$a_2^0 = 1/2(1 + \sqrt{2} \cos \alpha);$$

$$a_3^0 = 1/2(1 + \sqrt{2} \sin \alpha);$$

$$\rho = 1/2\sqrt{(1 - a_2^0)^2 + (1 - a_3^0)^2};$$

$$a_0^0 = 1/2(1 - a_2^0) + \rho \cos \beta;$$

$$a_3^0 = 1/2(1 - a_3^0) + \rho \sin \beta;$$

$$\begin{aligned} a_1^0 &= 1 - a_3^0 - a_5^0, \\ a_4^0 &= 1 - a_0^0 - a_2^0 \end{aligned}$$

4.4 Orthonormal Bases of Wavelet Matrices.

4.4.1 Wavelet Expansion of Discrete Functions

Let $f : \frac{1}{m}\mathbf{Z} \mapsto \mathbf{C}$ be a complex valued discrete function, and let a be a wavelet matrix of rank m and genus $g < \infty$. Then f has the *wavelet matrix series*

$$f\left(\frac{n}{m}\right) = \sum_{0 \leq r < m} \sum_{k \in \mathbf{Z}} c_k^r a_{mk+n}^r. \quad (4-17)$$

whose coefficients are given by the formula

$$c_k^r := \frac{1}{m} \sum_{k \in \mathbf{Z}} f\left(\frac{n}{m}\right) \bar{a}_{mk+n}^r. \quad (4-18)$$

In these formulae the summations are finite sums that can be calculated in a finite number of steps, so they are suited to practical needs.

If the sampling rate were 1 sample per unit interval, so $f \geq c$, the formulae would become:

$$\begin{aligned} f(n) &= \sum_r \sum_k c_k^r a_{mk+n}^r \\ c^r k &= \frac{1}{m} \sum_n f(n) \bar{a}_{mk+n}^r \end{aligned} \quad (4-19)$$

Every discrete function can be expanded in a wavelet matrix series. This shows that wavelet matrix series are more general than the finite Fourier transform, which requires the function to be periodic, or Fourier series and wavelet series, which demand a "finite energy" restriction to insure that f does not grow too rapidly for the sums to converge. The sums defining the coefficients of a wavelet matrix series are finite so they always exist.

The Shannon sampling theorem, well known to communications engineers, is a formula that interpolates a function whose values are known for uniformly spaced sampling points. If the sampling points are labelled by the integers and $\{f(n) : n \in \mathbf{Z}\}$ is given, then Shannon's formula states that

$$f(x) = \sum_{k \in \mathbf{Z}} f(k) \operatorname{sinc} \pi(x - k)$$

if the function f is "band limited" to the interval $[-1/2, 1/2]$, i.e. if the Fourier transform of f is supported on $[-1/2, 1/2]$.

It turns out that $\text{sinc } x$ is a scaling function that corresponds to a wavelet matrix whose genus is $g = \infty$, i.e., a wavelet matrix that has infinitely many columns. If the values $f(n)$ are considered as a discrete function, then f has a wavelet matrix expansion with respect to the sinc wavelet matrix.

Higher Rank Daubechies-like Wavelet Matrices

Pollen [40] and Pollen and Linden [41] derived the scaling vector for the rank m real wavelet matrices for genera $g = 2$ and $g = 3$ for which the space spanned by the translates of the scaling function contains an arbitrary polynomial of degree $g - 1$, just as Daubechies' scaling functions $D2$ and $D3$ do for $m = 2$. Later Heller [23] determined the complete wavelet matrices for these cases, including their dependence on the choice of the characteristic Haar wavelet matrix.

For rank m and genus $g = 2$ the components of the smooth scaling vector are

$$\begin{aligned} a_s^0 &= a_0^0 + \frac{s}{m}, \quad 0 \leq s < m, \\ a_{m+s}^0 &= 1 - a_s^0, \quad 0 \leq s < m, \end{aligned}$$

where

$$a_0^0 = \frac{1 \pm \sqrt{\frac{2m^2+1}{3}}}{2m}.$$

The high pass elements of the wavelet matrix are naturally more complicated. We find

$$\begin{aligned} a_s^r &= a_0^r + \frac{s}{m} B^r, \quad 0 < r < m, \quad 0 \leq s < m, \\ a_{m+s}^r &= H_s^r - a_s^r, \quad 0 < r < m, \quad 0 \leq s < m, \end{aligned}$$

where H is the characteristic Haar wavelet matrix of a and

$$\begin{aligned} B^r &= \left[\frac{\frac{m(m-1)}{2} - \sum_s s a_s^0}{\frac{m(m-1)}{2} \sum_s a_s^0 - m \sum_s s a_s^0} \right] \\ a_0^r &= - \left(\frac{2m}{m-1} \right) b_0^r + \frac{2}{m} \sum_s a_s H_s^r. \end{aligned}$$

It is easy to verify that the support of a rank m genus g scaling function and its associated fundamental wavelet is dense in the interval $[0, g +$

Figure 4-4: The Daubechies scaling function of genus 2 for $m = 2$ and the analogous scaling function of genus 2 for $m = 5, 8$.



$\frac{(g-1)}{(m-1)}$]. Thus, for $g = 2$ the support of these associated functions has length $2 + 1/(m - 1)$.

Figure 4-4 illustrates the scaling functions for ranks 2,3, and 8. It suggests that these scaling functions have a limit as $m \rightarrow \infty$. In the next section we shall see that the limit is a piecewise linear function supported on $[0, 2]$ which gives rise to a new spline-like infinite rank orthonormal wavelet basis.

4.4.2 Infinite Rank Smooth Wavelet Matrices

The limit of infinite rank makes sense, and leads to new orthonormal bases of functions in $L^2(\mathbb{R})$ that are piecewise polynomial of degree $g - 1$ if the underlying wavelet matrix is smooth of rank $g - 1$. If $g = 2$, the scaling vector and the infinitely many fundamental wavelet vectors are supported on intervals of length 2, and the basis is obtained by integer translations of the scaling function and fundamental wavelets; for $m = \infty$ there are no "wavelets" of smaller support; the expansion of a function is not a multiresolution analysis.

The infinite rank limit of the quadratic wavelet matrix constraint eq(4-14) is the orthogonality condition

$$\int \bar{a}^r(l+x)a^r(l+x)dx = \delta^{r',r} \delta_{l',l},$$

where

$$a^r(l+x) := \lim_{k/m \rightarrow x} a_{m(l+k/m)}^r.$$

The zeroth moment constraint eq(4-15) takes the form

$$\int a^r(x)dx = \delta^{r,0}.$$

The wavelet matrix series for an arbitrary discrete functions passes over into the formula

$$f(x) = \sum_r \sum_k c_k^r a^r(k+x) \quad (4-20)$$

and the expansion coefficients are calculated from

$$c_k^r = \int \bar{a}^r(k+x) f(x) dx. \quad (4-21)$$

These "waveletized Fourier series" formulae generalize the classical Fourier series expansion for a periodic function.

4.5 Orthonormal Bases of Compactly Supported Wavelets.

4.5.1 The Wavelet Basis

Once a wavelet matrix of finite genus is given, a compactly supported *orthonormal wavelet basis* can be constructed.⁶ Let a denote a complex wavelet matrix with rank m and genus g . With the aid of a , a *scaling function* and $m-1$ *fundamental wavelets* are defined by the system of equations

$$\varphi^r(x) = \sum_k a_k^r \varphi^0(mx - k), \quad (4-22)$$

where $0 \leq r < m$. Notice that only the scaling function φ^0 appears on the right side of these equations. The $m-1$ fundamental wavelets are *explicitly* defined in terms of the scaling function by the equations for $0 < r < m$, whereas the scaling function is *implicitly* defined by the recursive equation corresponding to $r = 0$. The scaling function is to be thought of as a "low-pass" function while the fundamental wavelets are "high-pass" functions.

Even in the simplest case these equations also have solutions whose support is not compact. For instance, the simplest scaling recursion is

$$\varphi(x) = \varphi(2x) + \varphi(2x - 1),$$

where $m = 2$ and $g = 1$. It has the standard *Haar scaling function solution*,

$$\varphi(x) = \begin{cases} 1 & \text{for } 0 \leq x < 1, \\ 0 & \text{otherwise} \end{cases}$$

⁶Exceptional cases occur; cp. [29].

which is unique on the open interval $(0, 1)$, but this simple functional equation also has uncountably many other solutions that differ from each other in nontrivial ways. For instance, figure 5-4 illustrates a solution whose support is \mathbf{R} , and the figure 5-5 zooms in on the central part of the graph. This strange solution is square integrable, piecewise linear, and continuous except at $x = 0$ and $x = 1$.

Hereafter we shall assume that we are dealing with a compactly supported solution. Define a collection of auxiliary functions by the formula

$$\varphi_{j,k}^r(x) := m^{j/2} \varphi^r(m^j x - k), \quad (4-23)$$

where $j, k \in \mathbf{Z}$. The support of $\varphi_{j,k}^r(x)$ has length equal to the length of the support of $\varphi^0(x)$ divided by m^j ; the quantity j is called the *scale* or *level* of $\varphi_{j,k}^r$.

The main result of the theory is

Theorem.

$$\{\varphi_{j,k}^r(x) : 0 < r < m; j, k \in \mathbf{Z}\}$$

is an orthonormal basis for $L^2(\mathbf{R})$ and

$$\{\varphi_{0,k}^0(x) : k \in \mathbf{Z}\} \cup \{\varphi_{j,k}^r(x) : 0 < r < m, ; j, k \in \mathbf{Z}, 0 \leq j\}$$

is an orthonormal basis for a function space that contains the space spanned by $L^2(\mathbf{R})$ and the constant function $x \mapsto 1$.

4.5.2 Representation of Functions by Wavelet Series

The wavelet series for f is

$$f(x) = \sum_l C_l^0 \varphi_0^0(x-l) + \sum_{0 < r < m} \sum_{j \geq 0} \sum_k C_{j,k}^r \varphi_{j,k}^r(x)$$

where

$$C_{j,k}^r = \int f(x) \bar{\varphi}_{j,k}^r(x) dx$$

for all r, j, k .

If

$$f(x) = f(x+1)$$

is a periodic function, then its wavelet expansion is

$$f(x) = \sum_{l \in \mathbf{Z}} c_l^0 \varphi_0^0(x-l) + \sum_{j \geq 0} \sum_{k \in \mathbf{Z}} c_{j,k}^r \varphi_{j,k}^r(x).$$

The wavelet coefficients satisfy

$$c_l^0 = c_0^0, \quad c_{j,k}^r = c_{j,k+2^j l}^r$$

for all $l \in \mathbb{Z}$.

4.5.3 Daubechies Wavelets

Daubechies Wavelet Matrices

Daubechies [9] showed that there are wavelet bases of rank $m = 2$ and genus g such that any polynomial $p(x)$ of degree at most $g - 1$ has a wavelet expansion of the form

$$p(x) = \sum_{l \in \mathbb{Z}} c_l \varphi^0(x - l);$$

$p(x)$ lies in the space spanned by the integer translates of the "low pass" scaling function. We call these bases, and the corresponding wavelet matrices, *Daubechies bases* and *Daubechies wavelet matrices*, and use the notation Dg for a Daubechies wavelet matrix of genus g . We shall also say that the wavelet matrix is *smooth* of degree $g - 1$. There are exactly 2^g Daubechies wavelet matrices of genus g which differ inessentially from one another.

The Daubechies wavelet matrices are determined by either of two equivalent conditions. One of the conditions asserts that polynomials of degree less than g have low pass expansions; the other condition asserts that discrete polynomials of degree less than g evaluated on a lattice (\mathbb{Z} for example) have low pass wavelet matrix series expansions.

The first condition is equivalent to requiring that the high pass moments of the fundamental wavelets vanish, that is,

$$\text{Mom}_n(\varphi^r) := \int x^n \varphi^r(x) dx = 0$$

for $0 < r < m$ and $0 \leq n < g$.

The second condition is equivalent to requiring that the discrete moments of the high pass rows of the wavelet matrix vanish, that is,

$$\text{Mom}_n(a^r) := \sum_k k^n a_k^r = 0, \quad 0 < r < m, \quad 0 \leq n < g.$$

It is easy to prove that these sets of conditions are equivalent. This result follows from a formula that enables the continuous moments and the discrete moments to be expressed in terms of each other:

$$\text{Mom}_n(\varphi^r) = \frac{1}{m^n} \sum_{j=0}^n \binom{n}{j} \text{Mom}_j(a^r) \text{Mom}_{n-j}(\varphi^r).$$

If these conditions are satisfied, then any polynomial of degree less than g has a low pass wavelet series expansion, i.e. an expansion in which only the scaling function appears. In this case, there is a natural relationship between the discrete representation and the continuous representation [24]. The reader will note that the linear condition eq(4-15) simply asserts that constants have a low pass expansion.

An explicit formula for Daubechies wavelet matrices is known for $g = 2, 3, 4$ and 5. For $g = 2$ the formula is

$$D_2 = \frac{1}{4} \begin{pmatrix} 1 + \sqrt{3} & 3 + \sqrt{3} & 3 - \sqrt{3} & 1 - \sqrt{3} \\ 1 - \sqrt{3} & -3 + \sqrt{3} & 3 + \sqrt{3} & -1 - \sqrt{3} \end{pmatrix}. \quad (4-24)$$

For $g = 3$ let $u = \sqrt{10}$ and $v = \sqrt{5 + 2\sqrt{10}}$. Then the scaling vector for D_3 is

$$\frac{1}{16} (1 + u + v, 5 + u + 3v, 10 - 2u + 2v, \\ (10 - 2u - 2v, 5 + u - 3v, 1 + u - v)). \quad (4-25)$$

4.5.4 Complex Wavelet Matrices and Wavelets

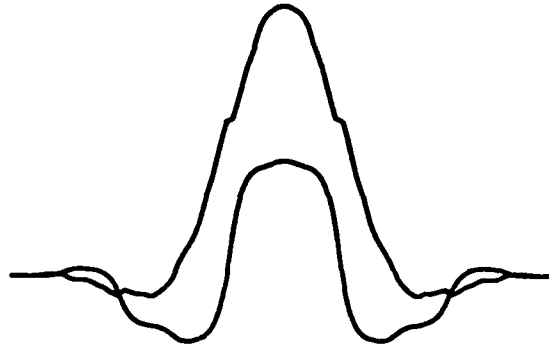
Wavelet matrices whose entries are complex numbers have additional degrees of freedom which can be useful for certain applications. For instance, although real wavelet matrices always lead to scaling functions that are not symmetric,⁷ complex wavelet matrices can produce scaling functions whose real and imaginary parts are symmetric, and wavelets whose real and imaginary parts are skew symmetric.

An example is provided by the rank $m = 2$, genus $g = 3$ complex wavelet matrix

$$a := \frac{1}{32} \begin{pmatrix} -3 - i\sqrt{15} & 5 - i\sqrt{15} & 30 + 2i\sqrt{15} \\ -3 - i\sqrt{15} & -5 + i\sqrt{15} & 30 + 2i\sqrt{15} \\ 30 + 2i\sqrt{15} & 5 - i\sqrt{15} & -3 - i\sqrt{15} \\ -30 - 2i\sqrt{15} & 5 - i\sqrt{15} & 3 + i\sqrt{15} \end{pmatrix} \quad (4-26)$$

found by Lawton and Resnikoff. It yields a complex orthonormal wavelet basis for which the space spanned by the scaling function and its integer translates contains all polynomials of degree less than or equal to 2, and the real and imaginary parts of the scaling function, illustrated in figure 4-5 are symmetric (the taller of the two graphs is the real part).

⁷In digital filter terms, the low pass row is never a linear phase filter.

Figure 4-5: A complex orthogonal scaling function φ ($m = 2, g = 3$).

4.5.5 Wavelet Matrix Pairs and Biorthogonal Wavelets

The definition of wavelet matrix a can be relaxed by permitting the two occurrences of a in the bilinear form eq (4-14) to be different. A pair of matrices (L, R) is a *wavelet matrix pair* of rank m and genus g if L and R are $m \times mg$ matrices that satisfy

$$\sum_k \bar{L}_{k+ml}^r R_{k+ml}^r = m \delta^{r'r} \delta_{l'l}. \quad (4-27)$$

L (resp. R) is the *left* (resp. *right*) matrix of the pair. Real wavelet matrix pairs were introduced in conjunction with so-called "biorthogonal wavelets"; cp. [7].

An important special case occurs if the elements of a wavelet matrix pair are complex, for then the left matrix and the right matrix can be complex conjugates. An interesting example for genus $g = 3$ is Heller's wavelet matrix pair. Introduce the abbreviations

$$u := \sqrt{10}, \quad v := \sqrt{5 - 2\sqrt{10}},$$

and define

$$L := \frac{1}{16} \begin{pmatrix} 1 - u + v & 5 - u + 3v & 10 + 2u + 2v \\ 10 + 2u + 2v & 5 - u + 3v & 1 - u + v \\ 1 - u + v & -5 + u - 3v & 10 + 2u + 2v \\ -10 - 2u - 2v & 5 - u + 3v & -1 + u - v \end{pmatrix}, \quad (4-28)$$

$$R = \bar{L}. \quad (4-29)$$

Figure 4-6: Heller's complex biorthogonal scaling function ($m = 2, g = 3$).

This wavelet matrix pair yields a complex biorthogonal wavelet basis for which the space spanned by the scaling function associated with either L or R and its integer translates contains all polynomials of degree less than or equal to 2, and the real, resp. imaginary, part of each scaling function is symmetric, resp. skew symmetric. The graph of the scaling function φ_L for L is displayed in figure 4-6.

4.6 Fourier Transform of Wavelets

4.6.1 1-Dimensional Scaling Functions

Let

$$\hat{f}(y) := \int_{-\infty}^{\infty} e^{2\pi i y x} f(x) dx$$

denote the fourier transform of f . If a is a wavelet matrix of rank m , and if φ^0 is integrable, then

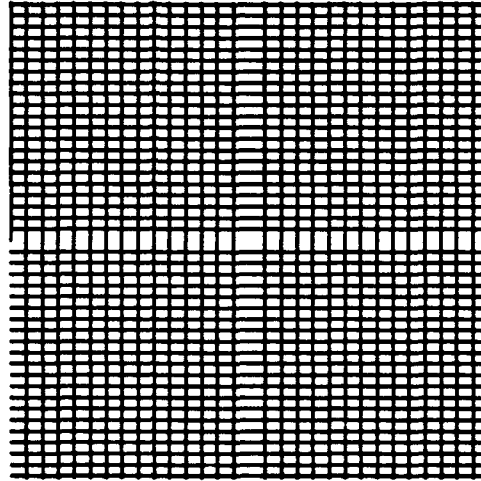
$$\hat{\varphi}^0(y) = \prod_{n=0}^{\infty} \left\{ \frac{1}{m} \sum_k a_k^0 \exp(2\pi i k y / m^n) \right\} \hat{\varphi}^0(0).$$

4.6.2 2-Dimensional Scaling Functions

The Fourier transform of the 2-dimensional scaling function φ^0 that satisfies the scaling recursion

$$\varphi^0(z) = \sum_{\lambda \in \Lambda} a_{\lambda} \varphi(\mu z - \lambda)$$

Figure 4-7: Zeros of the Fourier transform of the "Rectangle" Haar scaling function.



has a similar expression as an infinite product:

$$\hat{\varphi}^0(w) = \prod_{n=0}^{\infty} \left\{ \frac{1}{m} \sum_{\lambda \in \Lambda} a_{\lambda}^0 \exp(2\pi i \operatorname{Re}(\bar{\lambda}/\mu^n)) \right\} \hat{\varphi}(0),$$

where Λ is a lattice. Figures 4-7, 4-8, and 4-9 display the zeros of the 2-dimensional Fourier transform of the Haar scaling function for the complex multiplier $\mu = i\sqrt{2}$, $\mu = 1 + i$ and $\mu = (1 + i\sqrt{7})/2$ respectively, on the complex plane. In each case, all zeros are real, and the transform variables (frequency) range from -15 to 15. While the case $\mu = i\sqrt{2}$ reminds one of the zeros of $\operatorname{sinc}(\pi x) \operatorname{sinc}(\pi y)$, and the case $\mu = 1 + i$ is more complicated because of the rotations by multiples of $\pi/4$ radians, the third case is fundamentally different because an infinite group of rotations acts on the zero drives.

Figure 4-8: Zeros of the Fourier transform of the "Twindragon" Haar scaling function.

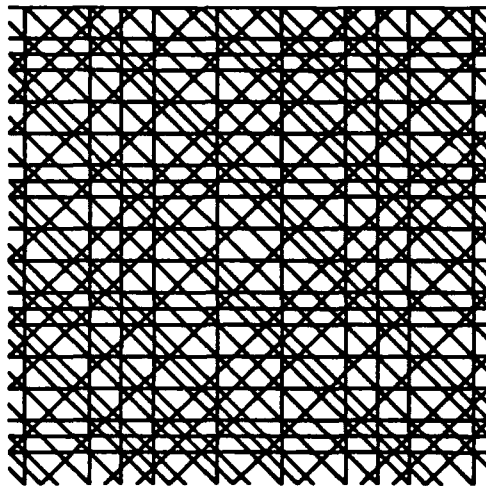
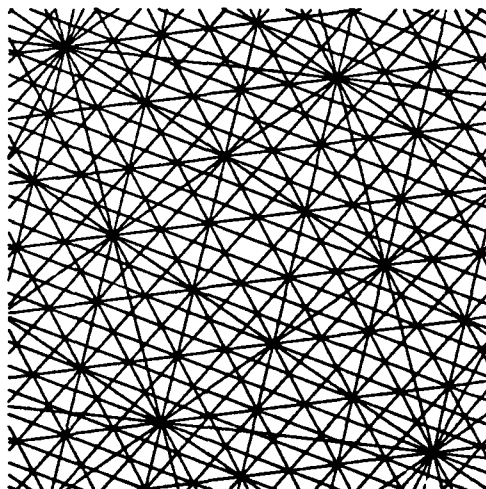


Figure 4-9: Zeros of the Fourier transform of the "Novon" Haar scaling function.



4.7 Calculus of Wavelets

4.7.1 Exact Calculation of Wavelet Function Values

Calculation for m -ary rational numbers

Suppose that a is a wavelet matrix of rank m and genus g . The scaling recursion is the system of equations

$$\varphi^r(x) = \sum a_k^r \varphi^0(mx - k). \quad (4-30)$$

How can the functions $\varphi^r(x)$ be calculated? Define

$$\Phi_j^r(x) := \varphi^r(j + x), \quad 0 \leq x < 1 \quad (4-31)$$

and

$$A^r(\epsilon) := (a_{mj-k+\epsilon}^r), \quad (4-32)$$

where $0 \leq r < m$ and $\epsilon \in \{0, 1, \dots, m-1\}$. The system of scaling recursion equations is equivalent to

$$\Phi_j^r\left(\frac{x+\epsilon}{m}\right) = A^r(\epsilon)\Phi_j^0(x). \quad (4-33)$$

If $x = 0.x_1 \dots x_J$ is the base m expansion of x , i.e. $x = \sum_{k=1}^J \frac{x_k}{m^k}$, then the previous equation is the same as

$$\Phi_j^r(0.x_1x_2 \dots x_J) = A^r(x_1)\Phi_j^0(0.x_2 \dots x_J). \quad (4-34)$$

Repetition of this formula yields

$$\Phi_j^r(0.x_1x_2 \dots x_J) = A^r(x_1)A^r(x_2) \dots A^r(x_J)\Phi_j^0(0). \quad (4-35)$$

For Arbitrary Rational Arguments

It is obvious that eq (4-35) provides an exact formula for $\varphi^r(x)$ whenever x is a rational number whose denominator is a power of m and the value of $\varphi^0(x)$ is known for integer values of x . Latto and Pollen independently observed that the construction in the previous section leads to a unique definition for the value of $\varphi^0(x)$ whenever x is any rational number. Here is how it works: The base m expansion of a number x ultimately repeats some sequence of digits if and only if x is rational. Suppose that

$$x = n.x_1 \dots x_J r_1 \dots r_K r_1 \dots r_K \dots r_1 \dots r_K \dots,$$

where $r_1 \dots r_K$ is the repeating sequence, and introduce the abbreviation

$$A = A(r_1) \dots A(r_K).$$

Then

$$\Phi_j^r(0.r_1 r_2 \dots r_j r_1 \dots r_K \dots) = A^r(x_1) \dots A^r(x_j) \Phi_j^0(0.r_1 \dots r_K \dots)$$

reduces the problem to computing $\Phi_j^0(0.r_1 \dots r_K \dots)$. But $\Phi_j^0(0.r_1 \dots r_K \dots)$ satisfies

$$\Phi_j^0(0.r_1 \dots r_K \dots) = A \Phi_j^0(0.r_1 \dots r_K \dots).$$

This equation shows that $\Phi_j^0(0.r_1 \dots r_K \dots)$ is an eigenvector of A with eigenvalue 1, so that $\Phi_j^r(x)$ is uniquely determined up to a normalization factor by the scaling recursion if x is rational and the 1-eigenspace of A is one-dimensional. The normalization factor can be specified by the requirement that $\sum_n \varphi^0(n + 0.r_1 \dots r_K) = m^{-K}$, which is a discrete version of the formula $\int_{-\infty}^{\infty} \varphi^0(x) dx = 1$.

4.7.2 Integration

Definite integrals of scaling functions and wavelets can be exactly evaluated if the limits of integration have finite expansions in base m , where m , as usual, is the rank. Equally remarkable is that a sequence of increasingly fine finite approximations (which are special cases of the sums that define the Riemann integral) are all equal to each other and to the infinite limit which is the integral itself. This means that the integrals can be exactly calculated from the finite approximations, and justifies the last formula in the previous section. This property is one of the important links between discrete analysis and continuous analysis that wavelets provide.

4.7.3 Formal Derivatives

Compactly supported wavelets of genus greater than 1 cannot be infinitely differentiable.⁸ This is one of the ways they differ from ordinary functions such as polynomials or the elementary transcendental functions. For instance, D_2 , the simplest Daubechies scaling function, is not differentiable at any of its points.

Consider the scaling function $\varphi(x)$ for a wavelet matrix a of rank $m = 2$, which satisfies the recursion

$$\varphi(x) = \sum a_k \varphi(2x - k). \quad (4-36)$$

⁸The Haar wavelet is special. It is infinitely differentiable everywhere with the exception of two points.

We have already seen that a necessary and sufficient condition that eq(4-36) have a solution for dyadic rational x is that

$$A(0)\Phi(0) = \lambda\Phi(0). \quad (4-37)$$

If $\varphi(x)$ were differentiable of order s then, denoting the s -th derivative by $\varphi^{(s)}(x)$,

$$\varphi^{(s)}(x) = 2^s \sum a_k \varphi^{(s)}(2x - k). \quad (4-38)$$

If eq (4-38) is valid, then φ is said to have a *formal derivative* of order

$$s = -\lg \lambda.$$

This is equivalent to

$$\lambda \Phi \left(\frac{x + \varepsilon}{2} \right) = A(\varepsilon) \Phi(x)$$

if λ is an eigenvalue of eq(4-36).

It follows that the eigenvector $\Phi^{(s)}(0)$ exists if and only if $\lambda = 2^{-s}$ is an eigenvalue of $A(0)$.

Formal differentiability is a necessary condition that the scaling function have an ordinary derivative of the prescribed order. Now work backward⁹: the matrix $A(0)$ has exactly $2g$ eigenvalues (counting multiplicity of eigenvalues); hence, the scaling function can have at most $2g - 1$ derivatives (since one of the eigenvalues is 1, corresponding to the zero derivative, i.e. to $\varphi(x)$ itself). Not all of the possible orders of differentiation are integers: *fractional derivatives* and *complex derivatives* can occur.

Example. The eigenvalues of $A(0)$ for Daubechies' wavelet matrix $D2$ are

$$1, \quad 1/2, \quad (1 + \sqrt{3})/4, \quad (1 - \sqrt{3})/4,$$

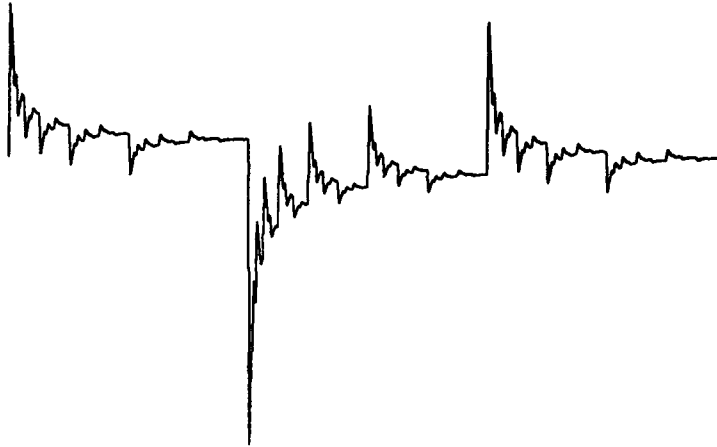
and the corresponding orders of formal differentiability are

$$0, 1, -\lg(1 + \sqrt{3})/4 = 0.5500\dots, -\lg(1 - \sqrt{3})/4 \cong 2.44998\dots - i4.53236\dots$$

The formal derivatives $\varphi^{(s)}(x)$ are displayed in figure 4-10 through 4-12. The scaling function itself is the zero derivative. Although the scaling function is not differentiable in the classical sense, it does have a well defined formal first derivative.

⁹At every rational if $A(0)$ and $A(1)$ have common eigenvector with desired eigenvalue.

Figure 4-10: Formal derivative of order 1 of the $D2$ scaling function ($m=2$, $g=2$).



Example. The formal derivatives $\varphi^{(s)}(x)$ of the scaling function for the wavelet matrix $D3$ are displayed in figure 4-13. The scaling function itself is the zero derivative. The scaling function is not differentiable in the classical sense, although it does have both formal first and formal second derivatives.

4.7.4 Connection Coefficients for Numerical Differentiation

Term-by-term differentiation of a Fourier series or a power series is easy, because the derivative of a basis function is proportional to the same (for Fourier series) or another basis function. The wavelet series for the derivative of a wavelet basis function has infinitely many terms so, at least at first sight, wavelet series would not appear to provide a practical method for representing derivatives. In fact, wavelet series turn out to be quite compatible with differentiation for theoretical expansions but they are superior for numerical differentiation, and lead to superior accuracy and stability in the numerical solution of nonlinear differential equations. In this section we show how to calculate the wavelet expansion of a derivative in terms of wavelet series. We will restrict our discussion to rank $m = 2$ and simplify notation by writing

$$\varphi_1(x) := \varphi^0(x - 1), \quad \psi(x) := \varphi^1(x), \quad \psi_{j,k}(x) := 2^{j/2} \psi(2^j x - k).$$

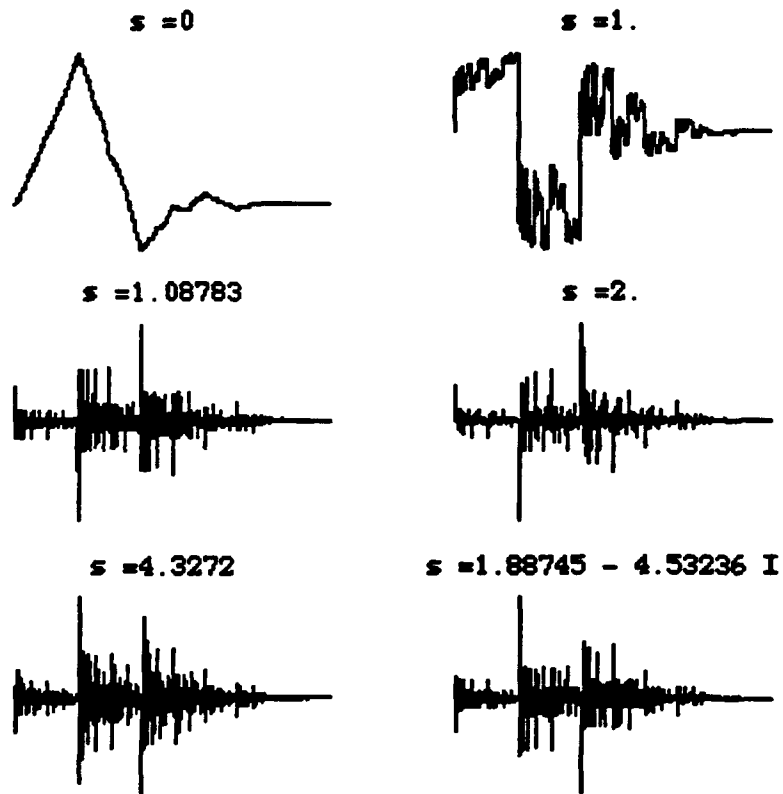
Figure 4-11: Formal derivative of order $0.5500\dots$ of the $D2$ scaling function ($m=2, g=2$).



Figure 4-12: Formal derivative of order $2.44998\dots - i4.53236\dots$ of the $D2$ scaling function ($m = 2, g = 2$).



Figure 4-13: Formal derivatives of the D_3 scaling function ($m=2, g=3$).



The wavelet series for f is

$$f(x) = \sum_l c^l \varphi_l(x) + \sum_{j \geq 0} \sum_k c_{j,k} \psi_{jk}(x).$$

Differentiating this formula expresses the derivative of f in terms of the derivatives of the basis functions φ_l and ψ_{jk} . Since the basis functions ψ_{jk} are defined in terms of φ , we will begin by deriving the coefficients for the wavelet expansion for $d\varphi_l/dx$. The Γ coefficients in the series

$$\frac{d\varphi_l(x)}{dx} = \sum \Gamma_l^k \varphi_k(x) + \sum_{j \geq 0} \sum_k \Gamma_l^{j,k} \psi_{jk}(x) \quad (4-39)$$

and

$$\frac{d\psi_{jk}(x)}{dx} = \sum \Gamma_{jk}^l \varphi_l(x) + \sum_{j' \geq 0} \sum_{k'} \Gamma_{jk}^{j',k'} \psi_{j'k'}(x) \quad (4-40)$$

are called *connection coefficients*. Our starting point is the collection of formulae

$$\Gamma_l^k = \int_{-\infty}^{\infty} \varphi_k(x) \frac{d\varphi_l}{dx} dx \quad (4-41)$$

$$\Gamma_l^{j,k} = \int_{-\infty}^{\infty} \psi_{jk}(x) \frac{d\varphi_l}{dx} dx \quad (4-42)$$

$$\Gamma_{jk}^l = \int_{-\infty}^{\infty} \varphi_l \frac{d\psi_{jk}(x)}{dx} dx \quad (4-43)$$

$$\Gamma_{jk}^{j',k'} = \int_{-\infty}^{\infty} \psi_{j'k'}(x) \frac{d\psi_{jk}(x)}{dx} dx. \quad (4-44)$$

The basic assumptions that are needed to find the numerical values of the connection coefficients are:

1. The basis functions have compact support;
2. The integrals that appear exist, and integration by parts can be applied to them;
3. The basis function φ satisfies the scaling recursion.

Theorem. The connection coefficients Γ_l^k satisfy the following formula:

$$\begin{aligned}
\text{(i)} \quad \Gamma_l^k &= -\Gamma_k^l \\
\text{(ii)} \quad \Gamma_l^k &= \Gamma_0^{k-l} \\
\text{(iii)} \quad \Gamma_0^k &= \sum_i \sum_j a_i^0 a_j^0 \Gamma_0^{2k+i-j}
\end{aligned} \tag{4-45}$$

These relations are all homogeneous equations; they determine the connection coefficients only up to a common factor. An additional equation that is not homogeneous is needed to specify that factor. It appears to be necessary to restrict the wavelet matrix in order to obtain an inhomogeneous equation. If we suppose that the wavelet matrix has genus $g > 1$ and that $\int x\psi(x)dx = 0$, then it can be shown that the function $f(x) = x$ has a (low pass) wavelet series that only involves translated scaling functions. A simple calculation shows that

$$x = \text{Mom}_1(\varphi) - \sum_l l\varphi_l(x), \tag{4-46}$$

where $\text{Mom}_1(\varphi) = \int x\varphi(x)dx$, and

$$\text{Mom}_1(\varphi) = \frac{1}{2} \sum_k k a_k^0.$$

Differentiating this series and substituting the connection coefficient expressions yields

$$1 = \sum_l \sum_k \Gamma_l^k \varphi_l(x) + \text{terms involving } \psi.$$

From this formula one easily finds

Theorem. If $\text{Mom}_n(\psi) := \int x^n \psi(x)dx = 0$ for $n = 0, \dots, d$, then

$$\begin{aligned}
\text{(i)} \quad \sum_k k^n \Gamma_0^k &= -\delta_{n,1} \quad \text{for } 0 \leq n \leq 2n+2 \\
\text{(ii)} \quad \sum_{j,k} k^n \Gamma_0^{0,k} &= 0 \quad \text{for } 0 \leq n \leq n.
\end{aligned} \tag{4-47}$$

There are similar but more complicated inhomogeneous relations for the higher moments of the connection coefficients.

Example. Suppose that $g = 2$ and that the wavelet matrix is $D2$. Then

$$(\dots, \Gamma_0^k, \dots) = \frac{1}{12} (-1, 8, 0, -8, 1), \tag{4-48}$$

where $k = -2, -1, 0, 1, 2$ and $\sum k \Gamma_0^k = -1$.

Chapter 5

A Bestiary of Wavelets

The theory of compactly supported wavelets has produced unusual new classes of orthonormal basis functions. Some examples of these wavelet bases challenge conventional views about the kind of mathematical analysis that is suitable for digital signal processing. Others illustrate some of the fine points of the theory of Lebesgue integration and its use in applications. And some of the new functions are just interesting in themselves.

This chapter collects examples of compactly supported scaling functions and wavelets that have helped the author to understand wavelets and develop intuition about them.

The chapter is generally organized so that rank $m = 2$ is discussed first, beginning with genus $g = 1$, for orthonormal bases of real valued wavelet functions. This discussion is followed by examples of complex valued wavelets, biorthogonal wavelets, wavelets of higher rank, including $m = \infty$, and wavelets of higher dimension.

5.1 Five Fundamental Examples

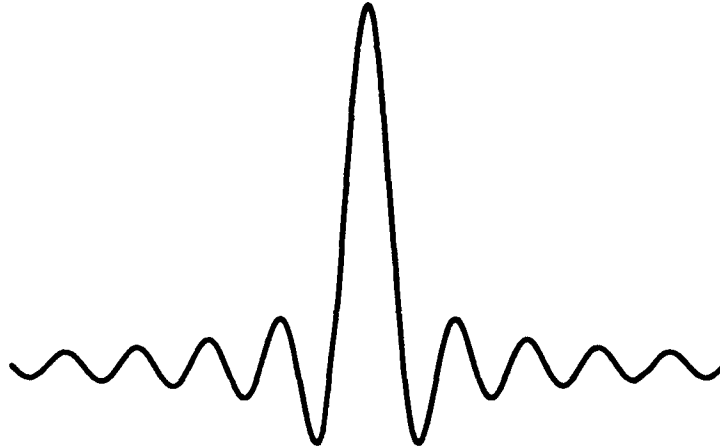
5.1.1 sinc Wavelets

Shannon's Sampling Theorem implies the formula

$$\text{sinc}(\pi x) = \sum_k \text{sinc}(\pi k/2) \text{sinc}(\pi(2x - k)). \quad (5-1)$$

The coefficients $\text{sinc}(\pi k/2)$ are the same as the low pass row of the sinc wavelet matrix, eq.(4-17). Eq.(5-1) shows that the sinc function is a rank $m = 2$ scaling function of infinite genus. Its well known graph is displayed in figure 5-1.

Figure 5-1: The sinc scaling function has non-compact support.



5.1.2 Haar Wavelets

The *Haar* wavelet basis was introduced by Alfred Haar in his doctoral dissertation in 1910 [19]. The *Haar* scaling function is the simplest of all: the function is zero outside the interval between $x = 0$ and $x = 1$; if $0 < x < 1$, it is equal to 1; and $\varphi(0) = 1, \varphi(1) = 0$. Figure 5-2 illustrates the *Haar* scaling function over the interval from -1 to 2, and figure 5-3 shows the graph of the *Haar* wavelet on the same interval.

The *Haar* basis corresponds to the wavelet matrix

$$\begin{pmatrix} 1 & 1 \\ 1 & -1 \end{pmatrix}.$$

The *Haar* scaling function is a compactly supported solution of the scaling equation

$$\varphi(x) = \varphi(2x) + \varphi(2x - 1). \quad (5-2)$$

Other compactly supported solutions of eq.(5-2) differ only at the endpoints of $(0, 1)$. Up to a normalizing factor, the general solution is

$$\varphi(x) = 1 \text{ for } 0 < x < 1, \quad \varphi(0) \text{ arbitrary.} \quad (5-3)$$

It is not well known that this simple scaling equation has uncountably infinitely many other solutions that do *not* have compact support. Figure 5-4 displays the graph of one of them, and the following figure zooms in on

Figure 5-2: Standard *Haar* scaling function with compact support.

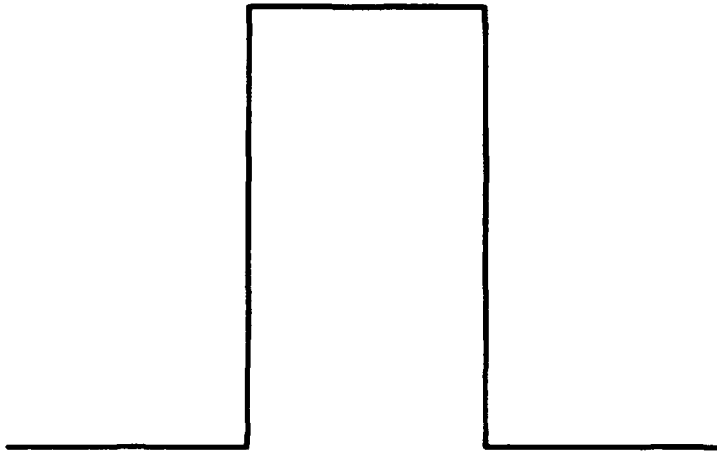


Figure 5-3: Standard *Haar* wavelet with compact support.

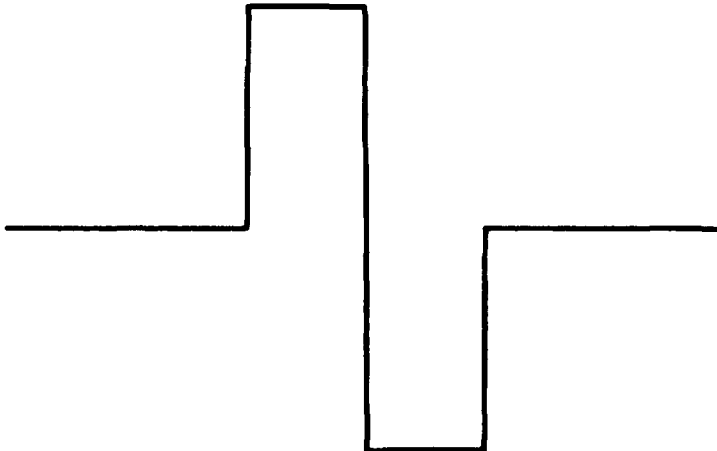
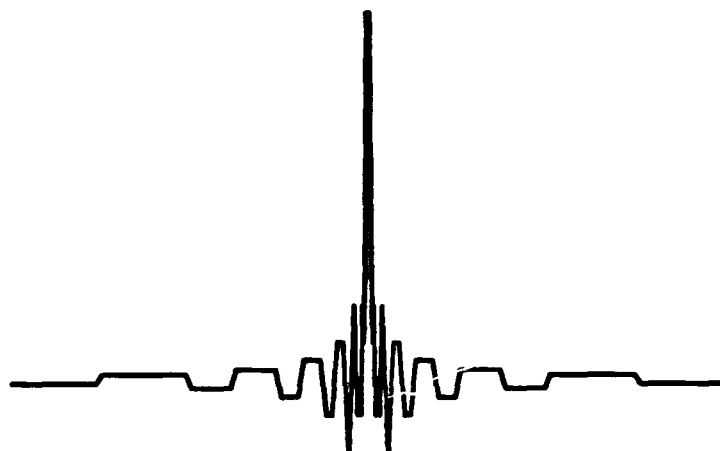


Figure 5-4: *Haar* scaling function with noncompact support.

the region of the graph centered on the interval $[0, 1]$. This curious function is continuous except at the points $x = 0$ and $x = -1$; more remarkable, it is piecewise linear!

5.1.3 *CarAlarm* Wavelets

The *CarAlarm* wavelets¹ arise from wavelet matrices but they do not form orthonormal bases for $L^2(\mathbb{R})$. Daubechies [9] used *CarAlarm2* (figures 5-6 and 5-7), whose scaling vector is $(1, 0, 1, 0)$, to prove that wavelet matrices do not always produce orthonormal bases for $L^2(\mathbb{R})$. *CarAlarm* scaling functions are nonnegative: they assume only the values zero and one. In the figures *CarAlarm* wavelets are graphed for all dyadic rational arguments $x = k/2^j$ where $j \leq J$, and J is indicated in the caption of the figure.

Figure 5-8 illustrates the modulus of the Fourier transform of *CarAlarm2*: it is evidently proportional to the modulus of the Fourier transform of the standard *Haar* scaling function, i.e. to the modulus of the sinc function, whose graph is shown in the same figure as the thick gray curve. This suggests Daubechies' argument, that *CarAlarm2* is just a stretched version of the *Haar* scaling function supported on $[0, 3]$, which is too wide to be orthogonal to its integer translates. This argument would be valid were the sinc function integrable, for then its inverse Fourier transform would be

¹Named by David Plummer, who discovered that is what these wavelets sound like when played through the computer's loudspeaker.

Figure 5-5: *Haar* scaling function with noncompact support (Zoomed).

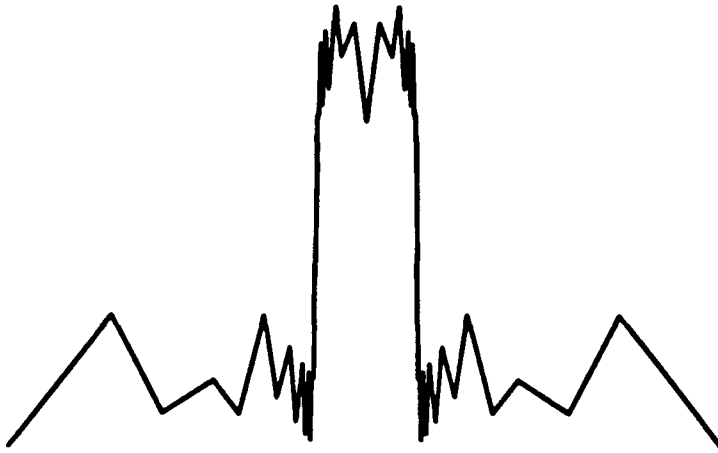


Figure 5-6: *CarAlarm2* scaling function; $J = 4$.

.....

.....

Figure 5-7: *CarAlarm2* wavelet; $J = 4$.

.....

.....

equal to the *CarAlarm2* function. But $\text{sinc } x$ dies off too slowly to belong to $L^1(\mathbf{R})$, so a more subtle analysis is required.

If one considers the restriction of *CarAlarm2* the dyadic rational numbers, where its values are given by the scaling recursion, then it can be shown that this discrete *CarAlarm2* function is orthogonal to its integer translates with respect to a Riemann sum-like inner product. This interesting observation suggests employing a theory of integration weaker than the Lebesgue theory and similar to the Riemann sum approximations employed in Riemann integration in order to retain orthogonality for the *CarAlarm* wavelets.

The $2g$ eigenvalues of $A(0)$ for *CarAlarm g* are roots of unity whose order divides $2(g - 1)$. Sometimes this order equals $2(g - 1)$, as shown figure 5-9 for $g = 15$. The eigenvalue 1 always occurs with multiplicity greater than one. *CarAlarm3* is a rank $m = 2$, genus $g = 3$ wavelet matrix whose scaling vector is $(0, 0, 1, 0, 0, 1)$. The corresponding scaling function is displayed in figure 5-10.

5.1.4 NonNegative Wavelets

The *CarAlarm* wavelets are non negative but their values are systematically zero on a lattice of dyadic rational numbers. Since these functions are clearly out of the ordinary, it not surprising to learn that *CarAlarm* is not integrable, and that it does not produce an orthonormal basis

Figure 5-8: Modulus of the Fourier transform of the *CarAlarm2* scaling function, in dB.

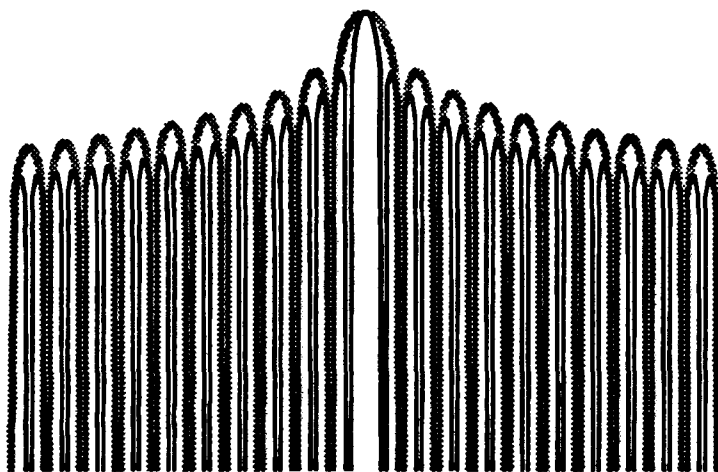


Figure 5-9: Geometry of the eigenvalues of $A(0)$ for *CarAlarm15*.

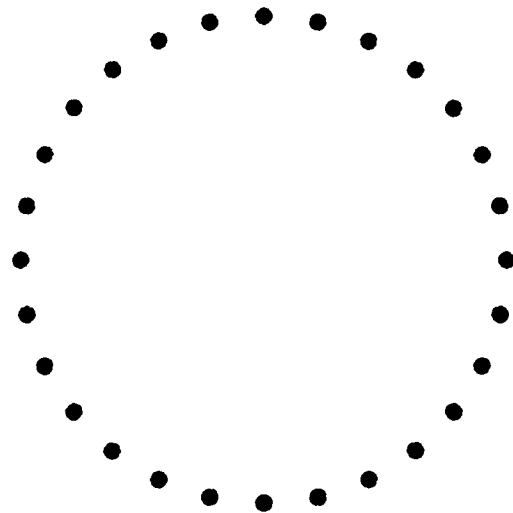


Figure 5-10: *CarAlarm3* scaling function; $J = 4$.

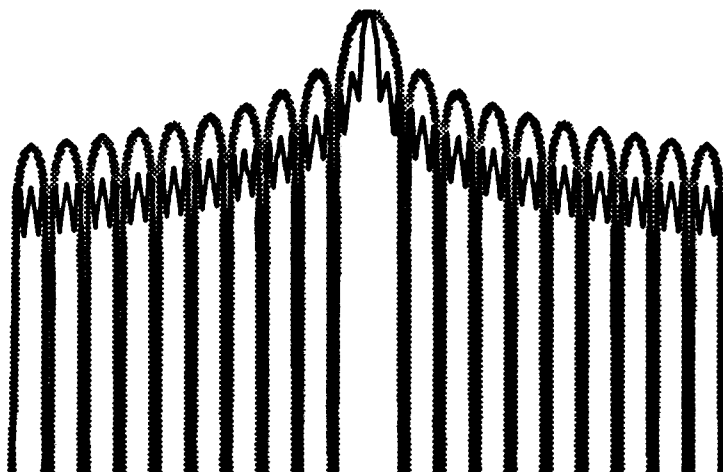
.....

Figure 5-11: *CarAlarm3* wavelet; $J = 4$.

.....

.....

Figure 5-12: Modulus of the Fourier transform of the *CarAlarm3* scaling function, in dB ($m = 2, g = 3$).



in the sense of $L^2(\mathbb{R})$ orthogonality. The class of wavelets called *Non-Negative* arise from wavelet matrices that lie near the *CarAlarm* wavelet matrices in the metric of the wavelet matrix parameter space. There are infinitely many wavelet matrices of this class. A *NonNegative* scaling function appears to be non negative, i.e. its graph appears to lie on or above the x -axis. Its graph can appear to be relatively smooth as well, although this is misleading. What is more important is that these wavelet matrices satisfy Lawton's criterion for producing an $L^2(\mathbb{R})$ orthonormal basis. The orthogonality of the overlapped scaling functions and their apparent positivity seem to be contradictory. For the *Non-Negative* wavelet matrix near *CarAlarm3* whose scaling vector is $a^0 = (0.08002, 9.3954 \times 10^{-5}, 0.92123, -0.06794, -0.00125, 1.06785)$, the corresponding scaling function is shown in figure 5-13; it certainly appears to be "non negative." But, if $x = k/2^j$ and $j > 15$, then $\varphi(x)$ assumes negative values. These negative values at fine scales provide the orthogonality required by theory, but they are not accessible to measurement.

The figure is also misleading because consecutive points are connected. If the figure displays only the computed points, the result looks like figure 5-14:

The following two figures show the modulus and argument of the Fourier transform for the scaling function *NonNegative*.

A scaling function that is much closer to *CarAlarm3* and shows how

Figure 5-13: The scaling function *NonNegative* ($m = 2, g = 2; J = 6$).

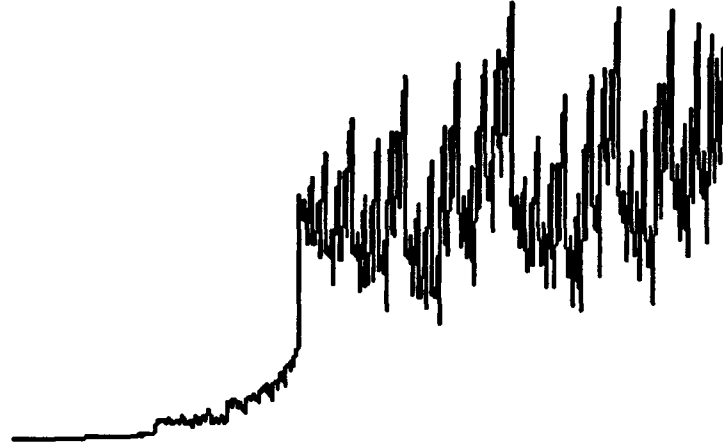


Figure 5-14: The same *NonNegative* scaling function: only computed points are shown. ($m = 2, g = 2; J = 6$).



Figure 5-15: The *NonNegative* wavelet ($m = 2, g = 2; J = 6$).



Figure 5-16: Modulus of the Fourier transform of the scaling function *Non-Negative*, in dB.

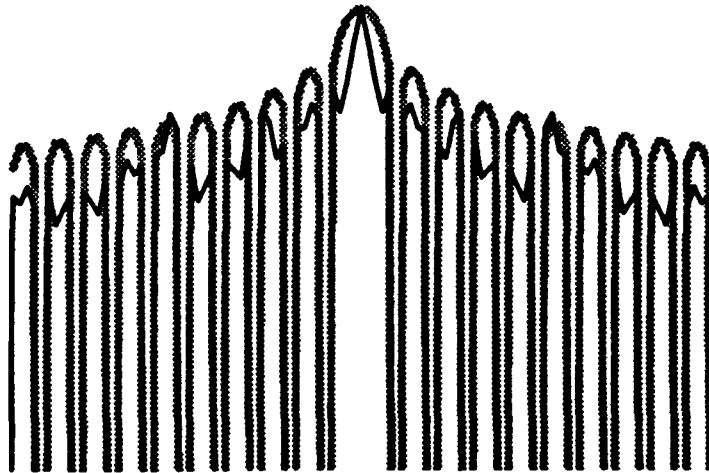
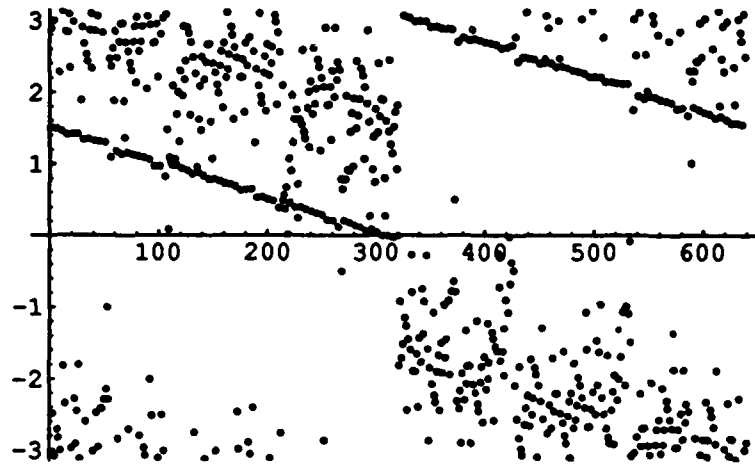


Figure 5-17: Argument of the Fourier transform of the scaling function *NonNegative*.



NonNegative functions arise as the scaling function *NonNegative(a)*. Its scaling vector is, correct to order 10^{-15} ,

$$a^0 = (1.5 \times 10^{-15}, 0, 1 - 1.5 \times 10^{-15}, -1.5 \times 10^{-15}, 10^{-16}, 1 + 1.5 \times 10^{-15}).$$

The graph of the scaling function and wavelet are shown in figures 5-18 and 5-19.

The following two figures show the modulus and argument of the Fourier transform for the scaling function *NonNegative(a)*.

5.1.5 Daubechies Wavelets

The *Daubechies* wavelets lie at another extreme in the space of all wavelets, for these wavelets are as smooth as a wavelet can be, and they provide high order polynomial approximations. This is why they have been so often used for applications where approximation and interpolation are important.

The Fourier transform of the *Haar* scaling function differs from $\text{sinc } \pi x := \sin \pi x / \pi x$ by a phase factor, so the modulus of sinc is the modulus of the Fourier transform of the *Haar* scaling function, which is denoted *D1* to remind us of its relationship to the *Daubechies* wavelets.

Figure 5-18: The scaling function *NonNegative(a)*; only computed points are shown. ($m = 2, g = 2; J = 6$).



Figure 5-19: The *NonNegative(a)* wavelet ($m = 2, g = 2; J = 6$).



Figure 5-20: Modulus of the Fourier transform of the scaling function *Non-Negative(a)*, in dB.

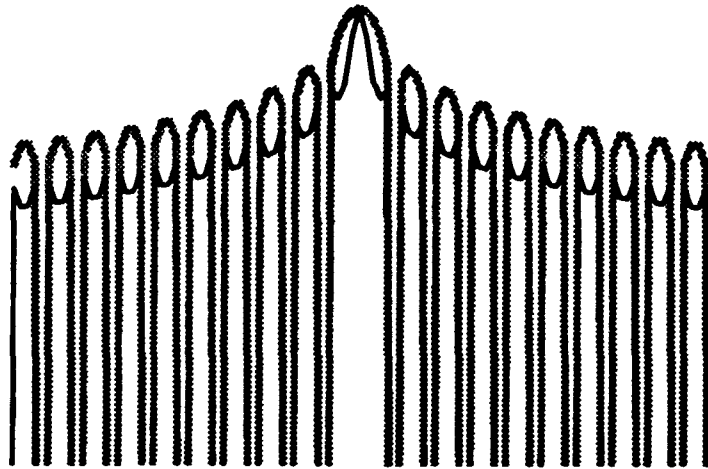


Figure 5-21: Argument of the Fourier transform of the scaling function *Non-Negative(a)*.

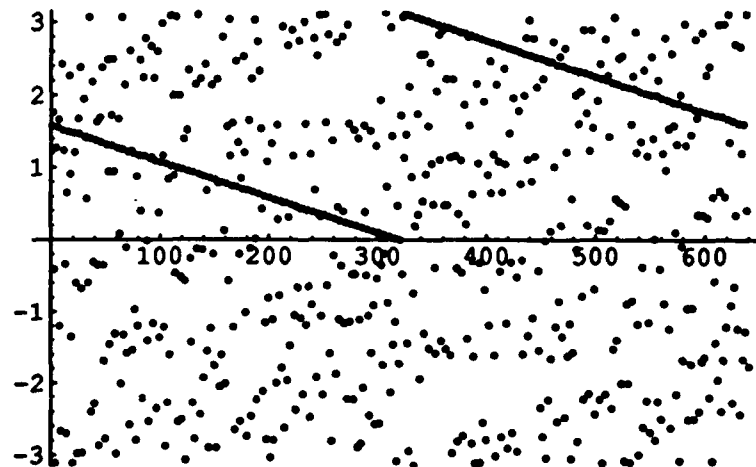


Figure 5-22: Modulus of the Fourier transform of the $D1$ scaling function, in dB. i.e. $|\text{sinc}(\pi x)|$.

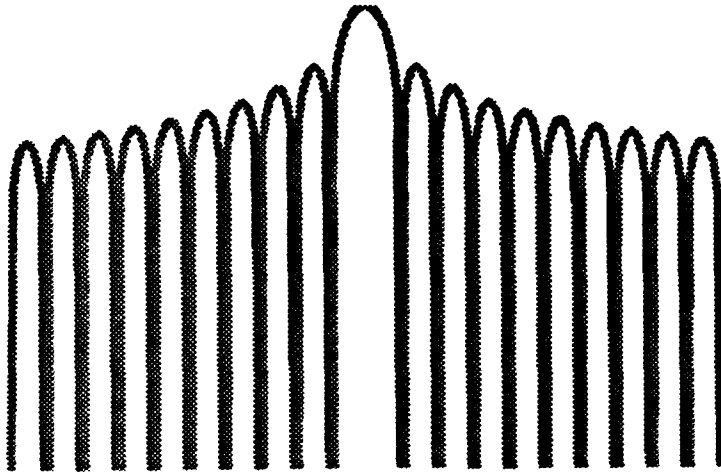


Figure 5-23: Modulus of the Fourier transform of the $D2$ scaling function, in dB.

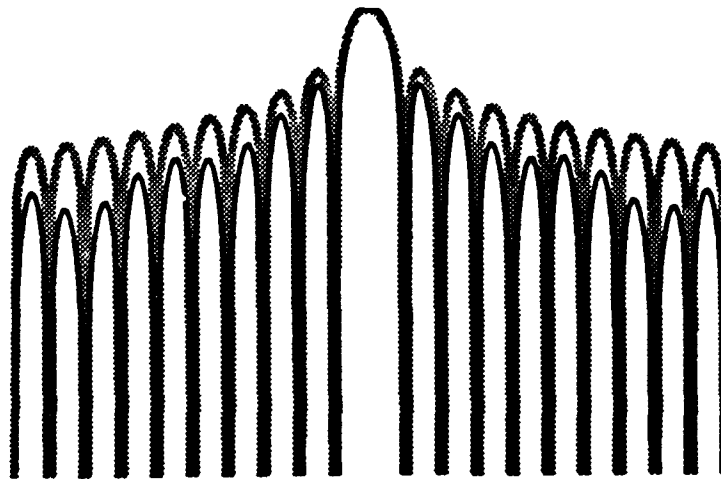


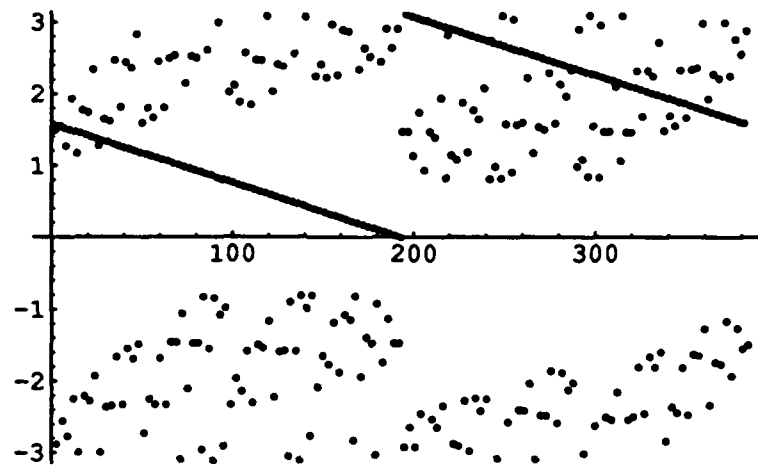
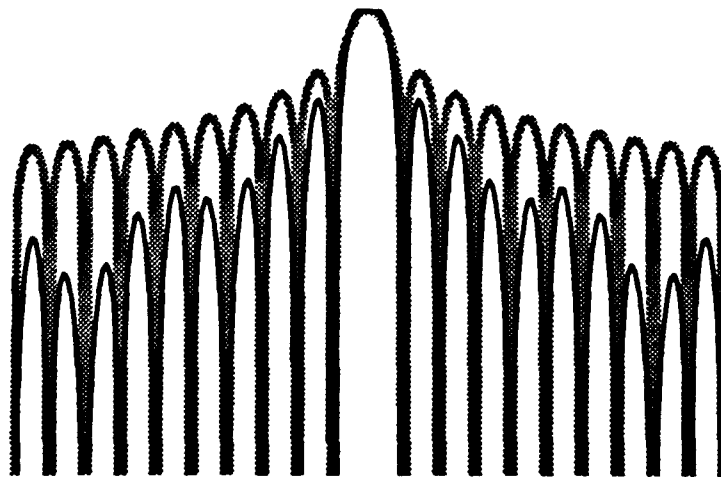
Figure 5-24: Argument of the Fourier transform of the D_2 scaling function.Figure 5-25: Modulus of the Fourier transform of the D_3 scaling function, in dB.

Figure 5-26: Daubechies scaling function D_5 ($m = 2, g = 5$).

Figures 5-29 and 5-30 display the scaling function and wavelet for the *Daubechies* wavelet matrix of genus $g = 15$. The basis formed from these functions can perfectly interpolate polynomials up to degree 14. While the scaling function is supported on an interval of length 29, figure 5-29 shows that the effective support, i.e. the length of the interval where the function is significantly different from zero, is only about 10 units long.

5.2 Real Orthogonal Wavelets

5.2.1 A wavelet basis of genus $g = 2$.

There are only two essentially distinct rank $m = 2$ wavelet matrices of genus $g = 2$ that lead to formally differentiable wavelets: one is the *Daubechies* wavelet matrix D_2 ; the other is a wavelet matrix called R_2 . The R_2 wavelet matrix is

$$a = \frac{1}{2} \begin{pmatrix} 1 & 1 + \sqrt{2} & 1 & 1 - \sqrt{2} \\ 1 - \sqrt{2} & -1 & 1 + \sqrt{2} & -1 \end{pmatrix}$$

Figure 5-27: Daubechies wavelet $D5$ ($m = 2, g = 5$).

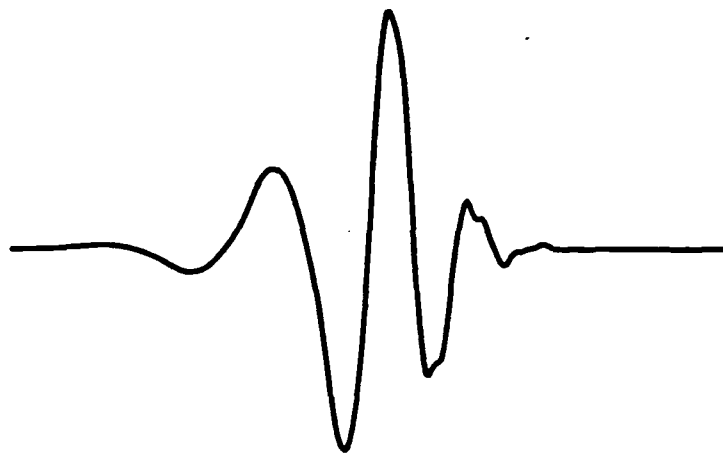


Figure 5-28: Modulus of the Fourier transform of the $D5$ scaling function, in dB.

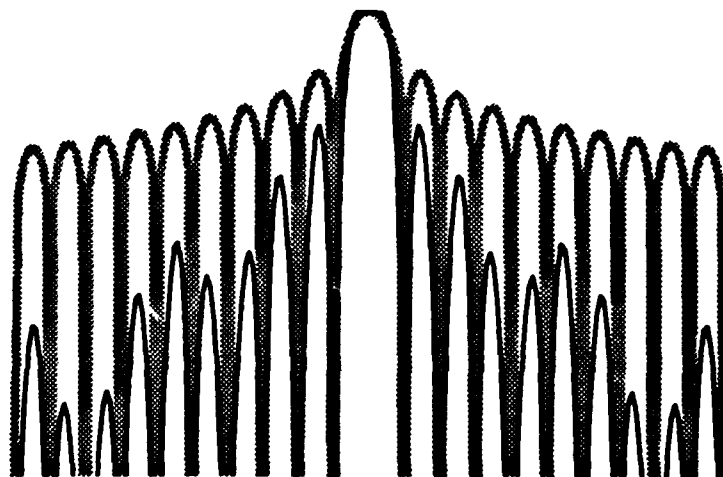


Figure 5-29: *Daubechies* scaling function D_{15} ($m = 2, g = 15$).

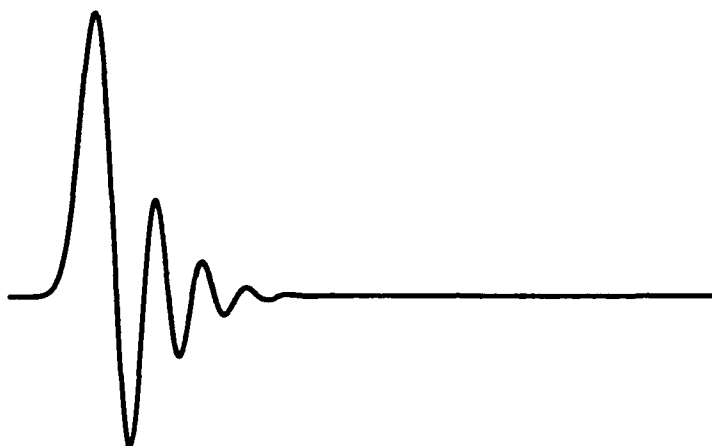


Figure 5-30: *Daubechies* wavelet D_{15} ($m = 2, g = 15$).

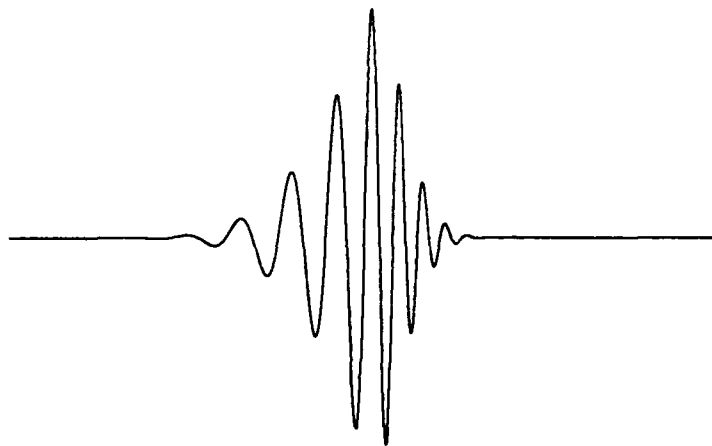
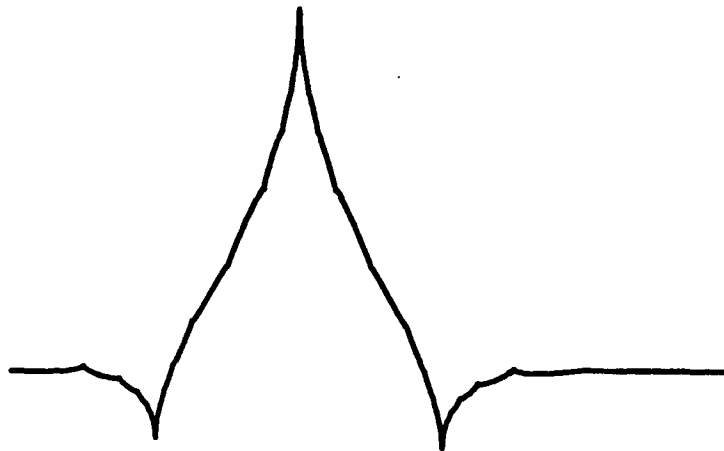


Figure 5-31: Formally differentiable scaling function $Rt2$ ($m = 2, g = 2$).



Figure 5-32: The wavelet $Rt2$ ($m = 2, g = 2$).



Figure 5-33: The scaling function Hat ($m = 2, g = 3$).

5.2.2 *Hat* Wavelets

Scaling functions derived from a wavelet matrix can never be symmetric, but they can be very nearly symmetric. The wavelet system *Hat* is an interesting example for genus $g = 3$; the scaling function and wavelet are illustrated in figure 5-33. The scaling vector for *Hat* is

$$a^0 = (-0.0943, 0.4966, 1.2066, 0.5246, -0.1123, -0.0213).$$

5.3 Flat Wavelets

If the entries of the wavelet matrix a are, up to a common factor, equal to ± 1 we say that a is a *flat real* wavelet matrix; if the entries of a are, up to a common factor, complex numbers of modulus 1 we say that a is a *flat complex* wavelet matrix.

The flat real matrices of genus $g = 1$ are Hadamard matrices, and the flat complex matrices of genus $g = 1$ are (up to a normalizing factor) modifications of the Finite Fourier Transform matrix.

Figure 5-34: The wavelet *Hat* ($m = 2, g = 3$).



Figure 5-35: Modulus of the Fourier transform of the scaling function φ for *Hat* ($m = 2, g = 3$).

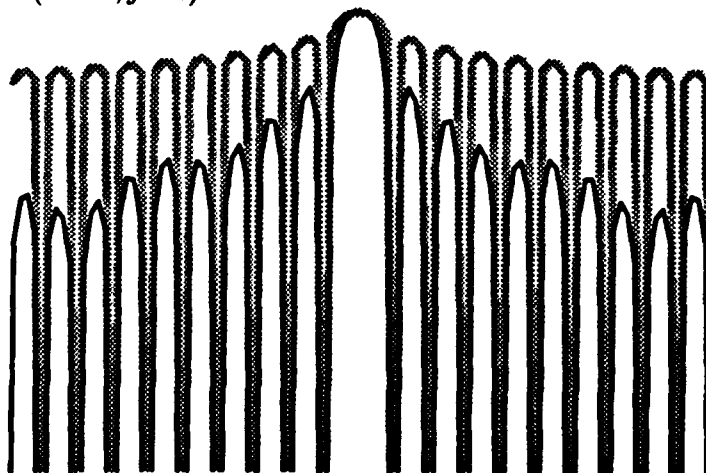


Figure 5-36: The scaling function for a flat wavelet ($m = 2, g = 4$).

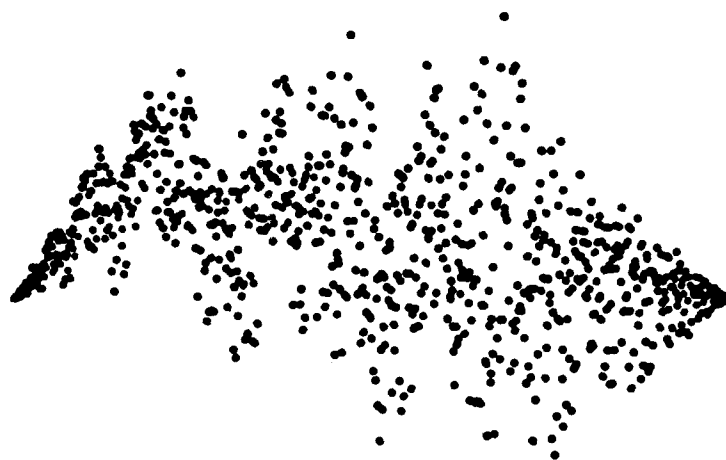


Figure 5-37: The modulus of the Fourier transform of the previous scaling function, in dB ($m = 2, g = 4$).

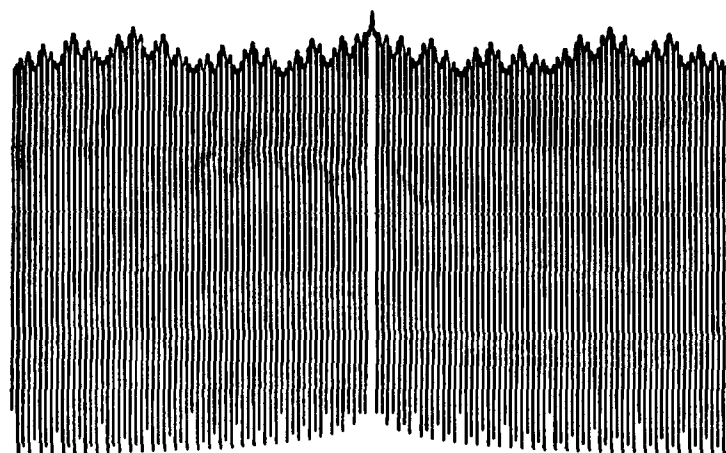


Figure 5-38: The argument of the Fourier transform of the previous scaling function, in dB ($m = 2, g = 4$).

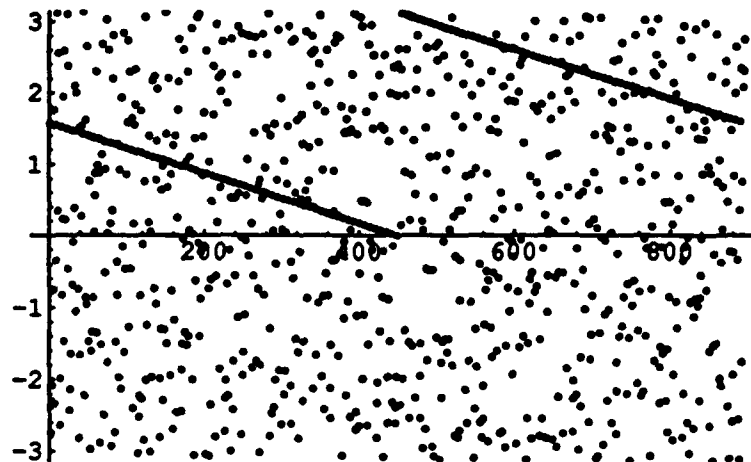
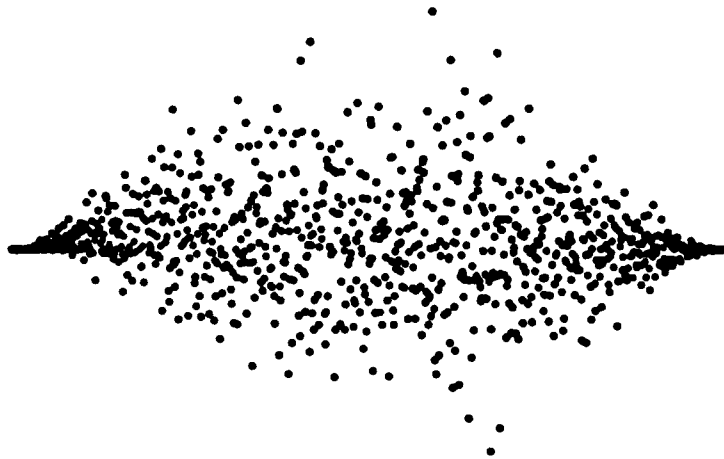


Figure 5-39: The wavelet for the same flat wavelet matrix ($m = 2, g = 4$).



Figure 5-40: The scaling function for a flat wavelet ($m = 2, g = 16$).



5.4 Complex Orthogonal Wavelets

5.4.1 Lawton-Resnikoff Wavelets

The real and imaginary parts of compactly supported complex wavelets can be symmetric, in contrast to real compactly supported wavelets. The rank $m = 2$, genus $g = 3$ complex wavelet matrix given in eq. (4-26) produces the symmetric complex scaling functions and skew symmetric wavelet displayed in figures 5-45 - 5-49.

Figure 5-41: The modulus of the Fourier transform of the previous scaling function, in dB ($m = 2, g = 16$).

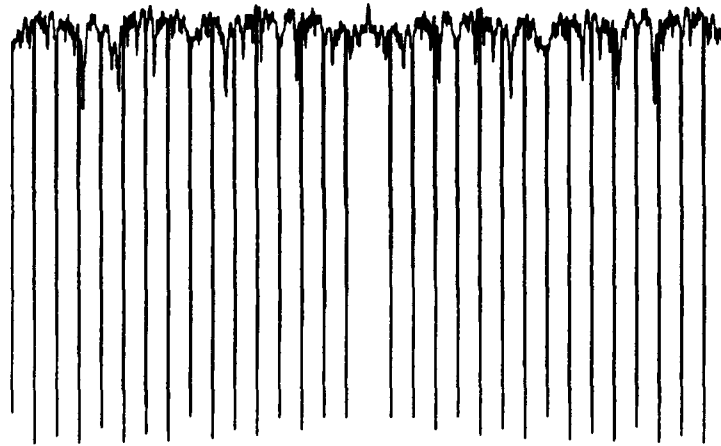


Figure 5-42: The argument of the Fourier transform of the previous scaling function, in dB ($m = 2, g = 16$).

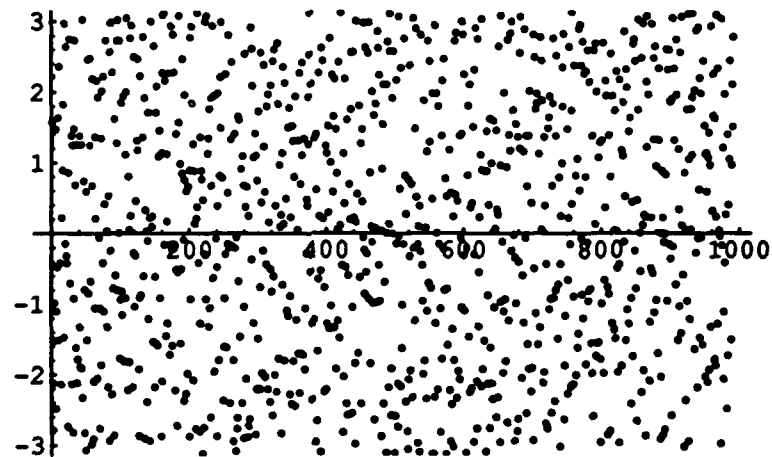


Figure 5-43: The wavelet for the same flat wavelet matrix ($m = 2, g = 16$).

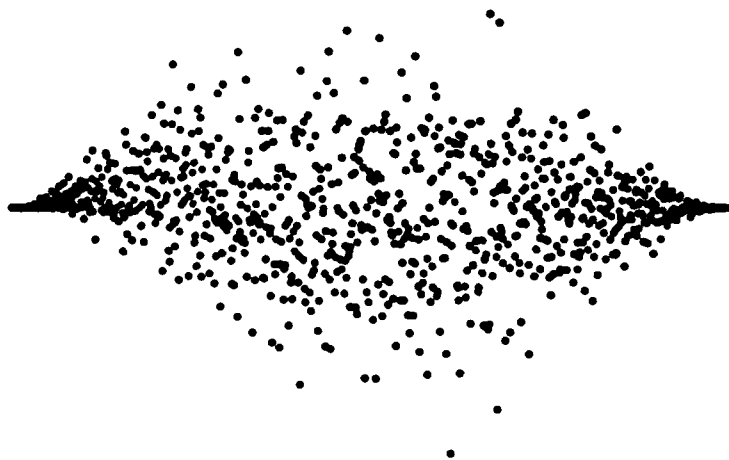


Figure 5-44: Geometry of the eigenvalues for a real flat wavelet matrix of rank $m = 2$ and genus $g = 16$.

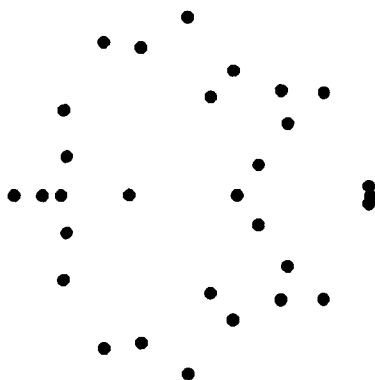


Figure 5-45: The real part of the *Lawton-Resnikoff* complex scaling function, $m = 2, g = 3$.

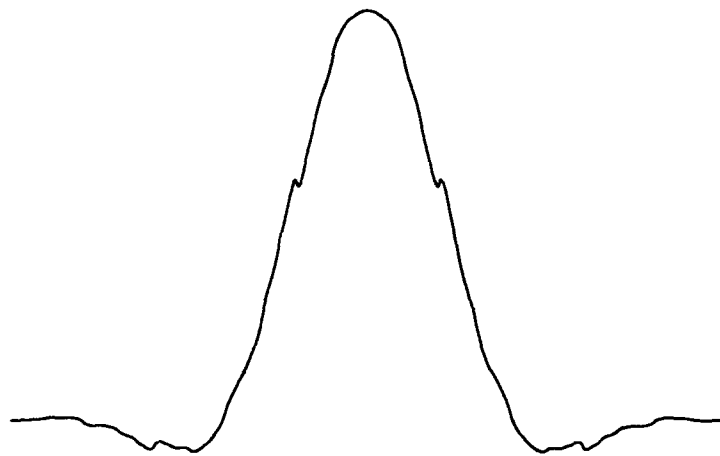


Figure 5-46: The imaginary part of the *Lawton-Resnikoff* complex scaling function, $m = 2, g = 3$.

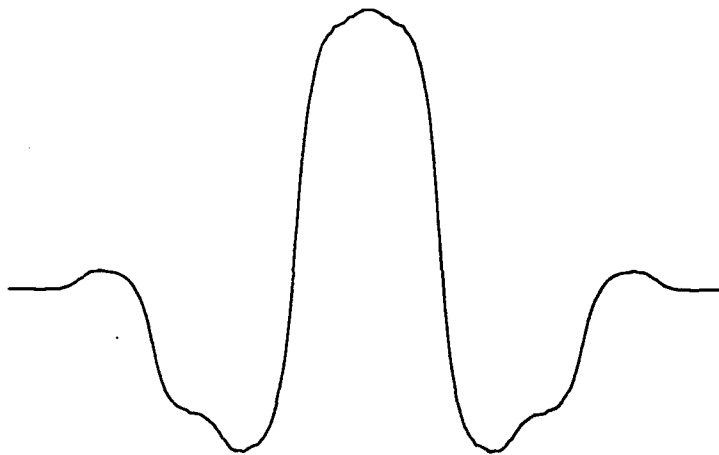


Figure 5-47: The real part of the *Lawton-Resnikoff* complex wavelet, $m = 2, g = 3$.

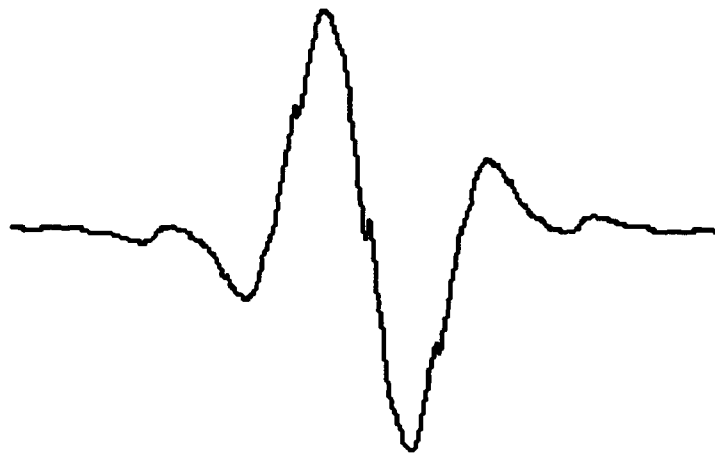


Figure 5-48: The imaginary part of the *Lawton-Resnikoff* complex wavelet, $m = 2, g = 3$.

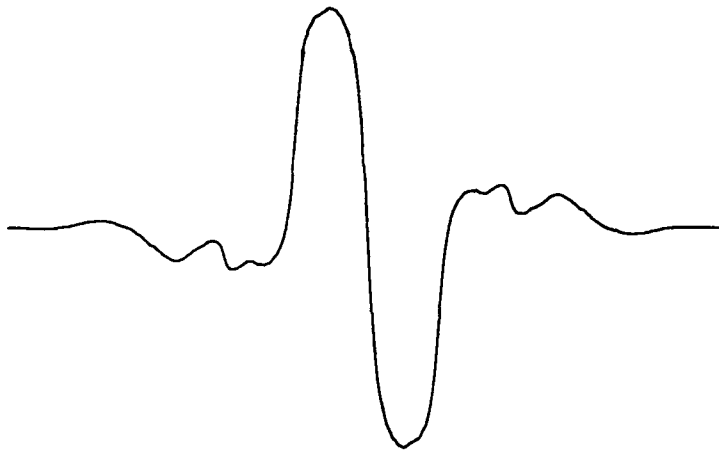


Figure 5-49: Modulus of the Fourier transform of the *Lawton-Resnikoff* scaling function, $m = 2, g = 3$.

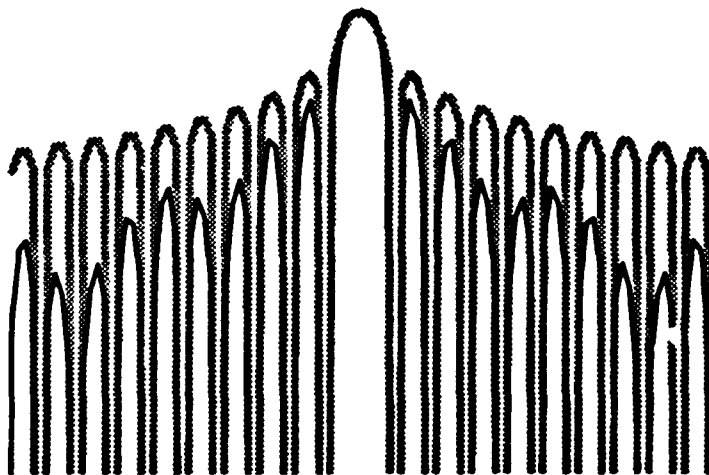
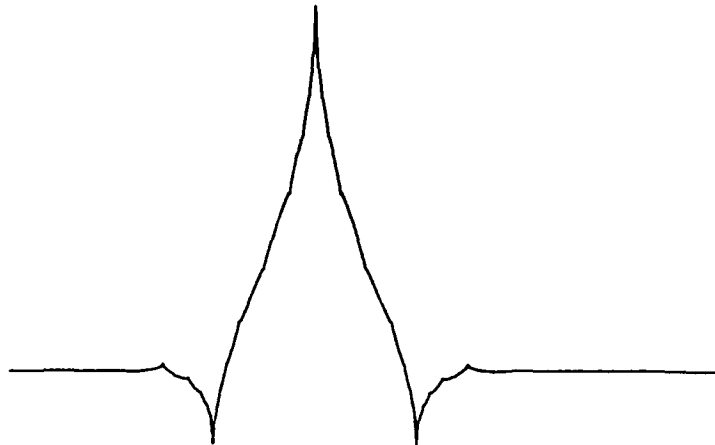


Figure 5-50: *Cohen-Daubechies-Feauveau* left biorthogonal scaling function ($m = 2, g = 4$).



5.5 Biorthogonal Wavelets

Biorthogonal wavelets are a generalization of the wavelet idea obtained by weakening the assumptions that constrain the wavelet matrix. In general, these “weakened wavelets” have little to offer that is really new. But there is one case where biorthogonal wavelet matrices and biorthogonal wavelet functions do add something: biorthogonal wavelets can be symmetrical. An important example was discovered by Heller [23], whose complex biorthogonal wavelets are illustrated in figures 5-56 -5-60. The wavelet matrix was given in eq(4-28).

5.5.1 *Cohen-Daubechies-Feauveau* Wavelets

The following real biorthogonal wavelet matrix pair of genus $g = 8$ is particularly useful for image compression when the amount of computation is not a major constraint.

Figure 5-51: *Cohen-Daubechies-Feauveau* left biorthogonal wavelet ($m = 2, g = 4$).



Figure 5-52: $\varphi_L - \varphi_R$ for *Cohen-Daubechies-Feauveau* biorthogonal wavelet ($m = 2, g = 4$).

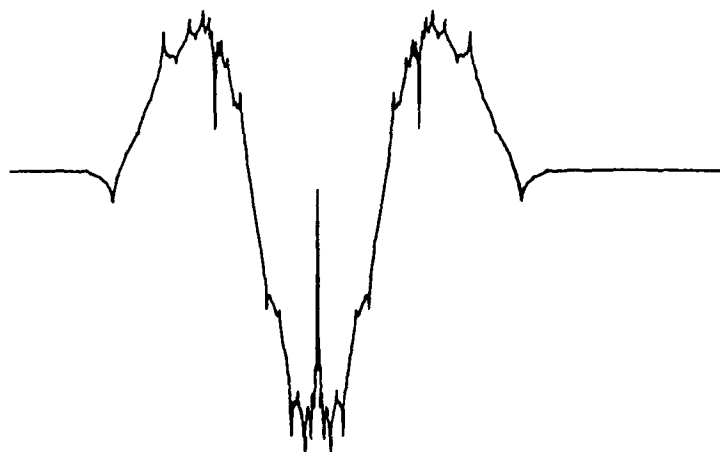


Figure 5-53: φ_L for a biorthogonal wavelet matrix of genus $g = 8$. ($m = 2, g = 8$).

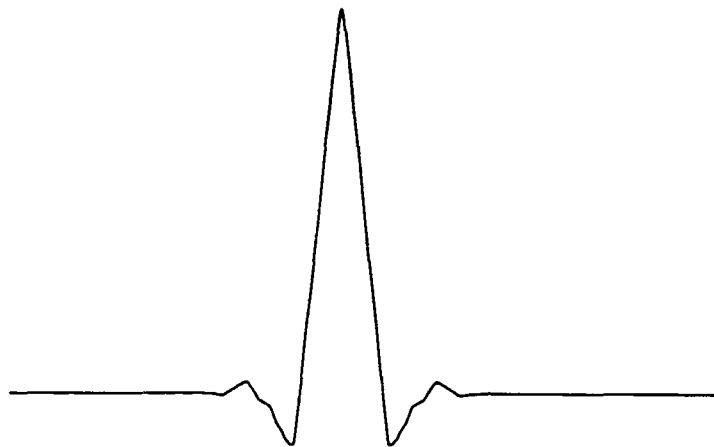
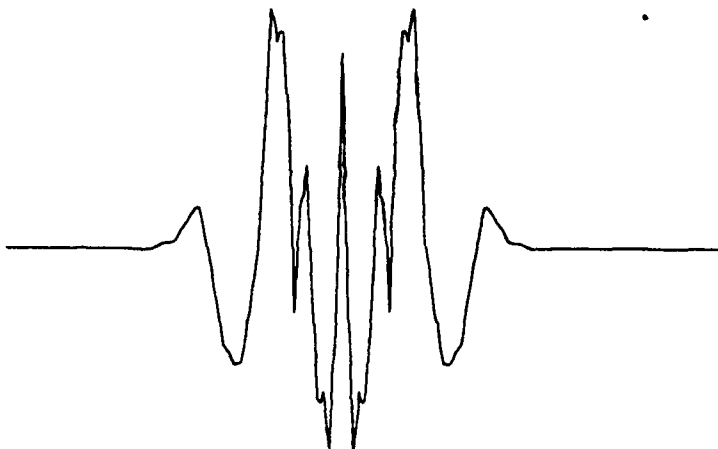


Figure 5-54: ψ_L for a biorthogonal wavelet matrix of genus $g = 8$ ($m = 2, g = 8$).



Figure 5-55: $\varphi_L - \varphi_R$ for a biorthogonal wavelet matrix pair of genus $g = 8$ ($m = 2, g = 8$).



The absolute value of the difference $\varphi_L - \varphi_R$ is less than 0.02.

5.5.2 *Heller Wavelets*

Heller's wavelets are complex biorthogonal functions with useful symmetries. The simplest example is for $g = 3$. The wavelet matrix given in eq. (4-28) produces the scaling function and wavelets shown in figures 5-56 - 5-60.

Figure 5-56: Real part of the 6-coefficient *Heller* biorthogonal scaling function φ_L

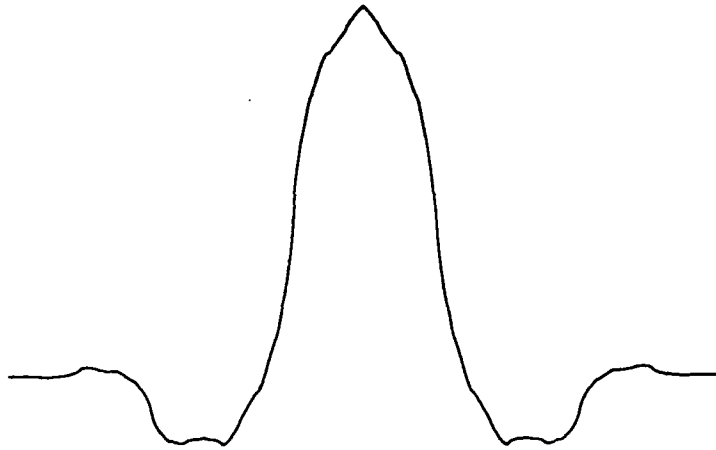


Figure 5-57: Imaginary part of the 6-coefficient *Heller* biorthogonal scaling function φ_L

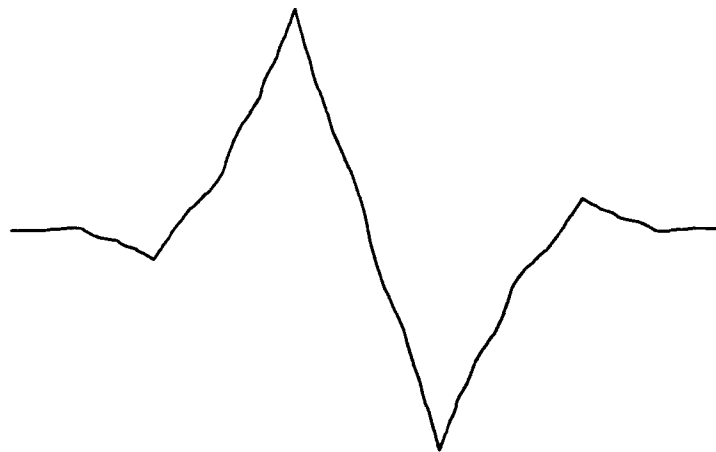
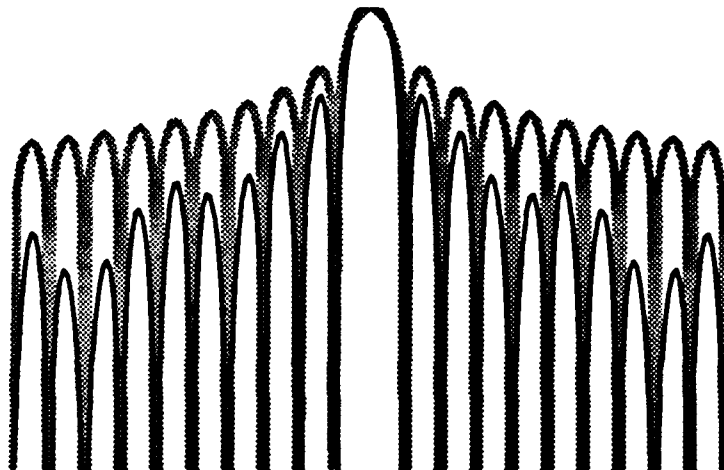


Figure 5-58: Modulus of the Fourier transform of the *Heller scaling function*, $m = 2, g = 3$.



5.6 Negative Multiplier *Daubechies* Wavelets

The equations that define a wavelet matrix can be extended to *negative multipliers*. Let m be an integer and suppose that $|m| > 1$. The extended equations defining a wavelet matrix are

$$\sum_k \bar{a}_{k+ml}^r a_{k+ml}^r = |m| \delta^{r',r} \delta_{l',l}. \tag{5-4}$$

The linear constraint is

$$\sum_k a_k^r = |m| \delta^{0,r}. \tag{5-5}$$

m is called the *multiplier*; the rank is $|m|$. It is easily seen that the solutions of these equations for negative multiplier m coincide with the solutions for the positive multiplier $|m|$. Although the wavelet matrices are the same for positive and negative multipliers of the same rank, the scaling functions and wavelets are different. Recall that the defining equations for these functions are

$$\varphi^r(x) = \sum_k a_k^r \varphi^0(mx - k).$$

Figure ?? displays the scaling function for multiplier $m = -2$ with wavelet matrix $D2$. Comparison with figure 4-1 shows that the negative multiplier

Figure 5-59: Real part of the 6-coefficient *Heller* biorthogonal scaling function ψ_L

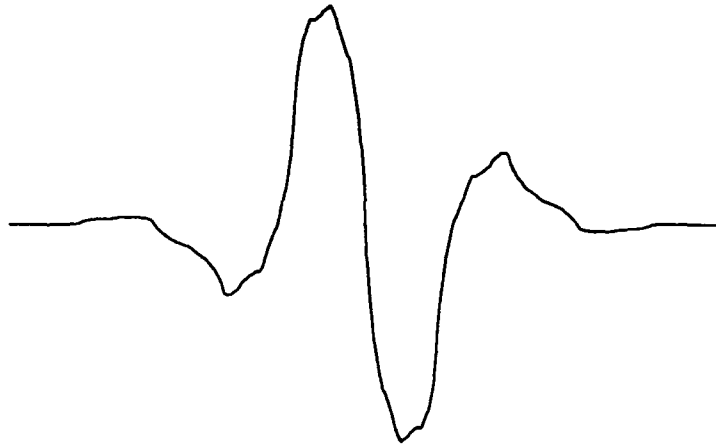


Figure 5-60: Imaginary part of the 6-coefficient *Heller* biorthogonal scaling function ψ_L

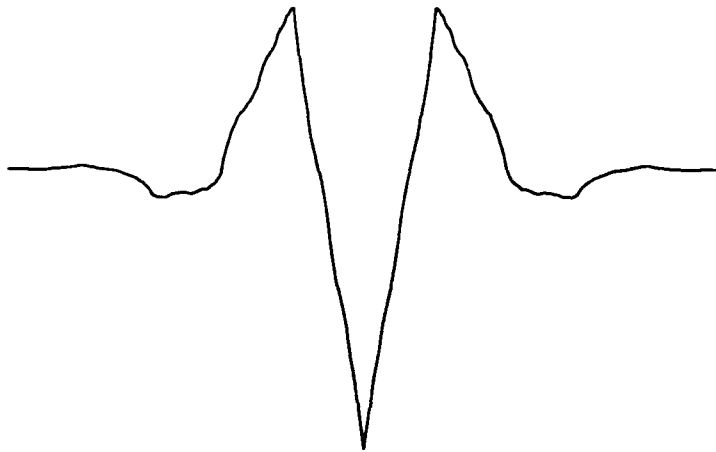


Figure 5-61: *Daubechies* wavelet with negative multiplier ($m = -2, g = 2$).

scaling function is more symmetrical and appears to the eye to be smoother than Daubechies' function, although it shares the property that polynomials of degree 1 can be represented as a low pass sum of linear combinations of the negative multiplier scaling function and its integer translates.

The Fourier transforms of the two scaling functions differ only in phase.

5.7 Higher Rank Wavelets

5.7.1 *Pollen-Plummer* Higher Rank Wavelets

The *Pollen-Plummer* higher rank scaling functions are generalizations of the rank 2 scaling functions discovered by Daubechies. They satisfy the scaling recursion

$$\varphi(x) = \sum_{k=0}^{mg-1} a^0 \varphi(mx - k) \quad (5-6)$$

and all moments of order less than g of each fundamental wavelet

$$\varphi^r(x) := \sum_{k=0}^{mg-1} a^r \varphi(mx - k)$$

Figure 5-62: Formal derivative of *Daubechies* wavelet with negative multiplier ($m = -2, g = 2$).



vanishes for $0 < r < m$. For genera $g = 2$ and $g = 3$ Heller has found all possible ways of completing the first row of the corresponding rank m wavelet matrix to a full rank m wavelet matrix.

The *Pollen-Plummer* scaling functions for genus $g = 2$ and multipliers $m = 3, 5$ and ∞ are illustrated in figures 5-66 and 5-67.

As $m \rightarrow \infty$ these scaling functions tend to a limit which coincides with the limit of the first row of the wavelet matrix. In terms of the variable $x = k/m$, and letting k and m approach ∞ so that their ratio tends to a finite limit yields a function $\varphi_\infty(x)$ of the continuous variable x (displayed in figure 5-68) that is supported on $[0, 2)$ and generates a complete orthonormal system for $L^2(\mathbb{R})$ in the usual way. In particular, the set $\{\varphi_\infty(x - l) : l \in \mathbb{Z}\}$ of translations of the scaling functions are orthonormal, and every polynomial of degree 1 can be expressed as a linear combination of them.

Figure 5-63: Previous figures on a common scale.

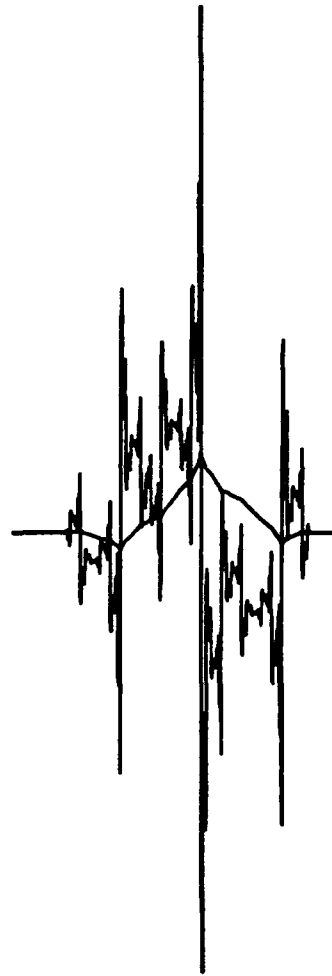


Figure 5-64: *Daubechies* scaling function with negative multiplier ($m = -2, g = 3$).

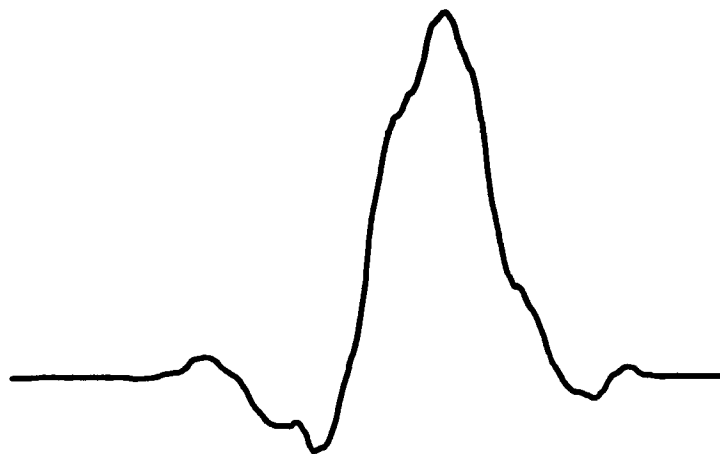


Figure 5-65: *Daubechies* scaling function with negative multiplier ($m = -2, g = 5$).



Figure 5-66: $PPD(3,2)$ scaling function ($m = 3, g = 2$).

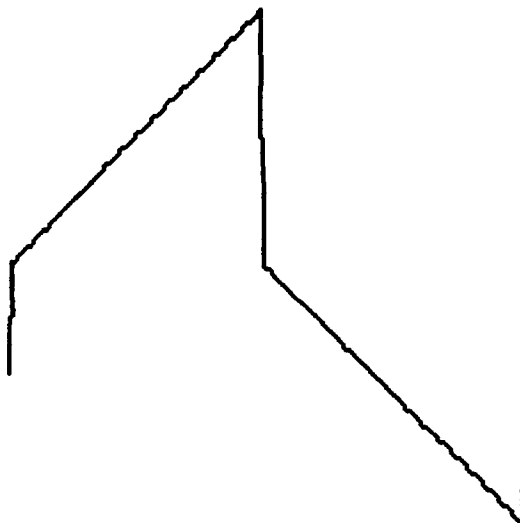
3 = n



Figure 5-67: $PPD(5,2)$ scaling function ($m = 5, g = 2$).

5 = n



Figure 5-68: $PPD(inf, 2)$ scaling function ($m = \infty, g = 2$).

5.8 Higher Dimensional Wavelets

5.8.1 Irreducible Two-Dimensional Wavelets

Λ is a lattice in the complex plane and $\mu \in \Lambda$ is a complex number such that

$$\mu\Lambda \subset \Lambda$$

A 2-dimensional wavelet matrix is a $\bar{\mu}\mu \times g\bar{\mu}\mu$ matrix a of complex numbers

$$a := \begin{pmatrix} a_0^0, & \dots, & a_{g\bar{\mu}\mu-1}^0 \\ \dots & a_\lambda^r & \dots \\ a_0^{\bar{\mu}\mu-1}, & \dots, & a_{g\bar{\mu}\mu-1}^{\bar{\mu}\mu-1} \end{pmatrix}$$

that satisfies the wavelet scaling conditions

$$\left. \begin{aligned} \sum_{\lambda \in \Lambda} a_\lambda^r &= \bar{\mu}\mu \delta_{0,j} \\ \sum_{\lambda \in \Lambda} \bar{a}_{\lambda+\mu\nu}^{r'} a_{\lambda+\mu\nu}^r &= \bar{\mu}\mu \delta^{r',r} \delta_{\nu',\nu} \end{aligned} \right\} \quad (5-7)$$

Matrix Formulation

The mapping

$$z = x + iy \mapsto \pi(x) := \begin{pmatrix} x & -y \\ y & x \end{pmatrix}$$

is a 2-dimensional real representation of the field of complex numbers \mathbb{C} . It is easily verified that

$$|z|^2 = \bar{z}z = \det \pi(z)$$

and

$$\bar{z} + z = \operatorname{tr} \pi(z).$$

The scaling equation can be written in terms of addition and multiplication in the matrix ring.

Consider multipliers $\mu \in \mathbb{C}$ such that $2\operatorname{tr} \pi(\mu)$ and $m := \det \pi(\mu)$ are integers. These multipliers can be classified according the values of the determinant and trace. The case where $m = 1$ is not interesting. For $m = 2$ there are three possibilities.

The Three Cases for $m = 2$

If $\operatorname{tr} \pi(\mu) = 0$ then

$$\mu = \pi(\pm i\sqrt{2}) = \begin{pmatrix} 0 & \mp i\sqrt{2} \\ \pm i\sqrt{2} & 0 \end{pmatrix}$$

are the only possibilities.

Figure 5-69: One-dimensional to two-dimensional mapping for the *Rectangle Haar* scaling function $\varphi(z)$ ($m = 2, g = 1$).

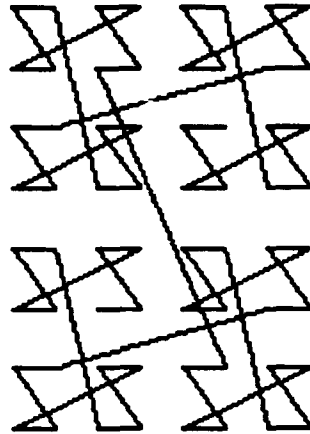


Figure 5-70: *Novon Haar* scaling function $\varphi(z)$ ($m = 2, g = 1$).



Figure 5-71: One-dimensional to two-dimensional mapping for the *Novon Haar* scaling function $\varphi(z)$ ($m = 2, g = 1$).

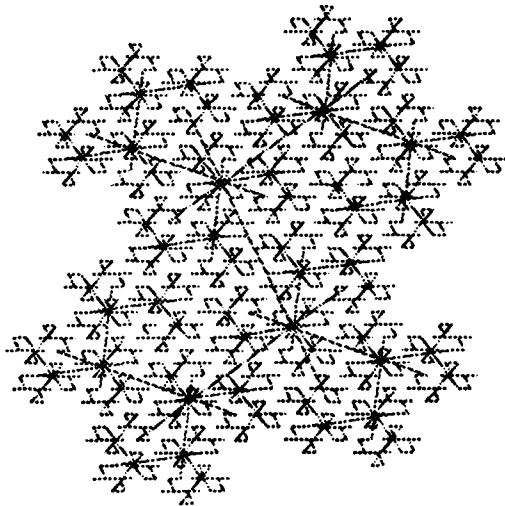


Figure 5-72: *Twindragon* Haar scaling function $\varphi(z)$ ($m = 2, g = 1$).

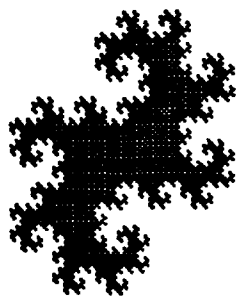


Figure 5-73: Two dimensional row and column transformed image *Lenna* image employing the $D3$ product basis.



Part III

**Applications of Wavelet
Technology to Bandwidth
Management**

Chapter 6

Bandwidth Compression

6.1 Image Compression

6.1.1 Imagery

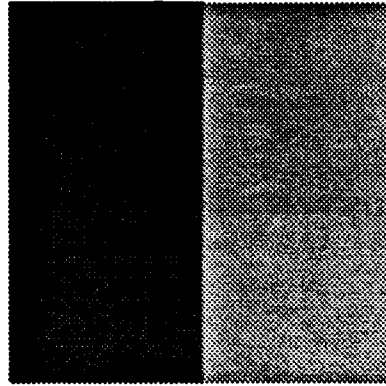
The human eye and the ear capture an amazing amount of data every second – much more than the brain can consider. For instance, in normal daylight vision, the color sensitive receptors of the retina in each eye collect about 800 megabits of visual information each second. The first step in making what the eye sees available to the brain is the reduction of this enormous amount of data by selective omission of less important information. The neural network that connects the eye to the visual cortex does this in real time, continuously and automatically. This automatic culling or “compression” reduces the amount of information that reaches the brain by a factor of at least 100. This fact shows that most of the physical information represented in the light signal that falls on the eye is not needed by the brain – this basic fact about vision is the psychophysical cornerstone of practical compression algorithms for video and other natural images.

6.1.2 Measures of Image Quality

The decompressed image produced by a lossy compression process is not the same as the original. The problem of defining image quality is to provide a method for comparing different image compression methods. Although this question is a natural one, a satisfactory answer still eludes the research community.

For many years engineers adopted “mean squared error” as a measure of quality. For a decompressed gray scale image, the mean squared error is the

Figure 6-1: Simultaneous contrast enhances edges.



sum of the squares of the differences between the corresponding pixel values of the source image and the decompressed image. Mathematically, this is the discrete $L^2(\mathbf{R})$ norm of the difference of the two images; physically, the $L^2(\mathbf{R})$ error measures the energy in the difference image. The mean squared error per pixel is often used to compare the quality of images of different size.

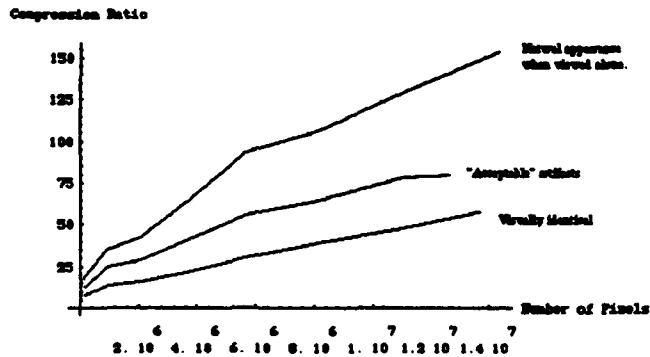
Misplaced image energy is certainly a quality measure: if the misplaced energy is large, the quality cannot be high. But a small $L^2(\mathbf{R})$ error need not imply that the two images are subjectively interchangeable. There are several reasons for this. Nonlinearities in the human visual system result in a nonuniform weighting of different types of visual phenomena which is not captured by the $L^2(\mathbf{R})$ norm. Moreover, if the energy in the difference image is localized, it may appear as an artifact but if the error energy is more or less randomly distributed through the image, it may not be perceived at all. Image compression experts know that mean squared error is not proportional to subjective image quality, but it is frequently used as a substitute nevertheless.

The maximum error, i.e. the largest of the absolute values of the pixel differences, is a measure that may correspond better to subjective quality assessments.

For a fixed quality level, the amount of compression that is inherent in an image depends on the size of the image and the rate at which it is sampled.

Images sampled at higher resolution have greater redundancy because uniform regions of the image account for a greater number of samples. For

Figure 6-2: Trade-off between compression ratio and image size for three fixed levels of quality for Aware's compression.



a fixed level of absolute resolution, natural images and images of a larger scene typically have greater redundancy than images of a smaller scene because of the local uniformity of physical objects.

Let N denote the number of pixels in a rectangular image. We will normalize storage requirements so that the amount of computer memory required to store one pixel of image information is 1 storage unit. Let $C(N)$ be the number of storage units required to store a compressed version of the image. Then $N/C(N)$ is the compression ratio.¹

Figure 6-2 displays three graphs that show how $C(N)$ varies with N for a fixed image sampled at increasing resolution and compressed by a wavelet image compression algorithm. The graphs were constructed by starting with a digital image sampled at a high resolution. To obtain subsampled lower resolution versions of the image, it was partitioned into 2×2 blocks of adjacent pixels which were averaged. The average value was assigned to each of the pixels. This procedure was repeated a number of times to reduce the sampling resolution.

Each curve in the figure corresponds to a different subjective quality measure. The lowest curve corresponds to compressed image whose decompressed form is visually identical to the original; the next higher curve corresponds to decompressed images that are visually different from the original but do not produce "unacceptable" artifacts. The highest curve

¹ Here we are omitting the overhead storage required to decompress the image. Since this is - for wavelet compression - a small fraction of the total, we shall ignore it.

corresponds to decompressed images that appear natural when viewed alone but have obvious natural looking artifacts when compared with the original.

The first and third curves appear to be asymptotically linear, and the second appears to lie between the other two. If we assume that the curves are asymptotically linear, this implies the relation

$$N/C(N) = (\alpha + N)/\beta$$

for constants α and β , at least for N very large, so

$$C(N) = \frac{\beta N}{\alpha + N}. \quad (6-1)$$

As $N \rightarrow \infty$, we find

$$\lim_{N \rightarrow \infty} C(N) = \beta.$$

This formula states that if N is sufficiently large, then there is no further information gained by sampling the image at increasingly fine scales.

6.2 Transform Image Compression Systems

6.2.1 System Block Diagram

The block diagram of a transform image compression system is shown in figure 6-3.

A transform compression encoder consists of three subsystems: a *transform* subsystem; a *quantization* subsystem, and an *entropy coder* subsystem. As shown in the figure, the input signal progressively passes through these subsystems.

The Transform

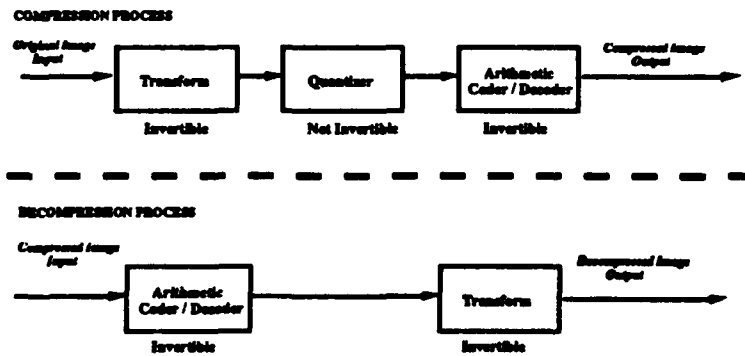
The transform is invertible; no information is lost in this stage of the compression process. The transform merely reorganizes the input image data in a way that makes the quantization stage more effective. Since the transform is invertible, it is not directly responsible for any compression: for a gray scale image, for instance, the transformed image provides one transform coefficient for each input pixel value.²

The purpose of the transform is to reorganize the image data to concentrate large scale/low spatial frequency image signal energy into a small number of coefficients for subsequent quantization. Selection of a transform is governed by the following criteria:

²The transform may change the dynamic range of the input values, and thereby require more or less storage for a transform coefficient. We shall ignore this factor in our discussion.

Figure 6-3: Diagram of a transform image compression system.

Transform Image Compression ----- System Diagram



- Transforms that concentrate large scale/low spatial frequency energy better are preferred.
- Transforms that are computationally efficient are preferred.
- Transforms that retain localized image information (e.g. edges, specular reflection) in the low frequency transform coefficients are preferred.

The Quantizer

The quantizer allocates different numbers of bits for the representation of different transform coefficients. The allocation of zero bits is the same as omitting the transform coefficient. Typically, the transform coefficients that correspond to the highest spatial frequencies will be omitted. Since noise populates all spatial frequency states, and there are more high spatial frequency states than low, it follows that omission of the high spatial frequency transform coefficients preferentially eliminates noise and hence may actually enhance the appearance of the image. A more refined approach to quantization enables some high spatial frequency information to be retained at the expense of low spatial frequency information.

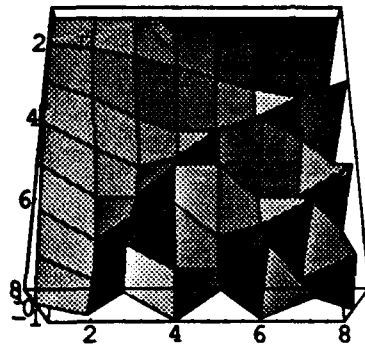
The quantizer provides all of the lossy compression – quantization is not invertible. The selection of a quantizer is governed by the following criteria:

- Quantizers that provide a good model of the source imagery are preferred.
- Quantizers that incorporate a good human psychovisual model are preferred.
- Quantizers whose quantization rules are computationally efficient are preferred.

The Entropy Coder

The final step in the compression process is removal of redundancy from the stream of quantized transform coefficients by means of an entropy coder. Entropy coding is invertible: no information is lost in this stage of the compression process. Nevertheless, when entropy coding is applied to a suitably transformed and quantized image, it provides a significant compression increment – there can be as much as a 30% reduction in the size of the compressed file. Entropy coders are not all equal. The selection of a quantizer is governed by the following criteria:

Figure 6-4: Discrete cosine transform ("DCT") matrix for JPEG: $m = 8, g = 1$.



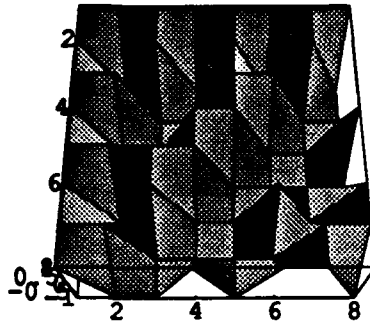
- Entropy coders that limit the number of pixels that can be affected by communications channel errors are preferred.
- Entropy coders that have smaller memory and/or processing requirements are preferred.

6.2.2 Conventional Block Transform Image Compression

Conventional block transforms have been used for image compression for several decades. Today, the best known, if not most effective, block transform is the discrete cosine transform ("DCT") [47]. The ISO JPEG³ still image compression standard employs a rank $m = 8$ DCT block transform. The graph of this 8×8 matrix is shown in figure 6-4 where the matrix is depicted as a surface by interpolating the matrix entries. The top row is the (constant) low pass scaling vector. The other seven rows are high pass. The matrix elements are the top values of the DCT digital filter. In section 6.3.1 DCT compression is compared with compression employing rank $m = 2$ wavelets matrices of higher genus.

Experiments to compress images using the Hadamard transform of rank $m = 64$ yielded poor results (cp. [42]), as one would expect from examining figure 6-5 which, although it illustrates the rank $m = 8$ Hadamard wavelet matrix, already begins to show the roughness in the transform matrix that

³The International Standards Organization Joint Picture Experts Group is the body charged with establishing standards for still image transmission and compression formats.

Figure 6-5: Hadamard transform matrix: $m = 8, g = 1$.

leads to characteristic artifacts and low compression ratios.

6.3 Wavelet Image Compression

Today, the most successful general image compression method is based on the two dimensional product basis constructed from the *Daubechies* wavelet matrix $D3$. Recall that $D3$ provides a low pass representation of polynomials of degree less than 3. From this it follows that the product basis provides a low pass expansion of polynomial functions of two variables, say x and y , each of degree less than 3. These surfaces are good models for light reflected from smooth surfaces such as walls, or the cheeks and forehead of a face. The ability to represent reflected light energy that produces surfaces in a digital image means that this transform is effective in concentrating a large fraction of the image energy in a small number of low pass ("near dc") transform coefficients.

Figures 6-6 and 6-7 show the scaling function and fundamental wavelet for $D3$.

Figure 6-6: *Daubechies* scaling function φ for $D3$ ($m = 2, g = 3$).

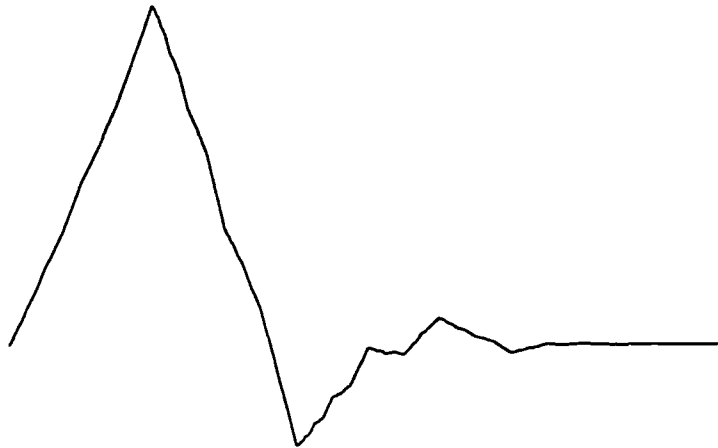
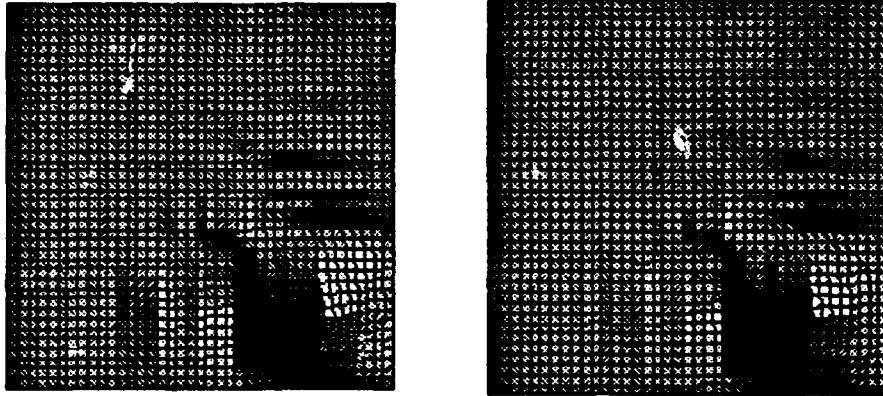


Figure 6-7: *Daubechies* wavelet ψ for $D3$ ($m = 2, g = 3$).



Figure 6-8: Stereogram of the product of scaling functions $\varphi(x)\varphi(y)$ for $D3$. (The origin of coordinates is at the lower right.)



Figures 6-10 through 6-13 display the product basis functions

$$\varphi(x)\varphi(y), \quad \varphi(x)\psi(y), \quad \psi(x)\varphi(y), \quad \psi(x)\psi(y),$$

each of which corresponds to a two dimensional digital filter. The filters that correspond to these basis functions transform the original image into four components: the low-low, low-high, high-low, and high-high parts of the transform. Each of these outputs contains one quarter as many coefficients as the input image, so the total number of output coefficients is the same as the number of input coefficients. This fact makes it possible to conveniently display the transform coefficient output as an image also by scaling the coefficients to fall in the range of the input pixel values – say the range 0 to 255 for an 8 bit grayscale image.

The *Lenna* figures 2 and 5-73 were constructed this way. They illustrate the first stage in applying the wavelet transform for compression.

Figures 6-8 and 6-9 are stereograms of the graph of the “Lo-Lo” function $\varphi(x)\varphi(y)$, and the “Hi-Hi” function $\psi(x)\psi(y)$, respectively. The reader should focus at infinity to view these stereograms.

Figure 6-9: Stereogram of the product of wavelet functions $\psi(x)\psi(y)$ for D_3 . (The origin of coordinates is at the lower right.)

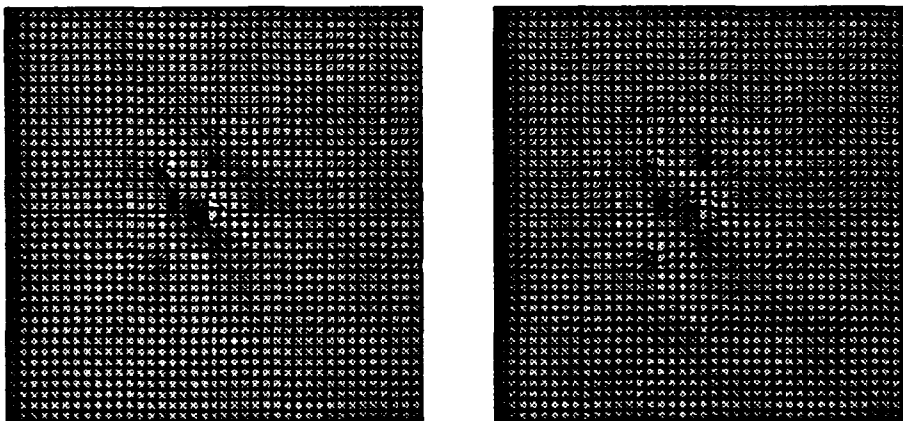


Figure 6-10: Two-dimensional low-low product wavelet basis function built from $D3$: $\varphi(x)\varphi(y)$.

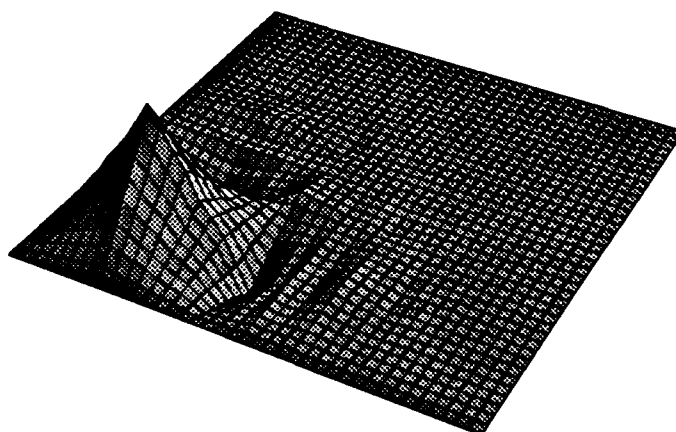


Figure 6-11: Two-dimensional low-high pass product wavelet basis function built from $D3$: $\varphi(x)\psi(y)$.

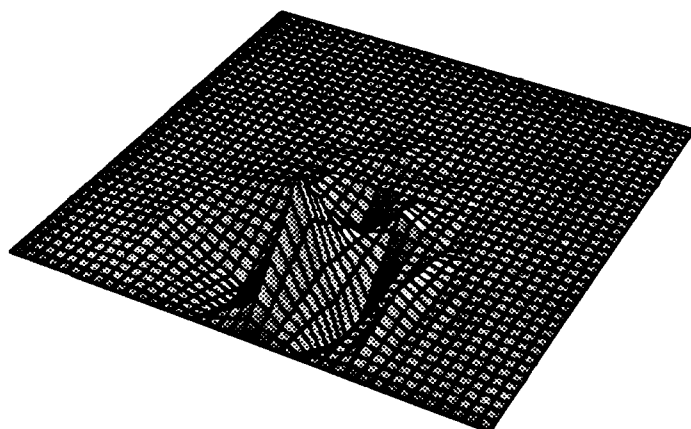


Figure 6-12: Two-dimensional high-low pass product wavelet basis function built from $D3$: $\psi(x)\varphi(y)$.

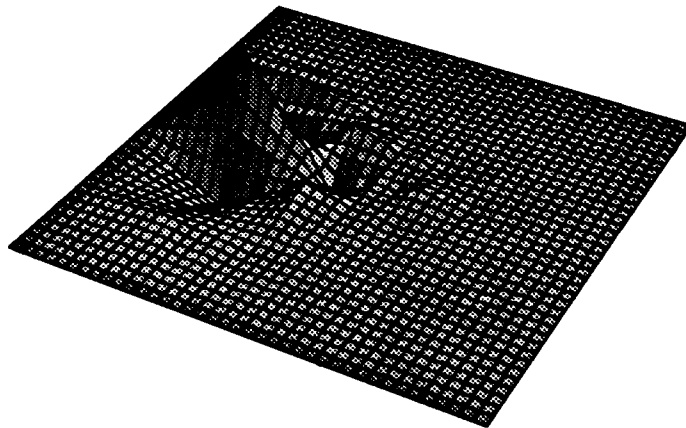
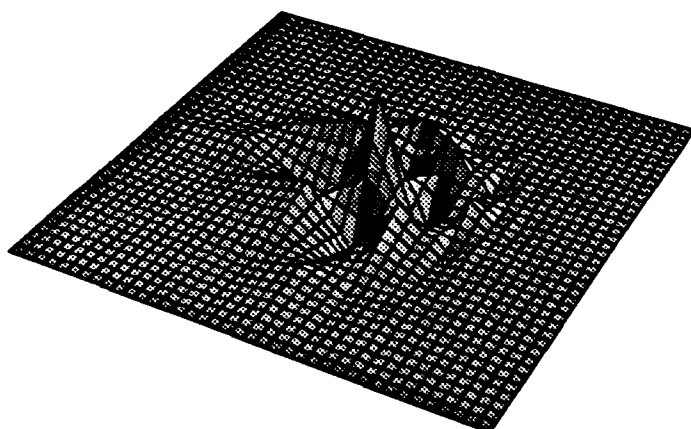


Figure 6-13: Two-dimensional high-high pass product wavelet basis function built from $D3$: $\psi(x)\psi(y)$.



6.3.1 Comparison of Conventional and Wavelet Image Compression

In this section we compare images compressed by conventional block transforms and their wavelet-unified higher genus versions, for various choices of the rank, genus, and characteristic Haar wavelet matrix.

The conventional block transform filters for image compression described in section 6.2.2 for the Discrete Cosine (DCT) and Hadamard transforms are the characteristic Haar wavelet matrices illustrated in this section. We consider ranks $m = 2, 3, 4$ and 8 , and genera $g = 1$ (the block transform), $2, 3$, and 4 .

In order to make even small differences perceptible, the source image, shown in figure 6-14, is a 64×64 pixel square centered on the right eye of the *Lenna* image. There are 8 bits of grayscale information per pixel. Each pixel in the original image has been magnified (without interpolation or smoothing) so that it is an 8×8 square that occupies 64 pixels.

The source image was compressed at a compression ratio of 32-to-1 using the two dimensional tensor product wavelet basis constructed from the designated 1-dimensional wavelet matrix. The grayscale pixel values - integers from 0 to 255 - were interpreted as values of a function on a two dimensional square lattice. Four levels of a Mallat tree decomposition were used to represent the grayscale image function as a wavelet matrix series. The resulting collection of wavelet matrix series coefficients was quantized but, in the interest of simplifying this discussion, the quantization algorithm is a simplified version of one that would be used to obtain the best quality.

Each eye image was equalized to provide better contrast for printing. The laser printer process used to print this volume employs dithering to create the gray tones displayed in the figures. The dithering process tends to interpolate and "low pass filter" the original digital image. Nevertheless, the dithered displays provide a useful indication of the systematic effects of using wavelet matrices of varying rank, genus, and characteristic Haar wavelet matrix for image compression.

Figures 6-15 through 6-18 demonstrate the importance of overlapping basis functions and *Daubechies* wavelet matrices for capturing the polynomial smoothness inherent in the source image and reducing blocking artifacts in the decompressed image. As the genus g increases, the blocking artifacts are decreased, but so too is faithful representation of edge information because the larger support of the scaling function is less sensitive to localized detail. The optimum combination of polynomial smoothness and sensitivity to edge detail appears to occur for $g = 3$ or $g = 4$.

Figure 6-14: *Lenna* eye source image.



Figure 6-15: *Lenna* eye decompressed at 32-to-1 via $D1$ ($m = 2, g = 1$).

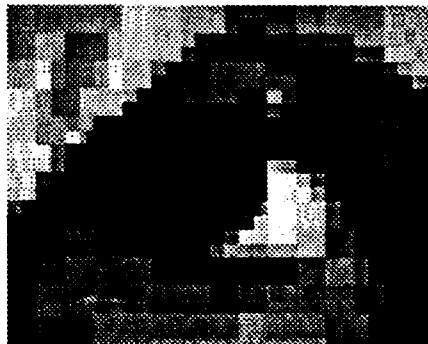


Figure 6-16: *Lenna* eye decompressed at 32-to-1 using $D2$ ($m = 2, g = 2$).



Figure 6-17: *Lenna* eye decompressed at 32-to-1 using $D3$ ($m = 2, g = 3$).



Figure 6-18: *Lenna* eye decompressed at 32-to-1 using $D4$ ($m = 2, g = 4$).



Figure 6-19 illustrates the characteristic properties of an image compressed with the rank $m = 8$ Discrete Cosine Transform used in the ISO JPEG still image compression international standard. The blocking artifacts due to the unoverlapped transform are obvious and distracting. The genus $g = 2$ "waveletized" DCT illustrates the benefit of employing overlapped basis functions.

Compared with the rank $m = 2, genus = 1$ block transform, the $m = 8$ DCT yields a much more faithful decompressed image because the higher rank is one way of increasing spectral resolution to capture more edge information. But the figures suggest that increasing spectral resolution by increasing the genus of the transform rather than its rank is more effective. This observation has been confirmed by extensive studies at Aware, Inc.

Figure 6-19: *Lenna* eye decompressed at 32-to-1 using the DCT ($m = 8, g = 1$).



Figure 6-20: *Lenna* eye decompressed at 32-to-1 using the “waveletized” DCT ($m = 8, g = 2$).



Figure 6-21: *Lenna* eye decompressed at 32-to-1 using the Hadamard transform ($m = 8, g = 1$).



Figure 6-22: *Lenna* eye decompressed at 32-to-1 using the “waveletized” Hadamard transform ($m = 8, g = 2$).



Having seen so many compressed examples of *Lenna's* eye, let us see what happens when the entire NITF6 *Lenna* image is compressed using a "production code" multilevel transform, full quantizer, and entropy coder. The original NITF6 image is displayed in figure 6-23.⁴ For comparison, figure 6-24 is a 32-to-1 compressed image employing the *D3* wavelet transform.

6.4 Multiresolution Audio Compression

6.4.1 Audio Signals

It is much the same for sound. The ear selectively omits the less important information, which is usually most of an audio signal. Only a fraction of the audio information that activates the eardrum actually reaches the brain to be "heard." If, for instance, two tones are close in pitch, then the brain will hear the louder of the two but not the softer. The designer of an audio compression algorithm will take the auditory consequences of this psychoacoustic "masking threshold" this into account. Figure 6-25 schematically illustrates the masking threshold for human hearing. A good compression algorithm will selectively omit the same kind of information that the human sensory system selectively omits to achieve higher compression levels without compromising quality; cp. [57], [58], [59].

Figure 6-26 displays the energy density as a function of time and frequency for an audio signal. Time progresses along the axis from the lower center toward the upper right, and frequency increases linearly along the axis from the upper left to the lower center in the graph. The next figure shows the same information but the effect of the psychoacoustic masking threshold on audibility is indicated by printing the masked signal energy in light gray. Comparison of the figures shows that a relatively large fraction of the energy in an audio signal cannot be heard by the ear.

Designing a compression algorithm for audio that takes masking into account is thus a problem in nonlinear filter design.

⁴The original is an 8-bit per pixel gray scale image, which cannot be adequately reproduced by the laser printer. The image shown here is a dithered grayscale expressed by binary (black and white) pixels.

Figure 6-23: Original NITF6 *Lenna* image.



Figure 6-24: *Lenna* decompressed at 32-to-1 using the *D3* wavelet transform with quantization ($m = 2, g = 3$).



Figure 6-25: Schematic representation of the audio masking threshold function.

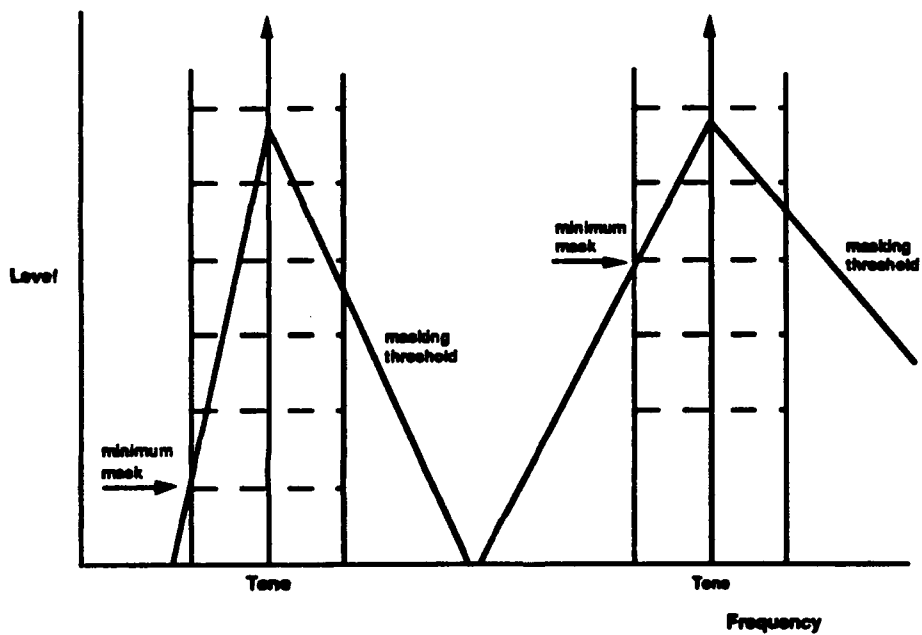


Figure 6-26: Energy density as a function of time and frequency for an audio signal.

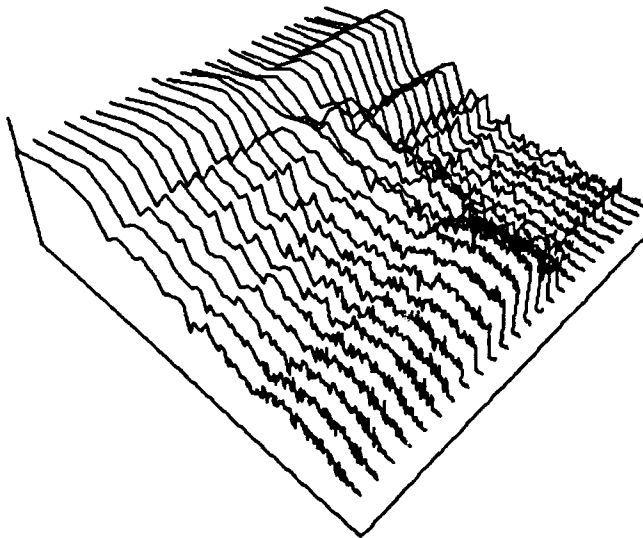
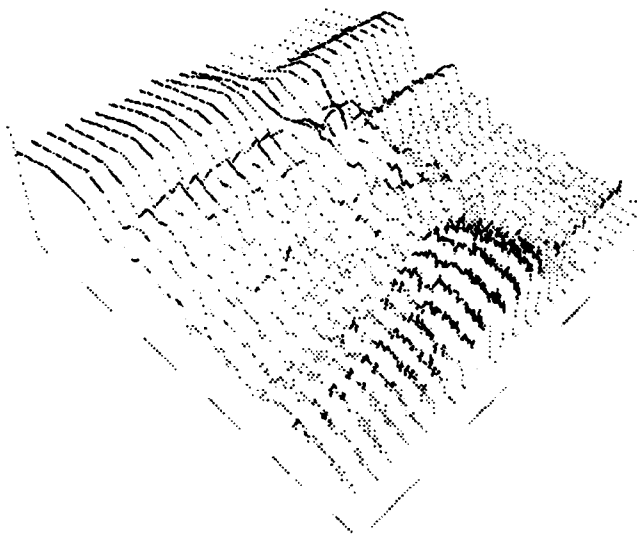


Figure 6-27: Psychoacoustic map of the same audio signal showing effect of the masking threshold.



Chapter 7

Channel Coding

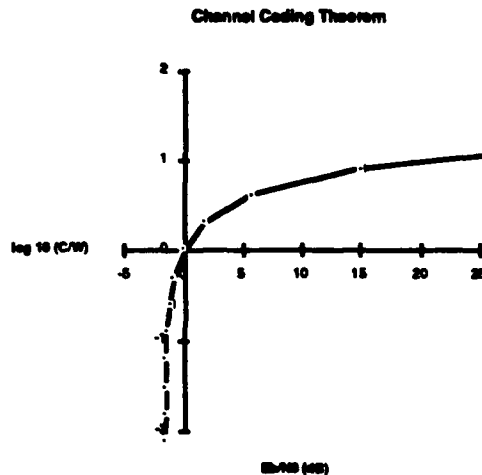
7.1 Relation to Shannon's Channel Coding Theorem

Claude Shannon, who founded information theory, proved that it is possible to add redundancy to the information so that a message can be received error-free and yet use all of the channel's capacity. The idea is simple although the conclusion is amazing. If the information in a message could be spread throughout the entire transmitted signal, like a hologram each of whose parts contains information about the whole, then noise bursts might corrupt some parts of the transmission but would be correctly received, and the whole message could be unraveled from the received parts. This is the intuitive idea behind Shannon's channel coding theorem. But the channel coding theorem doesn't show how to construct a good channel code "hologram." The problem has two parts: (i) Find a way to package some redundancy along with signal so that the redundant information spreads the signal throughout the entire message; and (ii) The fraction of redundant information added to the message becomes negligible as the messages become arbitrarily long. Then all of the channel capacity can be used without penalty.

Figure 7-1 illustrates the relationship between the noise energy per bit N_0 , the signal energy per bit E_b , the bandwidth in Hertz of the channel W , and the channel capacity in bits C for a binary symmetric channel. Error-free communications are possible for every point that lies below the curve.

A channel coding algorithm attempts to provide a constructive and practical realization of Shannon's Channel Coding Theorem, which loosely

Figure 7-1: Shannon's channel coding theorem.



asserts that *arbitrarily reliable communication is possible at any rate below channel capacity*; [37, 53, 54].¹

Although Shannon's theorem is not constructive, it does prescribe an unrealizable procedure that would code or "modulate" the message bit-stream onto the signal carrier so as to completely utilize channel capacity. This procedure employs modulating codewords that are overlapped random coding sequences or "waveforms" of infinite duration. If distinct codewords represent the message symbols "0" and "1", then the statistical orthogonality of random waveforms insures that cross-correlations are zero and the autocorrelation of each random waveform is the delta distribution. Hence, despite the presence of channel noise, the received message can be decoded by passing it through a set of filters matched to the random waveforms.

The key factors that make this procedure work are:

1. Codewords that are pairwise orthogonal;
2. Codewords that are infinitely long;

¹The Channel Coding Theorem was first proved for a Binary Symmetric Channel. It has been extended to more general channels.

3. Explicitly known matched filters for detecting the codewords.

- *Orthogonality* is used by the matched filter detectors to distinguish the different codewords from each other and from channel noise, with which (under suitable assumptions about the channel noise statistics) the codewords have small or vanishing correlations.
- *Infinite length* codewords are employed to spread the information represented by the encoded bit throughout the entire signal, thereby creating a kind of "hologram" whose smallest parts contain information about every part. This "de-localization" of the information makes the codeword resistant to localized noise effects and, in the limit, to arbitrary noise effects.

That the codewords are *random waveforms* is not essential; randomness, combined with infinite duration, simply guarantees orthogonality and delocalization.

The matched filters can be *statistical* or *deterministic*; deterministic filters are better in combination with soft decision detection procedures.

It appears that *in the limit of arbitrarily long waveforms, wavelet channel coding realizes the upper bound for information transmission given by Shannon's Channel Coding Theorem*. That is, wavelet channel encoded information can be transmitted at a rate that is as close as one pleases to channel capacity with arbitrarily small bit error rates. From a practical standpoint, the significance of this statement is that wavelet channel encoding provides a *constructive* and *practical* solution to design of efficient codes. Moreover, a wavelet channel codec can be efficiently implemented in VLSI technology.

7.2 Wavelet Channel Coding

The user of a digital communication system will primarily be concerned with the *bit rate* and the *error rate* of the communications channel.² The channel is controlled by allocating power and bandwidth, both of which are precious resources.

Every communications channel experiences noise. Additive white Gaussian noise (abbreviated "AWGN") is often a good first approximation because it results from thermal effects, which are always present. Other types of noise are important in specific applications. The communications system designer would like to achieve the objectives of high bit rate and low error

²The bit rate is the message throughput in bits per second. The error rate is the fraction of input message bits that are in error at the receiver.

rate with a minimum of power consumption and bandwidth requirements. These objectives are inconsistent; trade-offs must be made that prefer high bit rate to low error rate or low error rate to high bit rate; low power requirements to low bandwidth or low bandwidth to low power requirements. These trade-offs determine the type of modulation and error correction that will be selected.

Wavelet channel coding ("WCC") provides a systematic conceptual and design method for making these trade-offs through software selection within a common chipset-based hardware framework.

The advantages of wavelet channel coding result from the combination of the exact orthogonality of wavelet codewords, the spreading of message symbol information throughout the overlapped codeword symbols, and the ability to utilize soft decisions to decode wavelet channel coded symbols.

The main properties of WCC coding are summarized in the following list:

1. Wavelet Channel Coding is a new *class* of channel coding algorithms.
2. WCC offers a systematic and simple approach to the full range of coding problems, from low rate, power efficient codes to high rate, bandwidth efficient codes.
3. Wavelet Channel Coding can be applied in a *block coding* mode or in a *trellis coding* mode.
4. WCC codewords are strictly orthogonal.
5. WCC codewords have small correlations for non-codeword offsets.
6. WCC coding employs robust *soft decision* decoding.
7. WCC codes can be arbitrarily long.
8. WCC codewords have desirable Hamming distance properties and provide good error correction capability.
9. WCC codes can be efficiently coded and decoded with simple VLSI circuits.
10. Synchronization can be performed by correlation matching.

Analysis and computer simulations show that WCC with arbitrary length wavelets achieves the AWGN performance of coherent binary phase shift keying ("BPSK"). When compared under a constant channel rate criterion, WCC provides coding gains of approximately $10 \log_2(mg + 1)$ dB. On pulsed

interference and flat fading channels WCC outperforms BPSK with gains that are dependent of the wavelet sequence length.

Figures 7-2 through ?? display the performance improvements of wavelet channel coding in three environments:

1. An AWGN channel with 5% burst noise compared with Pulse Amplitude Modulation ("PAM").
2. An AWGN fading channel, compared with PAM.
3. A flat Rayleigh channel, compared with BPSK.

7.2.1 Modulation

There are three basic types of modulation. Each one corresponds to modulation of one of three parameters: *amplitude* A , *frequency* ω , and *phase* θ . To clarify this, suppose that the digital communication channel employs plane electromagnetic waves as the transmission medium. The modulator in a digital communications system maps the symbols that are to be transmitted to the amplitude, phase or frequency of the carrier. The modulator output can be represented as

$$s(t) := \text{Re} (u(t)e^{j2\pi f_c t}) . \quad (7-1)$$

This is a bandpass signal in which f_c represents carrier frequency and $u(t)$ the equivalent low pass message bearing waveform.

The form of $u(t)$ is dictated by the form of the modulation used. We distinguish:

1. *Amplitude Shift Keying*: more commonly called PAM (Pulse Amplitude Modulation). This is the modulation method in which the message symbols y_n are mapped to a discrete set of amplitudes so that

$$u(t) := \sum_{n=0}^{\infty} y_n g(t - nT) \quad (7-2)$$

2. *Frequency Shift Keying*: (FSK) in which the symbols y_n are mapped to a discrete set of frequencies so that

$$u(t) := \sum_{n=0}^{\infty} e^{j2\pi y_n t} g(t - nT) \quad (7-3)$$

3. *Phase Shift Keying*: (PSK) in which the y_n s are mapped to a discrete set of phases so that

$$u(t) := \sum_{n=0}^{\infty} e^{jy_n} g(t - nT) \quad (7-4)$$

In all of the above, the message symbol rate is assumed to be $1/T$ and $g(t)$ is assumed to be a pulse (square or other) of duration T .

In the remainder of this chapter, we examine the implications of using each of these modulation techniques for the transmission of WC encoded symbols. We limit our discussion to multiplier 2, flat WCM with maximal overlap trellis WCC. Extending the discussion to higher multiplier systems and arbitrary overlap signalling is straightforward.

Figure 7-2: Wavelet channel coding performance in a channel with 5% burst noise.

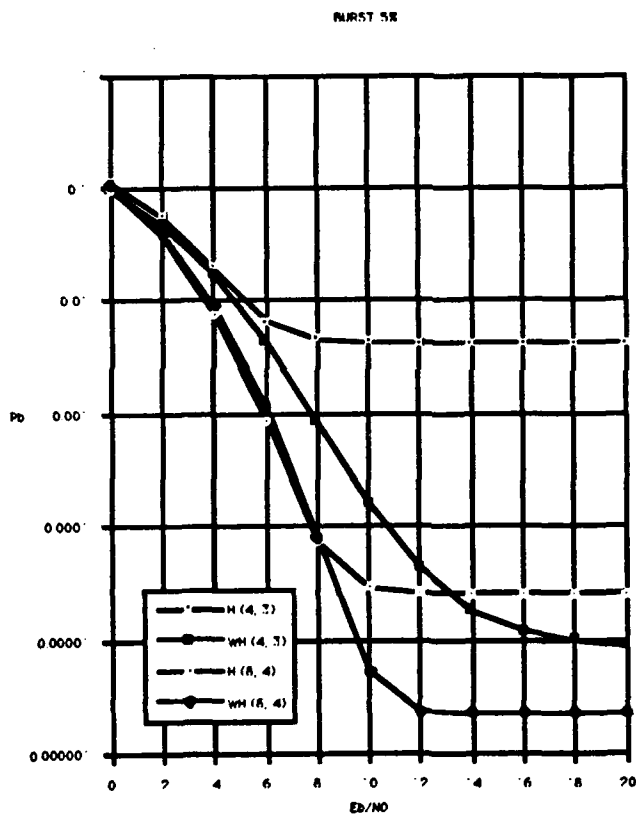


Figure 7-3: Wavelet channel coding performance in fading channels.

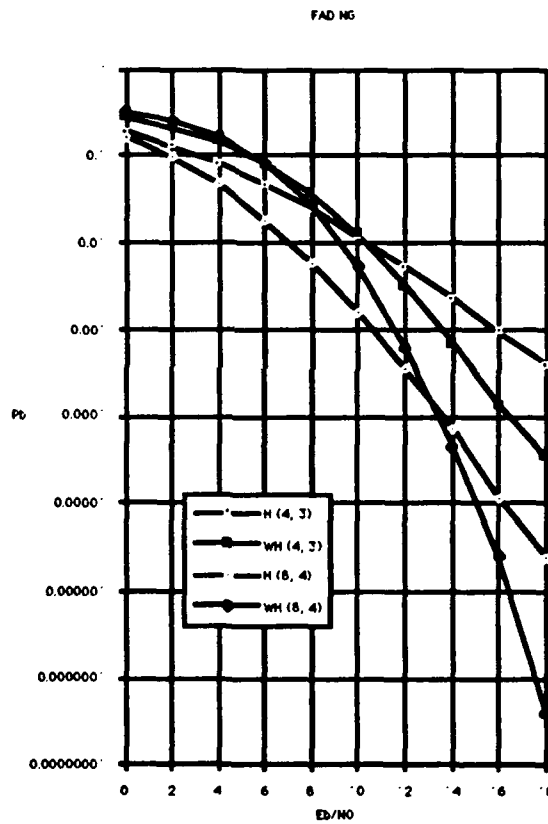
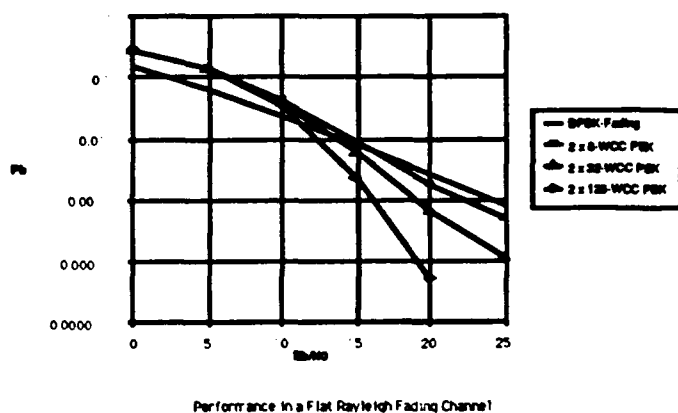


Figure 7-4: Wavelet channel coding performance in flat Rayleigh channels.



7.3 The Wavelet Channel Coding Algorithm

7.3.1 The Basic Idea: Trellis WC Message Coding for $m = 2$

For the purpose of illustration, let a message

$$x_1, x_2, \dots, x_n, \dots$$

consist of a sequence of bits represented by the signed units $\{+1, -1\}$, and let

$$\begin{pmatrix} a_0, \dots, a_{2g-1} \\ b_0, \dots, b_{2g-1} \end{pmatrix}$$

be a rank 2 wavelet matrix of genus g . Because the rows of multiplier 2 WCM's are mutually orthogonal when translated by steps of two, we can take advantage of the orthogonality of the a 's and b 's to code at a rate of two message bits per 2^k clock pulses, where $1 \leq k \leq \log_2 2g$. Message bits with odd sequence number will be coded using the WCM waveform

(a_0, \dots, a_{2g-1}) and message bits with even sequence number will be coded using the WCM waveform (b_0, \dots, b_{2g-1}) .

The coding procedure is illustrated in Table 7.1 for a system with *maximally overlapped* wavelet sequences. This corresponds to the case where the code rate is one information bit per WCC symbol (i.e. $k = 1$ above). The sequence of clock pulses is arranged above the upper rule of the table, and the sequence of transmitted symbols y_n is shown below the lower rule of the table. The encoding of each message bit x_n is shown in the n th row below the upper rule. The output code symbol for odd n the encoding begins on the n th clock pulse and that for even n the encoding begins on the $(n-1)$ th clock pulse. y_n is equal to the sum of the n th column of encoded message bit values and is therefore not restricted to the values ± 1 . The formula for computing the symbol y_n to be transmitted at the n th clock pulse is

$$y_n = \sum_k \{x_{2k+1}a_{n-2k-1} + x_{2k+2}b_{n-2k-1}\} \quad (7-5)$$

Some observations are in order:

1. It is evident that code rates as small as $1/g$ can be achieved by varying the overlap of the wavelet sequences; in the limit where the code rate is $1/g$, the wavelet sequences are non overlapped but adjacent.
2. When flat WCM are used, the WC encoded symbols that are generated by the trellis WCC algorithm are binomially distributed. We will discuss this in more detail in section 7.3.5 below.

7.3.2 Recovery of a Trellis WC Coded Message for $m = 2$

The sequence of message bits x_n can be recovered from the transmitted symbol sequence by a matched filter which uses the orthogonality of the WCM waveform sequences. For the illustrative implementation of waveform symbol generation described in the previous subsection, the message bit $x_n = \pm 1$ is identified with the sign of the output of a filter matched to the WCM waveform with input the received symbol sequence. To show this, suppose that the receiver has received the symbols

$$y_1, y_2, \dots, y_n, \dots$$

We will calculate the correlation of this symbol sequence with the WCM vectors (a_0, \dots, a_{2g-1}) and (b_0, \dots, b_{2g-1}) .

First, consider the output of the filter matched to (a_0, \dots, a_{2g-1}) , i.e.

$$\sum_n a_{n-2l-1} y_n, \quad (7-6)$$

where l is an arbitrary integer. Equation (7-5) implies

$$\begin{aligned} \sum_n a_{n-2l-1} y_n &= \sum_n a_{n-2l-1} \sum_{q \text{ odd}} \{x_q a_{n-q} + x_{q+1} b_{n-q}\} \\ &= \sum_{q \text{ odd}} \{x_q \sum_n a_{n-2l-1} a_{n-q} + \\ &\quad x_{q+1} \sum_n a_{n-2l-1} b_{n-q}\} \quad (7-7) \\ &= 2x_{2l+1}, \end{aligned}$$

where we have used the orthogonality of the WCM sequences to obtain the last line. A similar argument yields the formula for correlation with the sequence (b_0, \dots, b_{2g-1}) , which decodes the bits x_{2l} corresponding to even clock pulses.

More sophisticated WC coding and decoding techniques have been developed by Aware and are currently under investigation.

7.3.3 The Simplest Case: Block WC Message Coding with $m = 2$

Suppose that the message is periodic with period $2g$ equal to the length of the wavelet sequences employed by a trellis coder. In this case WCC performs the function of a block encoder, which we describe in this section.

If the message is the row vector

$$x := (x_0, \dots, x_{2g-1}) \quad (7-8)$$

where $x_i \in \{1, -1\}$, then the coded message is the codeword row vector

$$y := (y_0, \dots, y_{2g-1}) \quad (7-9)$$

where

$$y = xU \quad (7-10)$$

and

$$U := (U_{jk}), \quad (7-11)$$

$$U_{j,2k} := \frac{1}{2^j} a_{(j+2k) \bmod 2g}, \quad (7-12)$$

$$U_{j,2k+1} := \frac{1}{2^j} b_{(j+2k) \bmod 2g} \quad (7-13)$$

Theorem. U is a unitary matrix.

In the absence of noise, the decoding algorithm is simply

$$x = yU^{-1} = y\bar{U}^t \quad (7-14)$$

When a flat WCM is used for block coding, constant power encoded symbols are generated. This is not the case for trellis WCC, even when flat wavelet matrices are utilized.

7.3.4 Code Rate and Channel Rate for Arbitrary Overlap Signalling

We discussed in section 7.3.1 the ability to alter the *code rate* of the wavelet channel code by changing the amount by which the WCM waveforms overlap. In general we see that *arbitrary overlap signalling* is capable of producing variable rate codes. A *maximally overlapped signalling technique* produces a code rate of 1 (i.e. 1 information bit per codeword symbol); anything less than this will produce a lower rate code. A code with code rate equal 1 does not compromise information throughput; one information bit is transmitted per codeword symbol.

In addition to the code rate, it is informative to define the *channel rate* as the number of channel bits transmitted per clock pulse. In the maximally overlapped signalling case, this is identical to the channel rate. This relates to the modulation scheme that is necessary to transmit the encoded symbols. The channel rate for maximally overlapped wavelet sequences is given by the formula

$$R = \frac{1}{\log_2(mg + 1)} \quad (7-15)$$

By varying the overlap of the WCM waveforms, it is possible to obtain WC codes whose channel rate is arbitrary. This occurs because the number of values in the WCC symbol distribution decreases as the amount of overlap decreases. Another way to alter the channel rate is by limiting the modulation scheme to a number of levels less than the number of WCC symbols. This is essentially equivalent to performing *range truncation* on the WCC symbols. For example, a maximally overlapped trellis WCC using multiplier 2, length 8 flat real WCM will produce WCC symbols with possible values

$$-8, -6, -4, -2, 0, 2, 4, 6, 8 \quad (7-16)$$

The channel rate of this code is $\log_2 9$. It would require a 9-ary modulation scheme for transmission. By truncating the values ± 8 from the range

of WCC symbols, a 7-ary modulation scheme could be used reducing the channel rate to $\log_2 7$. Ultimately, the channel rate will approach one as the number of WCC symbol values is reduced to two. The redundancy inherent in WC coding suggests that altering the channel rate by range truncation may be beneficial and our simulations of WCC Phase Shift Keying ("PSK") bear this out.

7.3.5 Distribution of WCC Symbols

Monograph Distribution

WCC codeword symbols are not equiprobable. Indeed,

Theorem. Let $[a]$ be a $m \times mg$ flat real WCM. The $mg + 1$ codeword symbols for WCC share the common denominator m^J where J and g are related by the equation

$$m^{2J} = g, \quad (7-17)$$

and their numerators are

$$-mg, \dots, -2k, \dots, 0, \dots, 2k, \dots, mg. \quad (7-18)$$

These codeword symbols are binomially distributed according to the discrete probability density function (the notation for the probability displays only the numerator)

$$\text{Prob}(y_m = 2k - mg) = \binom{mg}{k} (0.5)^{mg}, \quad 0 \leq 2k \leq mg \quad (7-19)$$

where it is assumed that the message bits ± 1 have equal probability.

Theorem. The average value of the variance of a codeword symbol y is

$$\langle y^2 \rangle = \sum_{k=0}^{mg} (2k - mg)^2 \binom{mg}{k} (0.5)^{mg} = mg. \quad (7-20)$$

proof is by

7.4 Wavelet Channel Coding and Digital Modulation Techniques

7.4.1 Wavelet Channel Coding and M-ary Pulse Amplitude Modulation

When using a multiplier $m = 2$, flat real wavelet matrix of order gm in a maximal overlap trellis WCC, the encoded symbols take on the values

$$-mg, \dots, -2k, \dots, 0, \dots, 2k, \dots, mg. \quad (7-21)$$

M must equal $gm + 1$ for there to be a one-to-one mapping between the WC encoded symbols and the signals in the M -PAM constellation. As the length of the wavelet sequences increases, so does the average energy of the transmitted M -PAM signal. We see, therefore, that an increase in wavelet sequence length requires an increase in average transmitted symbol energy. However, for a fixed message rate, no bandwidth expansion is required to transmit WC codeword symbols using PAM.

7.4.2 Wavelet Channel Coding and M-ary Phase Shift Keying

Multiphase signaling is another means of transmitting digital data. The wavelet symbols are mapped to phases on the unit circle. At the demodulator it will be necessary to map the received signal phase back to the range of the codeword symbol distribution before processing by the matched filter wavelet decoder. A phase detector is therefore used to produce the soft decisions that are passed to the WC trellis decoder.

It is interesting to observe the distribution of WCC symbols when they are normalized to lie on a compact interval as $gm \rightarrow \infty$. The normalized WCC symbols cluster near zero as gm increases. A similar clustering behavior would obviously be observed on the unit circle, as seen by mapping the codeword symbols to the interval $[-\pi, \pi]$ and wrapping this interval around the unit circle.

The issue of optimally placing the codeword symbols around the unit circle is not a trivial one. We have shown that it is optimal to place the codeword symbols so that the distance between signal constellation points is proportional to the probability of symbol occurrence, i.e. a symbol that occurs frequently is placed further from its adjacent constellation points than a symbol that does not. The unit circle, however presents an additional problem. Wrap-around places the largest negative value adjacent to the largest positive value in the signal constellation. This is undesirable because

in the presence of noise, a sign reversal of the codeword symbol value is possible with catastrophic implications at the trellis decoder. Aware has found the following rules of thumb to be successful:

1. truncate the range of transmitted codeword symbols to those that occur on the order of 95% of the time.
2. map these to the unit circle so that approximately two thirds of the entire circle is used (thus keeping the most negative and most positive codeword symbols at a distance of approximately $\frac{2\pi}{3}$.) Ideally the optimum distance between these "end" values (i.e. the most positive and most negative codeword symbols) can be related to the signal to noise ratio (SNR) at which the communications system is operating. If for instance, the SNR is known in an additive white Gaussian channel, the end values can be placed on the unit circle to obey an a priori determined probability of sign reversal.

When M -PSK is used to transmit WCC symbols, an increase in the wavelet sequence length causes a decrease in the distance between adjacent signals in the constellation. No increase in symbol energy is incurred as the length of the wavelet sequences increases. Also, at a constant message rate, the code rate 1 trellis WCC requires no bandwidth expansion regardless of the wavelet sequence length. In the limit, as the wavelet sequence length goes to infinity, the WCC symbols map to the *entire* unit circle (assuming no range truncation is used.) This, in a sense, is equivalent to using analog phase modulation for digital data transmission and is an interesting prospect Aware is currently evaluating.

7.4.3 Wavelet Channel Coding and M -ary Frequency Shift Keying

The form of the message bearing low pass equivalent signal is given in eq. (7-3). The criteria for selecting the frequency separation between adjacent frequencies in the signal constellation are identical to those used in standard FSK modulation. At the receiver, the output from a set of $gm + 1$ bandpass filters (each tuned to an appropriate frequency) can be used to obtain a soft decision on the WCC symbol. Other, more sophisticated demodulation schemes are possible.

When FSK is used for the transmission of WCC symbols and a constant message rate is assumed, an increase in bandwidth is required for each increase in wavelet sequence length. The average energy of the transmitted wavelet symbol does not, however, increase with sequence length; it is given by the energy of the pulse $g(t)$.

7.5 Performance of Wavelet Channel Coding

7.5.1 Introduction

The performance of the multiplier 2 WCC algorithm presented in section 7.3.1 for a number of wavelet sequence lengths, and in communications channel environments including additive white Gaussian noise, pulsed interference and Rayleigh fading. The performance was compared with classical digital communications techniques for a constant *code rate* constraint as well as a constant *channel rate* constraint.

7.5.2 Performance of WCC in Additive White Gaussian Noise

In this section we discuss the theoretical performance of maximal overlap trellis WC coding when used in conjunction with M -PAM (heretofore denoted as WCC-PAM) in the presence of additive white Gaussian noise (AWGN).

Wavelet channel coding maps information bits into coded symbols that are $(mg + 1)$ -ary for an order mg WCM. The probability density function is binomial, and the average value of a codeword symbol y^2 is given by eq(7-20). For PAM the amplitudes of the equivalent low-pass waveforms are the symbols y_i . The energy of this waveform is proportional to y_i^2 , so the average signal energy is proportional to the average value of y_i^2 , i.e. mg ; cp. eq(7-20).

If we let $z_i = y_i + n_i$ be a noise-corrupted symbol, then y_i represents the signal component (i.e. a WCC symbol) and n_i a realization of mean 0, variance $N_0/2$ AWGN. We also let S_i and R_i represent the signal and noise components at the output of the wavelet matched filter, respectively.

The AWGN noise term in the R_i term has mean value zero and variance

$$\text{Var} = mg \frac{N_0}{2}. \quad (7-22)$$

It follows (using notation similar to that in section 7.3.2) that the probability of a bit error is (cp. [61])

$$\begin{aligned} P_b &= \frac{1}{2} \{ \text{Prob}(R_{2l+1} + S_{2l+1} > 0 \mid x_{2l+1} = -1) \\ &\quad + \text{Prob}(R_{2l+1} + S_{2l+1} < 0 \mid x_{2l+1} = +1) \} \\ &= \frac{1}{2} \{ \text{Prob}(R_{2l+1} > N \mid x_{2l+1} = -1) \\ &\quad + \text{Prob}(R_{2l+1} > N \mid x_{2l+1} = +1) \}. \end{aligned} \quad (7-23)$$

Since the noise term R_{2l+1} is independent of x_{2l+1} , this can be written as

$$P_b = \text{Prob}(R_{2j+1} > N) = Q\left(\frac{N}{\sqrt{NN_0/2}}\right) = Q\left(\sqrt{\frac{2mg}{N_0}}\right) \quad (7-24)$$

where

$$Q(\alpha) := \frac{1}{\sqrt{2\pi}} \int_{\alpha}^{\infty} e^{-y^2/2} dy. \quad (7-25)$$

Performance Results with Rate 1 WC Codes

Since rate 1 WC codes maintain the original bit rate, a comparison with classical binary modulation techniques (BPSK, BFSK, etc.) is appropriate. Let E_b represent the energy transmitted over the channel per message bit.

It can be shown that WCC-PAM in AWGN achieves the bit error rate (BER) performance of coherent BPSK for arbitrary length wavelet sequences, and WCC outperforms coherent BPSK in channel environments other than AWGN. This is due to the property of WCC to spread message bit information throughout the codeword symbols. As a result of this spreading, we see improvements in performance with increased wavelet sequence lengths in pulsed interference and fading channels.

Performance Results with Constant Channel Rate

We now compare WCC-PAM to uncoded PAM under a constant channel rate criterion. In order to maintain the message bit rate and since $\log_2(mg+1)$ bits are transmitted per WCC codeword symbol, it is necessary to assume that a bandwidth expansion factor of $\log_2(mg+1)$ is allowable on the channel without significant intersymbol interference.

Let E_c be the energy per channel bit. The BER performance is expressed in terms of E_c as

$$P_b = Q\left(\sqrt{\frac{2E_c \log_2(mg+1)}{N_0}}\right) \quad (7-26)$$

The simulated performance of WCC-PAM was compared to 9-PAM and 33-PAM, used for coded and uncoded PAM. As seen from the simulation curves, mg -WCC achieves gains of approximately $10 \log_2(mg+1)$ dB over $(mg+1)$ -ary PAM. Note that these curves are plotted in terms of channel bit SNR: E_c/N_0 . For PAM this is equivalent to information bit SNR E_b/N_0 . For WCC-PAM E_c/N_0 is equivalent to E_b/N_0 only with the bandwidth expansion assumption given above.

7.5.3 Performance on Pulsed Interference Channels

The pulsed interference (also called burst noise) channel is an AWGN channel that is occasionally corrupted by large bursts of noise or interference (either intentional or unintentional). The inherent property of WC codes to spread a message bit over a length mg WC codeword suggests that the use of WCC in burst noise channels would be beneficial. Indeed, as we show in this section, the effects of pulsed interference are ameliorated by using WCC, with performance improvements that increase with increasing wavelet sequence length.

Performance Results

The performance of WCC-PAM in pulsed interference was derived using computer simulation. It is assumed that the noise bursts occur randomly and are of duration no longer than that of a symbol. If an interleaver with length at least that of the burst is used, the results apply to longer duration bursts as well. Symbols affected by pulsed interference are simply blanked out at the receiver causing a symbol erasure. The justification for this is that all information in the amplitude of the PAM signal has been destroyed by the pulsed interference, hence setting the affected symbol to zero (the value of the most probable codeword symbol) is a reasonable choice.

It is apparent that WCC provides significant gains over uncoded BPSK in the presence of pulsed interference and that these gains grow with increases in the wavelet sequence length.

Table 7. Example of Wavelet Channel Coding

1	2	3	4	...	$2g$	$2g + 1$	$2g + 2$...
$x_1 a_0$	$x_1 a_1$	$x_1 a_2$	$x_1 a_3$...	$x_1 a_{2g-1}$
$x_2 b_0$	$x_2 b_1$	$x_2 b_2$	$x_2 b_3$...	$x_2 b_{2g-1}$
		$x_3 a_0$	$x_3 a_1$...	$x_3 a_{2g-3}$	$x_3 a_{2g-2}$	$x_3 a_{2g-1}$...
		$x_4 b_0$	$x_4 b_1$...	$x_4 b_{2g-3}$	$x_4 b_{2g-2}$	$x_4 b_{2g-1}$...
				...	\vdots	\vdots	\vdots	\vdots
y_1	y_2	y_3	y_4	...	y_{2g}	y_{2g+1}	y_{2g+2}	...

Chapter 8

Numerical Solution of Partial Differential Equations

8.1 Understanding PDE

The motion and interaction of physical things on the scale of human beings is described by Newton's laws, which mediate between the submicroscopic world, governed by quantum mechanics, and gravity, governed by general relativity. For the most part, these laws and relationships are expressed in terms of relations between physical quantities, such as *force* and *energy*, and the rate at which they change with *time* and *distance*. The equations that express the relations between a quantity and its rate of change are *differential equations*.

The differential equations that govern the diffusion of heat throughout an object (the "diffusion equation"), the propagation of electrical currents and radio waves ("Maxwell's equations"), the propagation of sound waves (the "wave equation"), the structural behavior of materials (the "continuum mechanics equation"), and the flow of viscous fluids, ranging from air to water and honey (the "Navier-Stokes equations") are the basic equations that govern the phenomena of daily life. Engineers who design complex products usually use numerical solutions of one or more differential equations as a tool.

The solutions of differential equations also relate the values of parameters that can be controlled by the user to the behavior of a process or

system, just as a driver rotates the steering wheel to control a car's direction.

It is usually difficult to calculate numerical solutions for differential equations in real time; in some cases, because of the large amount of calculation that would be needed or because the equation describes a transient or nonlinear phenomenon like a shock wave and is sensitive to numerical errors due to round-off or discretization of the space and time variables, it is impossible. For these reasons, real-time process control has not been practical for most processes. Recent advances in microcomputer performance and in wavelet mathematics create the possibility of broadly applying the numerical solution of differential equations to real-time control problems.

8.2 Wavelet numerical solutions for differential equations

Aware has developed numerical methods for solving nonlinear partial differential equations using wavelet functions. The relevant properties of wavelets are that they are compactly supported, orthogonal and define bases for Sobolev spaces. Being both compactly supported and orthogonal, wavelets combine the advantages of finite element, spline, and Fourier spectral methods that have been traditionally used to find numerical solutions. To test the feasibility of the wavelet methods we have studied nonlinear phenomena that exhibit singular behavior. These include shocks (e.g. Burgers equation, the Gas dynamics/compressible Navier Stokes equations) and turbulence (incompressible Navier Stokes). For shocks we found some remarkable results. The Galerkin method based on wavelets (the Wavelet-Galerkin method) accurately captured shocks for large Reynolds number and stably described their interactions. The solutions decayed to the correct limit for large times. In comparison, the spectral and finite difference solutions were unstable and inaccurate. The stability of the Wavelet-Galerkin method extended to infinite Reynolds number and by a simple modification of the *cutoff boundary condition* accurately captured shocks in the inviscid limit [30], [27]. For turbulence we ran simulations of the two dimensional Euler flow and examined the phenomena related to vortex merger, filamentation, the gradients of vorticity and the long time limit. Our initial results show that the Wavelet-Galerkin method is as accurate as the fully-dealiased spectral method, is far more stable, and, for each time step, (depending on the specific wavelet basis, algorithm and state of optimization), can be faster than the spectral method [68]. It seems that the wavelet discretization allows the implementation of numerical schemes for Euler flow that are useful

for long time studies and that cannot be implemented by spectral or finite difference methods. The basic numerical lesson is that scaling function expansions subdue the Gibbs's phenomenon, allow the stable calculation with oscillatory approximations that occur in inviscid calculations, and allow the efficient, iterative implementation of implicit time differencing methods.

Compact-support and the ability of scaling functions to exactly approximate features smoother than themselves, and hence to be able to better approximate discontinuous features, is essential. The orthogonality of the translated scaling function basis also guarantees the conservative approximation of the quadratic integrals (energy and enstrophy) by the Galerkin approximation to the Jacobian nonlinearity. The implicit time differencing with the Wavelet-Galerkin space discretization allows the control of, i.e. conserves, or monotonically increases or decreases, the energy and/or enstrophy. It seems clear that wavelet based numerical methods for turbulence simulations hold considerable promise and warrant further development.

We have also developed a wavelet-based method for the solution of boundary value problems in arbitrary geometries. This Wavelet-Capacitance Method is defined by a nontrivial extension of the classical Capacitance Matrix, and, unlike the classical method, it can be *spectrally accurate* [43]. We use compactly supported wavelets as a Galerkin basis and develop a Wavelet-Capacitance Matrix method to handle boundary geometry. For several geometries we have made a detailed comparison of methods, examining accuracy and rates of convergence. Specifically, we compared the Wavelet-Galerkin method to standard methods for the numerical solution of the Biharmonic Helmholtz equation and the Reduced Wave equation in nonseparable, two-dimensional geometries. We have used the Wavelet-Capacitance method to numerically resolve the long term limit of two-dimensional Euler and Navier-Stokes flows in rectangular and L-shaped domains. This has considerable relevance to the qualitative behavior of two-dimensional turbulence [70], [68], [69] and to practical applications of the method to problems in engineering. We have developed least-squares versions of our algorithm for the Helmholtz equation in nonseparable geometries and examined the accuracy and convergence of these methods.

We have also used the Hilbert transform of the compactly supported wavelets to define an extended basis for the exterior Acoustic Helmholtz problem. Surprisingly, the Hilbert transform of a compact wavelet is a noncompact wavelet verifying the same basic equation. The noncompact form can be used to match the Sommerfeld radiation condition. In summary,

- The Wavelet-Capacitance Matrix Method is stable and *spectrally accurate*. These results apply to general nonseparable domains and all

ranges of the parameters.

- The Wavelet algorithm is found to obtain accurate results for problems where, for instance, finite difference methods do not converge, or converge slowly, and where Fourier Spectral methods do not apply.
- For a fixed level of discretization, increasing the order of the wavelet basis spectrally decreases the error.
- The rates of convergence in sup norm appear to depend on the wavelet basis, DN , and discretization, δx , as $(\delta x)^{N-5}$.
- The rates of convergence in sup norm appear to be independent of the domain shape.
- Least-squares versions of the wavelet algorithm can preserve accuracy and decrease the computation by more than a factor of four. The finite difference algorithms would not allow effective least-square implementations.
- All errors (accuracy and convergence) are measured in the pointwise sup norm.
- Our implementation is fast, since it is based on fast (FFT) evaluations for periodic geometry adapted to nonseparable geometry.
- The basic algorithm applies to one, two and three space dimensions, without essential modification.
- The Wavelet-Galerkin method preserves symmetries of the domain and defines a type of discrete orthogonality that is very useful for further applications of the method. These applications include fast Domain Decomposition techniques.
- We have found a wavelet basis with prescribed rate of decay at infinity. This is based on the Hilbert Transform of compactly supported wavelets and will allow the fast direct solution of the exterior acoustic problem.
- To our knowledge, our algorithm is an unique extension of the classical Capacitance-Matrix method and should have several and diverse applications to problems requiring a higher order accuracy.

of the orthogonal spaces is useful in the numerical solution of nonlinear systems.

We have found that the Hilbert Transform of a scaling function is a scaling function with a prescribed rate of decay at infinity. Translates of this scaling function define a basis on the real line that is useful for the numerical solution of exterior boundary value problems. For instance, this would allow a direct solution of the acoustic radiation problem.

8.3 Summary of Current Results

8.3.1 Advantages of wavelets for the numerical Solution of PDE.

- Translates form orthogonal basis. Quadratic invariants, including energy and enstrophy, are preserved.
- Locally exact representation of polynomials by translates of the scaling function.
- Compact support of basis elements. Localization of gradients and stability of numerical methods. Attenuation of Gibb's Phenomena. Efficient parallel implementations.
- The degree of approximation of basis elements is greater than their degree of smoothness. Good approximation of smooth functions. Attenuation of Gibb's Phenomena at discontinuities.
- Multiresolution of scales. Connections with multigrid and adaptive methods.
- Fast evaluation of basis elements by use of the scaling relation.
- Exact evaluation of wavelet functionals by algebraic methods. Exact evaluation of functionals required in the Galerkin method.

8.3.2 Principal Results

- Development of Wavelet-Galerkin method. Exact evaluation of Connection Coefficients. Shock Capture and Turbulence Closure.
- Development of wavelet methods for PDE boundary problems by an extension of the Capacitance Matrix method. Comparison with standard finite difference methods. Spectral convergence of the wavelet methods.
- Long time limit of 2D-Euler and Navier-Stokes flows with geometry. Implications for Two-Dimensional Turbulence.

8.4 A One Dimensional Example: Burgers Equation

Burgers equation is an idealized mathematical representation for the development of a "breaker" as an ocean wave feels the bottom when it reaches a shallow beach. The bottom of the wave is retarded and the slope of the wavefront increases until it is nearly vertical. Then the wave breaks and crashes on the beach.

Aware developed the Wavelet-Galerkin method to solve this kind of problem. The results have been reported in several papers (cp. [27], [32], [66]) to which the reader is referred for the details.

Burgers equation is perhaps the simplest example of a non linear partial differential equation. The equation is

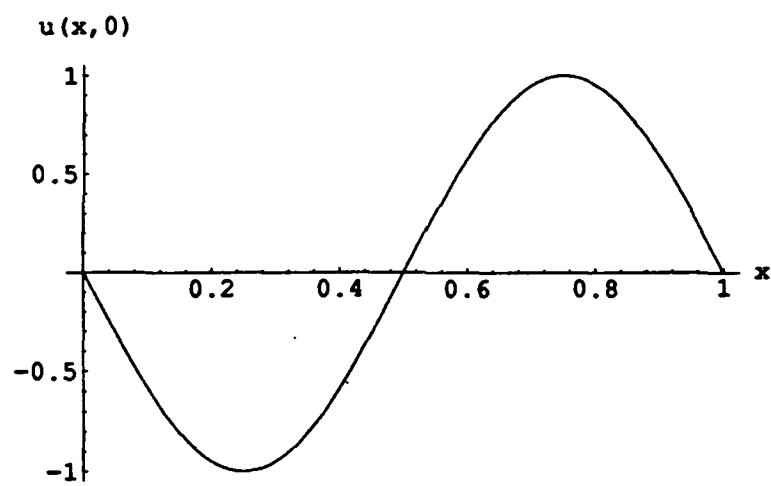
$$u_t + uu_x = \sigma u_{xx},$$

where σ is the viscosity. When the viscosity is null, the field will develop a *shock* in a time $t^* = \min\{1/u_x(x, 0)\}$. The nonlinearity is the quadratic term, uu_x , which causes small irregularities in $u(x, t)$ to grow as time passes. Ultimately, the gradient of u becomes too large to be accurately estimated by a difference quotient on a grid of fixed size, and the numerical solution becomes unstable and "crashes on the beach" too. Conventional numerical methods for solving this equation are unable to cope with the consequences of the instability of the numerical derivative. Wavelet methods, based on the use of connection coefficients to estimate derivatives, is much less sensitive to the grid size and tempers the instability. The result is an accurate solution without requiring fine grids or increased computational cost.

An example will help to demonstrate the power of the Wavelet-Galerkin method. For the sake of simplicity of description we will consider the Burgers' equation evolution of a one dimensional periodic wave; this is the same thing as considering a wave that travels around a circle. This assumption separates the problem of the general numerical stability and accuracy of the method from questions that concern the treatment of boundary conditions.¹

¹Aware and its associates at Rice University have developed powerful and efficient general methods for employing wavelets with boundary conditions. Cp. [66], [71], [43].

Figure 8-1: Initial condition for the solution of Burgers equation.



Suppose that at time $t = 0$ the initial waveform is the sinusoid

$$u(x, 0) = -\sin(2\pi x/64)$$

suitably normalized, and that a grid of 64 points per unit interval is employed in the space domain; the initial function is shown in figure 8-1.

Figure 8-2 illustrates the evolution of the solution employing the standard de-aliased spectral method on the 64 point grid. In the figure the time axis runs from the upper right to the lower left, so that the solution for the final time step is the leftmost cross section of the surface, and the initial sinusoid is the rightmost cross section. The vertical scale measures the wave amplitude $u(x, t)$. A total of 450 equispaced time steps are represented.

The figure shows that relatively soon a nearly vertical shock wave develops. Since the equation contains a diffusive term, the peak value of the shock decays as time passes. Then, as the figure illustrates, the shock give birth to an oscillation. The shock amplitude increase and the frequency oscillation rapidly grows in amplitude and propagates throughout the solution. The source of the oscillation is numerical error: error in estimating the gradient, and round-off error in the calculations. The final time slice shows an completely unreliable numerical solution.

Although the errors dominate the solution, their local space average appears to be less sensitive to these errors. Figure 8-3 shows the result of applying a 3-point average to the numerical solution at each time step. This simple average provides a generally accurate picture of the solution, but it is neither quantitatively correct nor is it accurate in the qualitative details - the shock front begins to grow again as time evolves. These problems are typical when the de-aliased spectral method is applied to non linear problems that describe transient, localized phenomena that have rapidly varying gradients.

The Wavelet-Galerkin method avoids these difficulties. The local support of the wavelet basis functions reduces or eliminates propagation of errors to distant regions, and the high accuracy of the connection coefficient derivative estimates (cp.[28], [36]) reduces the error in gradient estimates. When combined, these features lead - for a preset level of accuracy - to lower computational cost because the can employ a coarser grid.

Figure 8-4 displays the wavelet numerical solution of the same problem using the *Daubechies* wavelet basis $D3$. The solution has not been smoothed. Figure 8-4 shows the same solution with 3-point smoothing. This provides a small incremental improvement in the accuracy of the solution.

Figure 8-2: Evolution of the numerical solution of Burgers equation employing unsmoothed de-aliased spectral method.

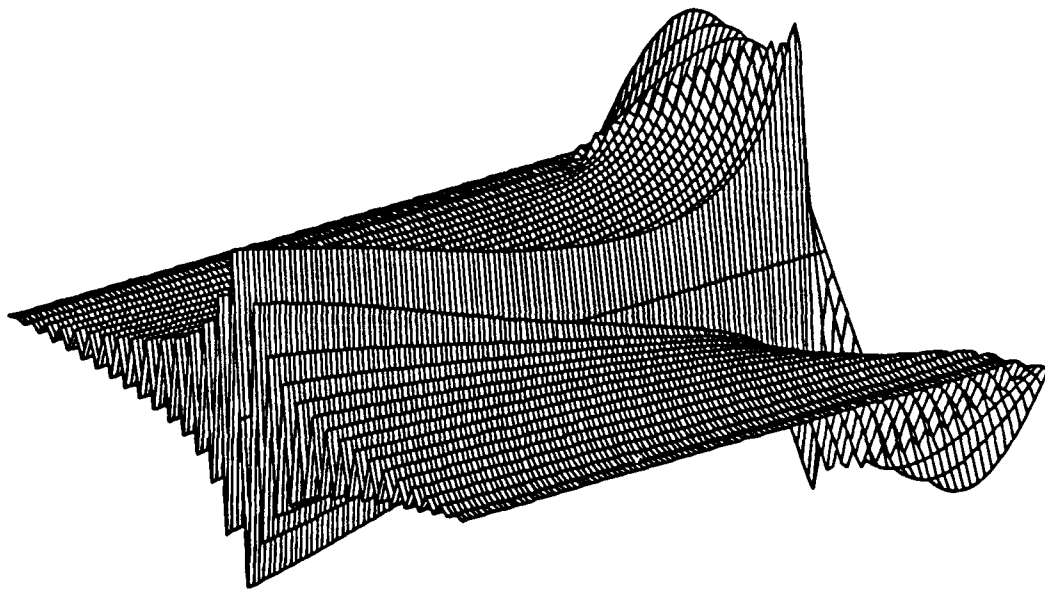


Figure 8-3: Evolution of the numerical solution of Burgers equation employing smoothed de-aliased spectral method.

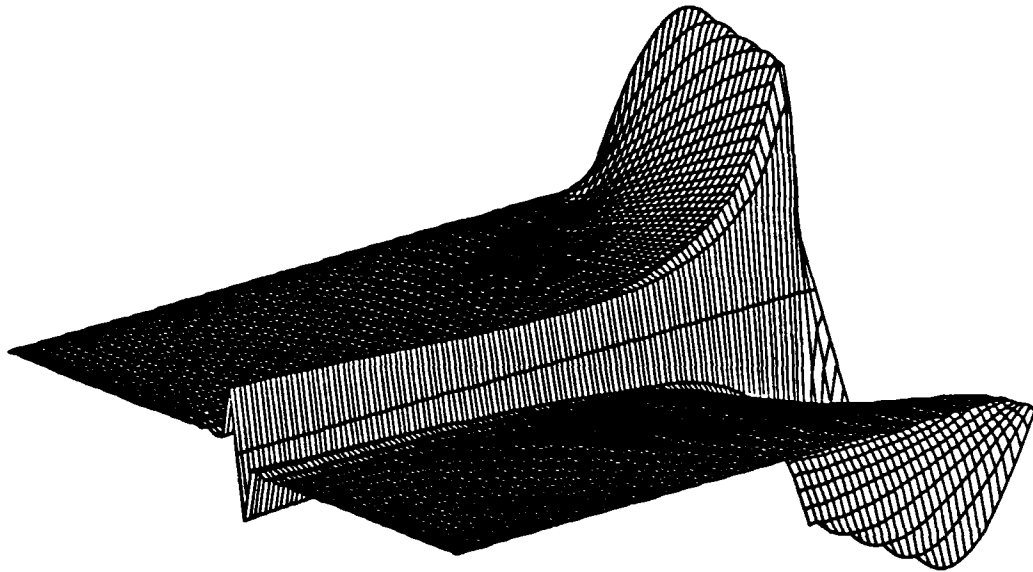


Figure 8-4: Evolution of the numerical solution of Burgers equation employing unsmoothed Wavelet-Galerkin method.

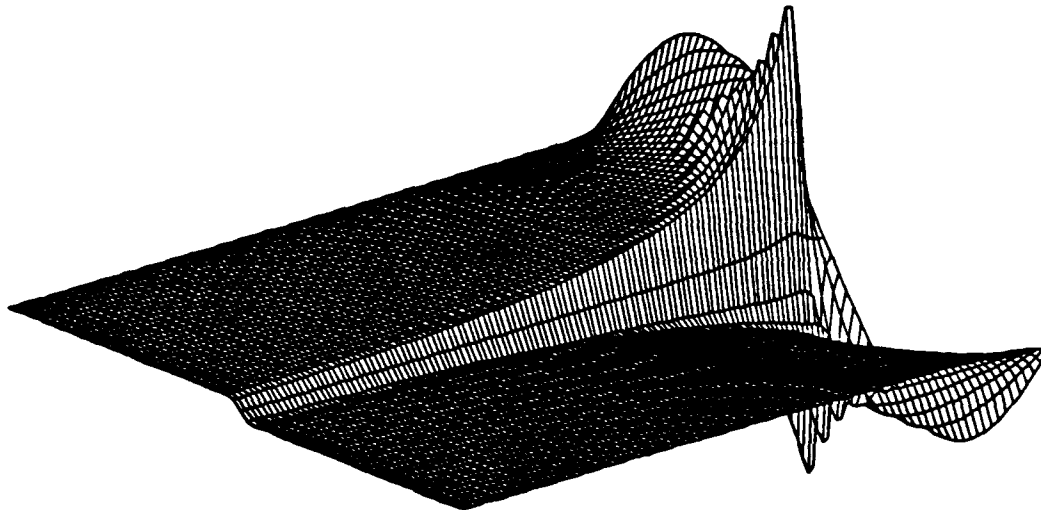
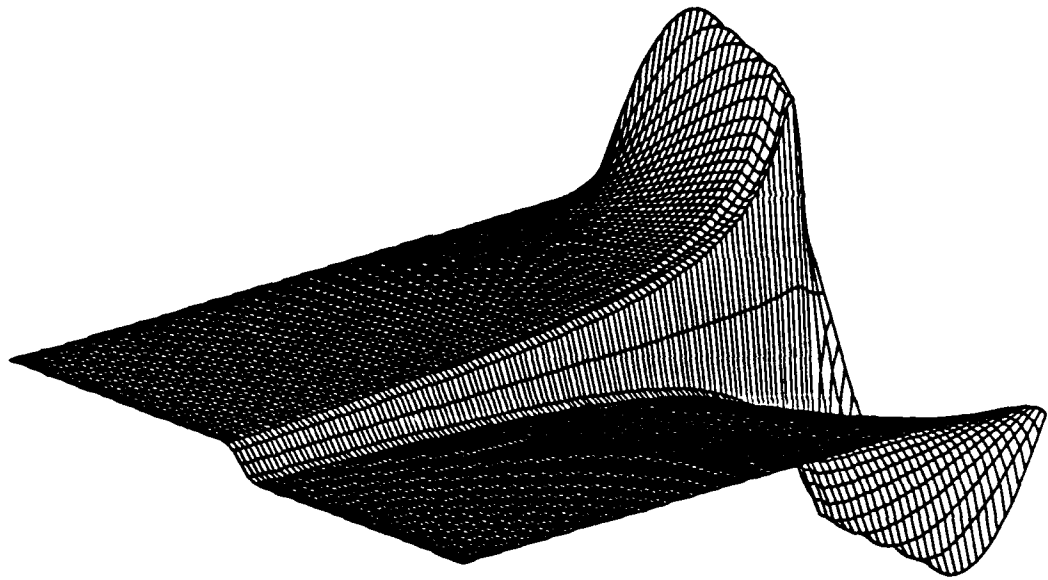


Figure 8-5: Evolution of the numerical solution of Burgers equation employing smoothed Wavelet-Galerkin method.



Bibliography

- [1] Abramowitz, M. and Stegun, I. *Handbook of Mathematical Functions with Formulas, Graphs, and Mathematical Tables*, National Bureau of Standards, Applied Mathematics Series No. 55, Second printing with corrections, Washington, DC, 1964.
- [2] Ahmed, N, Schreiber, H. and Lopresti, P., "On notation and definition of terms related to a class of complete orthogonal functions," *IEEE Trans. Electromagn. Compat.* EMC-15:75-80 (1973).
- [3] Alpers, S. (1983), *The Art of Describing*, Chicago: The University of Chicago Press.
- [4] Bishop, E. (1967), *Foundations of Constructive Analysis*, New York: McGraw-Hill Book Company.
- [5] Boltzmann, L. (1909), *Abhandlungen*, Vol. I, Leipzig: Barth.
- [6] Burt, P. and Adelson, E. , "The Laplacian pyramid as a compact image code," *IEEE Transactions on Communications*, vol. 31, pp. 532-540 (1983).
- [7] Cohen, A., "Biorthogonal wavelets," *Wavelets: a tutorial in theory and applications*, edited by Charles K. Chui, Academic Press, Inc., San Diego, 1992, pp. 123-152.
- [8] Cooley, J. W. and Tukey, J. W., "An algorithm for the machine calculation of complex Fourier series" *Math. Comp.*, vol. 19, pp. 297-301 (1965).
- [9] Daubechies, I., "Orthogonal bases of compactly supported wavelets," *Communications on Pure and Applied Mathematics*, vol. XLI, pp. 909-996 (1988).

- [10] Eddington (1928), A. S. *The Nature of the Physical World*, Cambridge: Cambridge University Press.
- [11] Einstein, A. (1955), *The Meaning of Relativity*, Princeton: Princeton University Press 5th Ed.
- [12] Fourier, J. , *Théorie analytique de la chaleur*, (1822, Paris); *Œuvres*, 1.
- [13] Gabor, D. , "Theory of communication," *J. IEEE*, vol. 93, pp.429-457 (1946).
- [14] Glowinski, R., Lawton, W., Ravachol, M. and Tenenbaum, R., *Wavelet Solution of Linear and Nonlinear Elliptic, Parabolic and Hyperbolic Problems in One Space Dimension*, in Proceedings of the 9th International Conference on Numerical Methods in Applied Sciences and Engineering SIAM, Philadelphia (1990)
- [15] Gödel, K. (1986), *Collected Works*, Vol. I, S. Feferman et al, eds. Oxford and New York: Oxford University Press.
- [16] Gombrich, E. H. (1960), *Art and Illusion*, A. W. Mellon Lectures in the Fine Arts 1956, Princeton: Princeton University Press.
- [17] R. A. Gopinath and C. S. Burrus, "On cosine-modulated wavelet orthonormal bases," Rice University Computational Mathematics Laboratory Technical Report CML TR92-06.
- [18] Goupillard, P., Grossman, A. and Morlet, J., "Cycle-octave and related transforms in seismic signal analysis," *Geoexploration*, vol. 23, pp. 85-102, (1984/85).
- [19] Haar, A., "Zur Theorie der orthogonalen Funktionensysteme," *Math. Ann.*, vol. 69, pp. 331-371 (1910).
- [20] Hadamard, J., "Résolution d'une question relative aux déterminants," *Bull. Sci. Math.*, ser. 2, vol. 17, pt. I, pp. 240-246 (1893).
- [21] Heideman, M. T., Johnson, D. H. and Burrus, C. S., "Gauss and the history of the FFT," *IEEE ASSP Magazine*, vol. 1, pp. 14-21 (1984) and *Archive for History of Exact Sciences*, vol. 34, pp. 265-277 (1985).
- [22] Heisenberg, W., "Über den anschaulichen Inhalt der quantentheoretischen Kinematik und Mechanik" *Zeit. f. Physik*, vol. 43, pp.172-198 (1927).

- [23] Heller, P., "Regular M -band wavelets," Aware Technical Report AD920608.
- [24] Heller, P. and Resnikoff, H., "Polynomials are generalized eigenfunctions of the wavelet transform," Aware Technical Report AD910912.
- [25] Heller, P., Resnikoff, H. and Wells, R., "Wavelet matrices and the representation of discrete functions," *Wavelets: a tutorial in theory and applications*, edited by Charles K. Chui, Academic Press, Inc., San Diego, 1992, pp. 15-50.
- [26] Heisenberg, W. (1927), "Über den anschaulichen Inhalt der quantentheoretischen Kinematik und Mechanik", *Zeitschrift für Physik* 49 (1927), 172-198.
- [27] Latto, A. and Tenenbaum, E., "Compactly supported wavelets and the numerical solution of Burgers' equation," *C. R. Acad. Sci. France, Série I*, pp. 903-909 (1990).
- [28] Latto, A., Resnikoff, H. and Tenenbaum, E., "The evaluation of connection coefficients of compactly supported wavelets", Aware Technical Report AD910708 (July 1991) and *Proceedings of the French - USA Workshop on Wavelets and Turbulence*, Princeton University, June 1991, Editor, Y. Maday, Springer - Verlag (1992).
- [29] Lawton, W., "Necessary and sufficient conditions for constructing orthonormal wavelet bases," *J. Mathematical Physics*, vol. 32, pp. 57-61 (1991).
- [30] Lawton, W., "Multiresolution properties of the Wavelet-Galerkin operator," *J. Mathematical Physics*, vol. 32, (1991).
- [31] Lawton, W. and Resnikoff, H. L., "Multidimensional Wavelet Bases," Aware, Inc., Technical Report No. AD910130, 1991.
- [32] Lawton, W., Morrell, W., Tenenbaum, E. and Weiss, J., "The Wavelet-Galerkin Method for Partial Differential Equations", Aware Technical Report AD901220 (1990)
- [33] R. Lidl and G. Pilz, *Applied abstract algebra*, Springer-Verlag, New York, 1984.
- [34] Mallat, S., "A theory for multiresolution signal decomposition: the wavelet representation," *IEEE Transactions on Pattern Analysis and Machine Intelligence*, vol. 11, No. 7, pp. 674-693 (1989).

- [35] Maxwell, J. C. (1908), *Theory of Heat*, London: Longmans, Green & Co..
- [36] Wells, R. O. and McCormick, K., "Wavelet calculus and finite difference operators," Aware Technical Report AD920915 = Rice University Computational Mathematics Laboratory Technical Report 91-02.
- [37] McEliece, R., *The theory of information and coding*, volume 3 of *Encyclopedia of Mathematics and its Applications*, Addison-Wesley Pub. Co., Reading, MA (1977).
- [38] Meyer, Y., *Ondelettes et operateurs, Tome I: Ondelettes*, Paris, Hermann 1990, ISBN 2 7056 6125 0.
- [39] Neumann, J. von (1955), *Mathematical Foundations of Quantum Mechanics*, Princeton: Princeton University Press, (translation of the original German edition).
- [40] Pollen, D., "Linear one dimensional scaling functions," Aware Technical Report AD900101.
- [41] Pollen, D. and Linden, D., "Real quadratic one-dimensional scaling coefficients," Aware Technical Report AD900109.
- [42] Pratt, W., Kane, J., and Andrews, H., "Hadamard transform image coding," *Proc. IEEE* 57, pp. 58-68 (1969).
- [43] Qian, Z. and Weiss, J., "Wavelets and the numerical solution of partial differential equations," Aware Technical Report AD920318; to appear in *J. Computational Physics*.
- [44] Rabbani, M. and Jones, P., *Digital image compression techniques*, SPIE Optical Engineering Press, Bellingham, WA (1991).
- [45] Qian, Z. and Weiss, J., "Wavelets and the numerical solution of boundary value problems," Aware Technical Report AD920714; to appear in *Applied Mathematics Letters*.
- [46] Rademacher, H., "Einige Sätze von allgemeinen Orthogonal-Funktionen," *Math. Ann.* vol. 87, pp. 122-138 (1922).
- [47] Rao, K. and Yip, P., *Discrete cosine transform*, Academic Press, Inc., Boston, 1990.
- [48] Reid, C. (1976), *Hilbert - Courant*, New York and Heidelberg: Springer-Verlag.

- [49] Resnikoff, H. L., *The Illusion of Reality*, New York and Heidelberg: Springer-Verlag, (1989).
- [50] Resnikoff, H. L. and Puri, M. L., "Information," chapter 18 (pp. 451-469) of *Acting under uncertainty: Multidisciplinary conceptions*, Georg von Furstenberg, editor, Kluwer Academic Publ., Boston (1990).
- [51] Robinson, A. (1966), *Non-standard Analysis*, Amsterdam: North-Holland Pub. Co.
- [52] Shannon, C. and Weaver, W. (1949), *Mathematical Theory of Communication*, Urbana: University of Illinois Press.
- [53] Shannon, C. E., "A mathematical theory of communication," *Bell System Technical Journal*, vol. 27, pp. 379-423 (1948).
- [54] Shannon, C. E., "A mathematical theory of communication," *Bell System Technical Journal*, vol. 27, pp. 623-656 (1948).
- [55] Shannon, C. E., "Communication in the presence of noise," *Proc. I.R.E.*, vol. 37, pp. 10-21 (1949).
- [56] Smith, M. J. and Barnwell, T. P., "Exact reconstruction techniques for tree-structured subband coders," *IEEE Transactions on ASSP*, vol. 34, pp. 434-441 (1986).
- [57] Stautner, J. P., "Coding for compression of entertainment quality audio signals: An overview of literature and techniques," Aware Technical Report Number AD910528.
- [58] Stautner, J. P., "High quality audio compression for broadcast and computer applications," Aware Technical Report Number AD920207. Presented at the 26th Annual SMPTE Advanced Television and Electronic Imaging Conference.
- [59] Stautner, J. P., "Scalable audio compression for mixed computing environments," Presented at the 93rd Convention of the Audio Engineering Society, 1-4 October 1992, San Francisco.
- [60] Tzannes, M. A., and Tzannes, M. C., Block biorthogonal channel coding using wavelets, Aware Technical Report AD920622, *Proceedings of MILCOM '92*, to appear.
- [61] Tzannes, M. A., and Tzannes, M. C., Bit-by-bit channel using wavelets. Aware Technical Report AD920629, *Proceedings of GLOBECOM '92*, to appear.